AAEC/PR 39-P

AAEC/PR 39-P

INIS-XA-N--161

AUSTRALIAN ATOMIC ENERGY COMMISSION

RESEARCH ESTABLISHMENT

LUCAS HEIGHTS

PROGRESS REPORT OF PHYSICS DIVISION

1st JANUARY – 31st DECEMBER 1973

AUSTRALIAN ATOMIC ENERGY COMMISSION

RESEARCH ESTABLISHMENT

LUCAS HEIGHTS

PROGRESS REPORT OF PHYSICS DIVISION

1st JANUARY-31st DECEMBER, 1974

ACTING DIVISION CHIEF - MR. W. GEMMELL

CONTENTS

CONTENTS

CONTENTS

CONTENTS

1.1 INTRODUCTION

The reactor MOATA is operating successfully at 100 kW with the higher available flux being much appreciated by all users. A uranium analysis service commenced and the various mining exploration companies are gradually availing themselves of it in an increasing fashion. The possible introduction of a similar service for neutron radiography is being explored following successful laboratory studies. Various other applications of nuclear science are under development.

The revised safety assessment carried out for 100 kW operation of MOATA led to a more generalised study of self limited, non boiling power transients and in particular the maximum reactivity limit for these transients. This involved a re-examination of the SPERT non boiling transients and the prediction of their outcome in quantitiative terms on purely physics considerations without resort to normalisation. The indications are that a 10 second period transient in MOATA would give rise to a power transient which would be self limited to 100 kW. A possible experiment to test this prediction is under examination.

Various physics aspects of MOATA operation were studied on a mockup of the reactor on the split table machine and the degree of understanding by staff of this reactor's behaviour much improved. The safety assessment of the split table machine (Critical Facility) was completed and should shortly be available from the printer for submission to the new Licensing and Regulatory Bureau for authority to operate.

Nubar measurements for the various fissile elements are complete, but studies of neutron emission from the individual fragments produced during the spontaneous fission of ^{252}Cf fission and the neutron energy spectrum of ^{252}Cf fission neutrons are being undertaken to clarify some of the remaining discrepancies.

Analysis of neutron capture cross section data obtained at Oak Ridge National Laboratory is continuing. Details of the analysis for some element studies are given. Progress has also been made in elucidation of the contribution of p-wave neutrons in neutron capture.

The complexity and variety of codes for reactor analysis and their interdependence has produced major shifts in design philosophy. An outline is given of the system in use within the Division.

2.1 MOATA REACTOR (T. Wall)

A full review of the reactor safety assessment was completed in anticipation of uprating the reactor's power from 10 kW to 100 kW operation. Appropriate modifications to the process system, the neutronic instrumentation and the control/interlock circuits, were implemented and following complete testing of the revised system, the reactor has been operated routinely at powers up to 100 kW.

The resulting increase in available neutron flux ($\sim 10^{12}$ neutron cm^{-2} s^{-1}) has increased the range of feasible experiments, as well as conveniently shortening activation irradiation times and lowering the detection threshold for elements in neutron activation analysis.

Based on data accumulated to date, it is estimated that the first full year's operation may result in an integrated power output of about 100 MWh compared with the maximum possible 170 MWh approximately, for continuous full power, single shift operation. This is a very encouraging initial response and augurs well for future utilisation of the reactor.

The following are some of the projects which involved significant use of the reactor.

Activation analysis of trace elements in ground waters and obsidian glasses
Prompt gamma ray detection in thermal column beam
Radiation damage to transistors
Reactor noise measurements
Uranium assay in ore and ground-water samples
Neutron radiography
Molecular decomposition by neutron bombardment
Labelling of river sands by neutron activation
Isotope production
Undergraduate and postgraduate training
Measurement of the absorption cross sections of soils

In addition, production of essential isotopes for medical applications and for ASNT was carried out during the extended HIFAR shutdown. The increased flux available allowed requirements to be met within the normal working day, instead of requiring special shift working arrangements as in the past.

Neutron Radiography

Neutron radiography is a potentially powerful tool for non-destructive examination of articles and specimens containing light atoms, particularly hydrogen, in their component structure, since these do not provide examinable contrast using the usual X-ray approach.

Preliminary studies of the neutron radiography technique have been carried out using the activation foil photographic film transfer method. The general IR1 neutron beam arrangement for this study is shown in Figure 2.1. Initially, sensitometric curves, Figure 2.2 (a),(b), relating the film dose from an activated foil to the film blackening, were obtained for indium and gold detectors exposed to D7 X-ray film. The neutron flux was of an intensity such that convenient, short irradiation and exposure times for indium detectors produce film densities of 2.0 and above. Radiography with gold as the transfer foil is also possible, but longer and less convenient irradiation and exposure times are necessary. Tables 2.1 and 2.2 show the times required to produce a radiograph of background density 2.8 for gold and indium respectively. The reactor beam characteristics and methods used to obtain the exposure data were described by Wall and Gillespie (1973). Using the thermal neutron beam, hydrogenous material in glass-to-metal seals and automobile fuel injectors have been radiographed.

Hydrogen Determination in Cellulose Acetate

In collaboration with Materials Division, an investigation was made into the Hysen technique for the detection of hydrogen. This followed the work by Konsanke (1971) in which the reactor beam is filtered by thick slabs of cadmium and indium (Figure 2.3). The filtered beam then passes through the radiographed object where some of the epithermal neutrons colliding with hydrogen impurities in the object are downscattered into the indium resonance region and subsequently absorbed on the indium transfer foil. The activated indium foil is then exposed to the X-ray film and the image of the object developed.

To obtain data on response times and film contrast, sheets of cellulose acetate of thickness 0.25 mm and hydrogen content 5.8×10^4 ppm were formed into a three layered step wedge 0.25, 0.5 and 0.75 mm thick and the step wedge radiographed through filters of 6 mm cadmium and 6 mm indium. The densities obtained are shown in Table 2.3 and are compared with data from a radiograph of the same step wedge in the unfiltered thermal neutron beam from IR1. Expressing the film contrast c as

$$c = 100|\Delta D|\ B^{-1}$$

where $|\Delta D|$ is the absolute value of the difference in density between a cellulose acetate region and background density B.

The values of c in Table 2.3 show the improvement in the contrast by the use of cadmium and indium filters.

Hydrogen Determination in Zircaloy

Having demonstrated the use of filters to improve the contrast for hydrogen in cellulose acetate, the filter method was used to determine the film contrast obtainable from radiographs of thin slabs of hydrided zircalloy. Five slabs of zircalloy metal, 10 mm square by 0.71 mm thick, with concentrations of hydrogen ranging between 125 and 1420 ppm were prepared by the Spectrometry and Radiochemistry group. These were radiographed by the Hysen technique using 6 mm cadmium and indium filters. The contrast ratios attained are shown in Figure 2.3 for both D4 and D7 X-ray film.

Although film densities in the range 1 to 3 were obtained for the 125 and 265 ppm specimens, the results showed large scatter in repeated experiments. Reliably reproducible contrasts were obtained only for the 495, 935 and 1420 ppm specimens, and at this stage, it appears that the technique might provide an accuracy of $\sim\pm$100 ppm at levels of $\sim$500 to 1500 ppm hydrogen.

Konsanke claimed that the Hysen technique can detect 50 ppm hydrogen in 0.62 mm thick zircalloy coupons, but it is not clear whether this refers to detectable contrast from a test specimen of known H content or to a quantitative H determination for an unknown sample. Our work with 125 ppm coupons suggests the former since measurable contrasts could be obtained, but quatitatively showed a large scatter in repeat runs.

Further work will be done to establish accuracy and reproducibility of results using fixed irradiation, decay and film exposure times and to allow a quantitative comparison with results from the standard thermal neutron radiography technique.

Uranium Ore Assay

A pneumatic transfer rig has been providing brief irradiations of crushed ore samples in MOATA. Determination of the delayed neutron activity on removal from the reactor provides an estimation of the uranium content of the ore.

Standard sample ampoules, each filled with a weighed sample of ore (~3 to 5 g) are loaded into the rig magazine. They are in turn then injected into the reactor for a 45 s irradiation, ejected to the centre of an annular ganged array of BF_3 proportional counters in an hydrogenous moderator. The delayed neutron output is counted for 40 s and the sample transferred to a shielded storage holder. A few standard samples of known U content are arranged in each magazine for calibration and standardisation of the irradiation/counting routine.

Up to ~60 samples can be determined in one hour under ideal conditions, with 40 being a reasonable working average.

Extensive tests and comparisons with other methods of analysis (particularly X-ray fluorescence and wet chemistry) have shown conclusively the very high reliability as well as the convenience of the technique. The practical limit of detection for the present sample size with 100 kW reactor operation is approximately 2 ppm natural uranium for an accuracy of about $\pm$20 per cent. The accuracy improves rapidly with increasing uranium content, reaching about $\pm$2 to $\pm$ 3 per cent at uranium concentrations of about 100 ppm and above.

An improved rig which will allow easier sample handling and more versatility in experimental conditions, has been designed and built and is undergoing out-of-pile testing prior to installation on the reactor.

Some preliminary tests have also been made of the feasibility of ore analysis for uranium by measurements of selected gamma rays. It appears that long counting times (~24 hours) are required, but that use of a uranium gamma ray at 1.001 MeV might enable the disequilibrium problem to be circumvented.

TABLE 2.1

GOLD EXPOSURE TIMES T_E (h)

PRODUCING FILM DENSITY OF 2.8 IN D7 FILM

(i) 10 kW beam flux = 1.4×10^6 neutron cm^{-2} s^{-1}

Irradiation time T (h) / Decay time t_1	4	6	8	10
0	82.7	47.0	33.3	25.9
2	84.1	48.4	34.2	26.6
4	88.7	49.8	35.1	27.3
6	92.0	51.2	36.0	27.9
8	95.4	52.7	37.0	28.7

(ii) 100 kW beam flux = 1.4×10^7 neutron cm^{-2} s^{-1}

Irradiation time T (h) / Decay time t_1	4	6	8	10
0	5.65	3.77	2.84	2.29
2	5.78	3.85	2.91	2.34
4	5.91	3.94	2.97	2.39
6	6.04	4.03	3.04	2.45
8	6.18	4.12	3.10	2.50

TABLE 2.2

INDIUM EXPOSURE TIMES T_E (m)

PRODUCING FILM DENSITY OF 2.8 IN D7 FILM

(i) 10 kW beam

Decay time t_1 \ Irradiation time T (m)	50	100	150	200
0	248.7	77.1	59.1	52.8
20	-	130.2	90.6	78.8
40	-	-	170.7	134.4

(ii) 100 kW beam

Decay time t_1 \ Irradiation time T (m)	50	100	150	200
0	7.86	5.06	4.26	3.96
20	10.3	6.60	5.55	5.12
40	13.6	8.64	7.25	6.68
60	18.1	11.4	9.50	8.75
80	24.3	15.0	12.5	11.5
100	33.1	20.0	16.6	15.2

TABLE 2.3

FILM DENSITIES FOR CELLULOSE ACETATE RADIOGRAPHS

Cellulose acetate thickness (mm)	0.25	0.5	0.75	Background
Film density Hysen technique	0.48	0.60	0.70	0.37
Film density thermal beam	1.17	1.15	1.09	1.19
Contrast Hysen technique	29.7	62.2	89.2	
Contrast thermal beam	1.7	3.4	8.4	

2.2 HIFAR SUPPORT (P. Duerden)

Considerable experimental effort has been made during the course of the year's operation and also during and following the major shutdown period for maintenance (28/5/73 to 7/9/73), to update and augment HIFAR physics operational data.

Measurements have included fuel reactivity coefficients, long lived poisons and temperature coefficients, statistical weights, coarse control arm reactivity worths and Xe-Sm transient poisoning. The results have been assessed and collated with other existing data and incorporated into revised operational information published for the reactor. A brief summary of only a few of the measurements is given below.

Statistical weights were determined at several core heights for a range of fuel element positions and experimental facilities. The collated available data are shown in Figure 2.4.

Individual CCA Reactivity Worths

(a) Removal of a CCA from the core

Reactivity balances with a rig in, and then removed from fuel element position C4 were made for the normal 6 arm bank and with each arm in turn held at 52^{o} (horizontal). The worth of the horizontal CCA in terms of the worth of the 6 arm bank was then determined:

(i) from comparisons of the bank movement in each configuration necessary to compensate the insertion of the rig, and

(ii) from the critical angle change with rod bank configuration.

It was found that the bank worth was reduced by 20, or 13, or 6 per cent of the 6 arm value for raising of an inner, intermediate or outer arm, respectively, corresponding to relative arm worths for these locations of 26: 16: 8.

(b) Lowering of arm into core

This experiment followed the long shutdown: the residual neutron source was therefore abnormally low (~0.01 Watt equivalent) and necessitated restriction of the core available excess reactivity to a maximum of 6.6 per cent $\Delta k/k$.

Two independent pulse counting channels in 6VGR3 and 6VGR4 were used in

a subcritical counts 'approach to critical' measurement in terms of CCA bank angle. A CCA bank parking angle was then chosen such that complete loss of the most effective CCA (assumed worth 26 per cent of the total bank worth) plus a temperature decrease of $5^{o}C$ would just make the system critical. With the remaining 5 arms held at this angle, each arm in turn was lowered to 13^{o}, 10^{o}, 7^{o} and 4^{o}, with count rates being measured at each step.

The subcritical inverse count rate changes were related to the known reactivity changes for movements of the 6 rod bank in the range close to critical. The resulting reactivity changes for lowering of each arm are shown in Figure 2.5.

The ratio of the reactivity change on lowering a given individual arm relative to that for lowering the whole bank through the same angle, was found to be sensibly constant, implying that the shapes of the ρ vs θ relation for individual arms and the full bank are the same over the range of angles used. This gives some confidence in using the current CCA calibration data for angles below 10^{o} where critical measurements of worth cannot be made.

The relative worths of the inner, intermediate and outer arms were found to be in the ratio 23:18:9 and to give reactivity changes corresponding to 25, 20 and 9.5 per cent of that which would result from lowering the full bank through a similar angle.

HIFAR Safety Analyses

The worst possible consequences of uncontrolled reactivity accidents in the AAEC reactor HIFAR have been estimated (Turner 1973)*. The study was done to find out how essential the principal reactor shutdown system, namely the coarse control arm scram, is to the safe operation of the reactor. Two reactivity accidents have been identified which, if they occurred in combination with a failure of this shutdown system could result in fuel melting, loss of the heavy water coolant and failure of the steel containment shell. These accidents are:

(a) Breakage of an inner coarse control arm at the worst time and with a new maximum allowable fuel loading, and

(b) uncontrolled withdrawal of the coarse control arm bank.

---

*Turner, W. J. (1973) - RP/TN153

Prior to the introduction of the Mark IV fuel elements in HIFAR in 1970, all subchannels of a HIFAR fuel element were identical; the mean outlet temperature and the subchannel outlet temperatures were therefore equal. This is not true for Mark IV fuel elements in which two of the five annual subchannels are heated on only one side and the other three on both sides. Thus the protection provided by the central fuel element trip must be reassessed. This has been done and after consultation with Operations Division, recommendations have been made for lowering the trip setting, connecting the trip to the hottest element and restricting the range of D_2O temperatures at the lower end.

2.3 CRITICAL FACILITY (D. B. McCulloch)

Work continued on the preparation of a comprehensive general safety assessment document for the Facility. The scope of the attendant studies broadened during the year, but the task is now essentially complete and a fully edited version of the document will be ready for appraisal of the appropriate Safety Committees shortly.

Meanwhile, clearance for operation on a series of experiments on MOATA (Argonaut Reactor) type cores was obtained on the basis of a safety appraisal specific to this type of assembly. Measurement programmes have been carried out on three cores of this general type and have given valuable data on MOATA physics parameters and on reactivity coupling effects between core tanks.

The operating experience on these experiments has been of considerable value in staff training and familiarisation with the new facility and in identifying areas of weakness in the equipment and in proposed administrative rules for its operation. A number of modifications have been devised and implemented as a result of the experience gained to date, which significantly improve reliability and convenience of operation, as well as enhancing inherent operational safety.

2.3.1 Safety Assessment (A. Dalton)

Analyses of the cell design, the design basis accident and consequent aerosol release and dispersion, were updated and revised in the light of newly and directly available facility data and parameters and new climatological and aerosol settling data. The administrative rules for operation were revised to take account of practical staffing arrangements and of precise physical arrangements of control and safety circuits which were not always exactly apparent from manufacturer's descriptions and drawings. Some

modifications were incorporated in control circuits to improve operational convenience and safety.

Major efforts were devoted to a reanalysis of the protection provided by the safety circuits and shutdown devices against a wide range of reactivity addition accidents. The reanalysis was undertaken to incorporate actual measured data which could now be obtained for response times, instruments, safety circuits and protection devices, under practical reactor power increase conditions. This work is described below.

Transients Terminated by Reactor Protective Devices (D. Culley)

Point reactor kinetics studies using digital methods (AIREK III code, Blue and Hoffmann 1963) have been made for a wide range of possible assemblies having prompt neutron lifetimes, ℓ^*, from 10^{-3} to 10^{-8} s. Assuming accidental fuel loading errors such that criticality was achieved before the tables were fully closed, the energy released for the resulting reactivity transients were calculated for a range of different instrument initiated shutdowns.

All systems were assumed to have $k_{eff} \sim 0.7$ at full table separation. Count rates or ionisation chamber output currents were obtained for a number of types of detectors appropriately located in the assemblies using flux spectra from the GYMEA code (Pollard and Robinson 1966) and the counter sensitivity to thermal neutron fluxes. Count rates for the selected detectors as a function of system subcriticality were thus established in terms of the neutron source strength. These count rates were, however, assumed to be lower by a factor of 10 in the kinetics model to ensure that a conservative estimate was always taken of instrument response.

Transient terminations by high flux trips and flux period trips were considered. For the latter, an extensive investigation of the periodmeter response function was made using the PACE analogue computer, and an empirical model of its response under reactor conditions for a wide range of initial count rates was derived and incorporated in the point kinetics code. Measured values of safety circuit delays, electromagnet release times, table stop and reverse times, etc., were also incorporated.

The negative reactivity insertion function for the safety rods was derived from SCRAM test data of rod displacement vs. time and an assumed cosinusoidal flux distribution in the assembly. Since core radius is less than rod travel for the small, shorter lifetime cores, withdrawal of fuel rods gives a more rapid reactivity reduction than insertion of absorber rods. However, it was

conservatively assumed that absorber type rods were used in all assemblies.

Four ramp reactivity addition rates were considered for the final table closure range (0.625 to 5.0 x 10^{-4} $\Delta k/k\ s^{-1}$) and 2 x 10^{-3} $\Delta k/k$ for the (incredible) situation where criticality is reached in the intermediate range. Sets of calculations were performed for several groupings of instrumentation and equipment failure. Delayed neutron data for Pu fuel were conservatively assumed to apply throughout.

The results (Table 2.4) show that for criticality occurring in the final speed range of table closure, in only one case is there a significant energy release even when period protection and safety rod action are assumed to fail simultaneously. A small reduction in the ultra-conservative factor of 10 allowed between assumed and expected count rate vs. flux relationships, renders the release negligible even for this case.

For the incredible case of criticality in the intermediate speed range, failure of the safety rods can be tolerated, but correct operation of the period protection circuits is essential if damaging energy releases are to be avoided.

The self limiting energy releases for several reactor systems fuelled with ^{235}U were calculated for the case of the maximum credible reactivity additions (step and ramp) coupled with the failure of all protective devices. The studies described below show that the maximum energy release is at least an order of magnitude lower than that chosen for cell design, namely 130 MJ. The fraction released as kinetic energy is more than two orders of magnitude lower again.

Transients Terminated by Reactor Inherent Shutdown Mechanisms

In fast reactor systems the components of the overall power reactivity feedback coefficients and rates of energy release are such that rather generalised analyses (e.g. Bethe-Tait method) usually suffice to give reasonable estimates of total energy releases in self-terminating reactivity excrusion situations.

For near thermal and thermal systems, however, the situation is less simple. The slower rates of energy release lead to complex heat transfer effects depending on precise fuel and core geometry, closeness of component contacts, etc. These effects in turn influence the overall feedback coefficient of reactivity, which is in any case often very small as a result of opposing contributions from fuel expansion and Doppler components.

TABLE 2.4

CALCULATED ENERGY RELEASES FOR TRANSIENTS TERMINATED BY REACTOR PROTECTION SYSTEM

Pu systems, $\beta = 2 \times 10^{-3}$.
Upper rows are with safety rod worth -0.01 k/k.
Lower rows are for table stop and reverse only.

H (cal cm^{-3}) for metallic fuels:

	U	Pu
Melting	840	562
Vaporisation	10500	7872

Ramp Rate	0.0625 \$ s^{-1}		0.125 \$ s^{-1}		0.25 \$ s^{-1}		1.0 \$ s^{-1}
	low level DT 5 s	ϕ_{max}	low level DT 5 s	ϕ_{max}	low level DT 5 s	ϕ_{max}	low level DT 5 s
10^{-3}	2×10^{-2}	0.1	1×10^{-2}	9×10^{-2}	5×10^{-3}	6×10^{-2}	1×10^{-3}
	2×10^{-2}	0.1	1×10^{-2}	0.1	5×10^{-3}	7×10^{-2}	1×10^{-3}
10^{-4}	8×10^{-3}	9×10^{-2}	4×10^{-3}	7×10^{-2}	2×10^{-3}	7×10^{-2}	1×10^{-3}
	8×10^{-3}	0.1	4×10^{-3}	7×10^{-2}	2×10^{-3}	8×10^{-3}	1×10^{-3}
10^{-5}	9×10^{-4}	4×10^{-3}	4×10^{-4}	2×10^{-3}	2×10^{-4}	4×10^{-3}	6×10^{-5}
	9×10^{-4}	4×10^{-3}	4×10^{-4}	2×10^{-3}	2×10^{-4}	5×10^{-3}	6×10^{-5}
10^{-6}	3×10^{-4}	2×10^{-3}	2×10^{-4}	1×10^{-3}	8×10^{-5}	3×10^{-2}	3×10^{-5}
	3×10^{-4}	2×10^{-3}	2×10^{-4}	2×10^{-3}	9×10^{-5}	0.1	5×10^{-5}
10^{-7}	3×10^{-4}	2×10^{-3}	2×10^{-4}	1×10^{-3}	9×10^{-5}	3.4	4×10^{-5}
	3×10^{-4}	2×10^{-3}	2×10^{-4}	2×10^{-3}	9×10^{-5}	✱	6×10^{-5}
10^{-8}	1×10^{-3}	4×10^{-3}	6×10^{-4}	2×10^{-3}	3×10^{-4}	3×10^{-3}	7×10^{-5}
	1×10^{-3}	4×10^{-3}	6×10^{-4}	2×10^{-3}	3×10^{-4}	5×10^{-3}	7×10^{-5}

✱Fuel melts approximately 290 ms, and vapourises approximately 300 ms after trip. Energy release reduces to 0.3 cal cm^{-3} for 50% increase in initial count rate.

TABLE 2.5

COMPONENT SPECIFICATION FOR $^{235}U/C$ REACTOR ASSEMBLIES

	Moderator	Fuel
Material	Graphite blocks	Metal Fuel strips 94% U5
Length (mm)	400,800	400
Width (mm)	100	50.8
Height (mm)	100, 50	0.076
Weight (kg)	12.8	0.029
Density ($t\ m^{-3}$)	1.6	18.5
Melting point (K)	3500	1133
Boiling point (K)	4200	3900
Coefficient of linear expansion (K^{-1})	8×10^{-6}	16×10^{-6}
Specific heat ($kJ\ kg^{-1}\ K^{-1}$)	0.25	0.163
Thermal conductivity ($kJ\ m^{-1}\ s^{-1}\ K^{-1}$)	5	30
Latent heat of fission ($kJ\ kg^{-1}$)	-	65.3
Latent heat of vaporisation ($kJ\ kg^{-1}$)	-	1630
Special features	Recess in top surface of block extending over its full length for fuel insertion 56 x 1.85 mm	Coated with PTFE of thickness 0.02

TABLE 2.6

PARAMETERS FOR THERMAL AND EPITHERMAL

^{235}U/C REACTOR CORE ASSEMBLIES

Volume ratio graphite/fuel	1000:1	2000:1	11250:1
Critical radius (cm)	46.0	52.0	96.5
Critical mass (kg)	5.1	7.1	7.9
Prompt neutron lifetime (sec)	3.1×10^{-4}	5.1×10^{-4}	1.9×10^{-3}
Doppler coefficient $\Delta k/k$ per ^{o}C	-1.6×10^{-6}	-7.1×10^{-7}	-10^{-7}
Thermal expansion coefficient $\Delta k/k$ per ^{o}C	1.1×10^{-6}	-6.4×10^{-7}	-1.0×10^{-5}
Thermal shift $\Delta k/k$ per ^{o}C	-8.5×10^{-5}	-1.5×10^{-4}	-1.5×10^{-4}

TABLE 2.7

CALCULATED QUANTITIES OF INTEREST FOR REACTOR TRANSIENTS

TERMINATED BY DISASSEMBLY

Volume Ratios graphite ^{235}U	1000:1	2000:1	11250:1
Inverse period (s^{-1})	42.2	25.3	6.85
Disassembly coefficient $\Delta k/k\ m^{-1}\ s^{-1}$	0.46	0.23	0.03
Total fission energy (MJ)	7.4	5.4	8.5
Energy before boiling of fuel begins (%)	60	59	58
Max. KE % of total energy	0.30	0.24	0.11
Amount of fuel vaporised (%)	16	17	15
Duration of transient after boiling point (ms)	22	33	85
Max. pressure (atmos)	14.5	7.0	2.0

Since near thermal and thermal assemblies of ^{235}U and graphite ($\sim 1000 \leq V_M/V_F \leq \sim 10^4$) are likely to be studied experimentally on the Critical Facility, it was considered necessary to analyse the self-terminating properties of such systems under reactivity transient conditions. Details of the components to be used in the assemblies are given in Table 2.5 and the results of calculations to give the coefficients of the inherent reactivity feedback mechanism components are given in Table 2.6 for a representative range of V_M/V_F values.

To study the energy release in transients in such systems, a model was developed and coded to solve the coupled thermodynamics-hydrodynamics neutron kinetics equations, yielding temperatures, pressures, quantity of fuel vaporised, total and kinetic energy releases as a function of time following a step insertion of reactivity from the delayed critical condition. Because of the uncertainties in reactivity feedback coefficients and heat transfer mechanisms referred to above, it was conservatively assumed that core disassembly was the only available shutdown mechanism. Furthermore, various models were assumed for the rate of heat transfer from fuel to other core components, including the limiting case of zero heat loss, which is closely applicable in rapid transients or where poor thermal contact exists between fuel and other core components.

A one dimensional, one energy group model was adopted for core neutronics and it was assumed that disassembly occurred by vertical motion of the components resulting from vapour pressure in the fuel slots. The latter is a reasonable assumption since the cross sectional area of the slots is very small compared with their length. Fission heat generation continues until the excess reactivity is reduced to zero and the transient terminates by either

(a) reduction in core density due to vapour pressure induced relative movement of components, or

(b) the gaps between components have increased sufficiently to allow significant fuel vapour to escape from the core.

Assuming zero heat transfer from the fuel, pressure generated by fuel vaporisation is the only mechanism for core movement. For this case, the energy balance equations become:

$$Q = NmL_m + \frac{1}{2} Mr^2 + Mg(r - r_o)$$

where

Q = fission heat input,

N = number of channels involved,

m = mass of vapour formed/channel,

L_m = latent heat of vaporisation of fuel,

M = mass of core + reflector moved vertically, and

r = height of fuel slot (initially r_o)

Assuming that the vaporised metal behaves as a perfect gas and incorporating the total resulting force in an equation for vertical movement of the core, then

$$Q = \frac{GL_m}{RAT_b} M(\ddot{r} + g)\ r + \frac{1}{2} M\dot{r}^2 + Mg(r - r_o)$$

where G = molar weight of ^{235}U

R = gas constant per mole

ΔT_b = boiling temperature -20^oC

The fission energy is given by

$$Q = \alpha S_f \Delta T_b V_f \int_0^t \exp(\alpha t' - \mu \int r dt') dt'$$

and α = reciprocal reactor period

μ = disassembly reactor feedback coefficient

S_f = specific heat of fuel

V_f = volume of metal fuel involved.

Combination of the equations above results in a fourth order differential equation which is numerically solved by the computer program.

If sharing of fission energy with graphite and air is allowed, the transient must be followed from room temperature because air pressure may now cause sufficient core movement to terminate the transient before any boiling of fuel occurs. The heat balance equation at temperature T is

$$Q = m_f S_f (T-T_o) + Am_a C_v (T-T_o) + BMS_g (T-T_o) + \frac{1}{2} M\dot{r}^2 + Mg(r-r_o)$$

where

m_f = mass of fuel

T_o = room temperature

A = fraction of heat absorbed by air

B = fraction of heat absorbed by graphite

m_a = mass of air

C_v = specific heat of air at constant volume

S_g = specific heat of graphite

Solutions were obtained using the computer program for a range of fractional heat losses to the air and graphite.

The studies were based on a \$3 reactivity addition at delayed critical and showed that when sharing of fission heat is permitted, the partial pressure of the heated air in the channels causes core disassembly either before fuel boiling occurs at all or with less vaporisation of fuel than in the zero-sharing case. Alternatively, heat-sharing with the graphite can terminate the transient without core disassembly via the thermal neutron spectrum shift, which requires graphite temperature rises of only 100 to 200°C.

The most severe excursions, therefore, are those in which all the heat is retained in the fuel plates. For this model, the results are given in Table 2.4 and show that for the range of cores considered, the maximum energy release is less than one tenth of the Critical Facility cell design release of 130 MJ; that the maximum fraction of the total energy release which appears as kinetic energy is only 0.3 per cent; and that the fraction of the core fuel inventory vaporised is always less than 0.2 per cent. The adequacy of the cell design criteria and conservatism of the cell design brief accident are therefore conclusively demonstrated even with complete failure of all protective devices in these reactor assemblies.

2.3.2 Critical Facility Operations (D. B. McCulloch)

Operation of the split table machine since March 1973 has led to a very favourable impression of the reliability and accuracy of the machine and its ancillaries. Particularly noteworthy are the accuracy and reproducibility of critical settings and the lack of spurious trips from the nucleonic safety channels.

Some of the problems which have occurred are:

(a) Difficulty with some rod drive assemblies failing to latch and failure of rod position control microswitches.

(b) Failure of the table buffer to drop as a consequence of the distortion of the buffer arrester plate.

(c) Failure of MO3 to drive the tables to the closed position due to dirty contacts and pole pieces of a motor control relay.

Modifications performed to improve the safety or efficiency of operation include:

(a) Console indication of the operation of the three FCTM microswitches defining the 1500 mm table position. This is a 2/3 system such that failure of two microswitches could lead to the tables not separating under a scram order. The modification enables the performance of the microswitches to be continuously monitored from the control console.

(b) After failure of the table buffer to drop, a microswitch was installed so that buffer action could be monitored from the control console.

(c) Automatic neutron source retraction under scram conditions was disabled since this presented a circular problem inasmuch as driving the neutron sources into the core can cause a 5 s doubling time trip which causes the sources to drive back into their shield flasks. Because of the risk that personnel might forget that the sources were in the core while working on an assembly, in-cell indication of source position has also been provided.

(d) The rod selection logic was altered to permit selection as safety or control rods prior to rod latching. This avoids reselection of all rod functions prior to each startup.

(e) The output of the four logarithmic amplifiers of the safety channels is now displayed at the control console, thus allowing approach to trip settings to be monitored during operation.

(f) A push-button switch has been interposed in the rod H electromagnet power supply to enable this rod to be individually 'scrammed' for experimental purposes. Similar modifications will be made to all rod electromagnet supplies when convenient.

A versatile computer-based fuel accounting system for the facility has been developed and is operational as the IBM 360/50 code 'COOK 53'. It will enable full data for any individual item of fuel to be available in the form of card or printed output, together with its location in store or core. Check total data by isotope, batch and location are also available for the complete fuel inventory.

2.3.3 Experiments (J. Connolly, J. Harries)

A mockup of the MOATA reactor was constructed and first taken to critical on March 20, 1973. This assembly was intended to provide experience with the operation of the split table machine and to allow measurements relating to the neutron kinetics of MOATA to be made.

The Mockup I core was a reasonably faithful replica of MOATA, the major differences between the two reactors being the type of U5/Al fuel plate, the use of polythene as moderator and the arrangement of the control and safety rods.

To investigate coupling effects between the two slab cores, two further assemblies, Mockup II and II have been built, with core slab spacings of 600 mm and 800 mm. The Mockup I spacing was 450 mm.

The critical mass of the assembly was found to be 2.85 kg U5, in good agreement with the 2.95 kg predicted by a 2-dimensional POW calculation.

The measured worth of the safety rods was found to be in good agreement with that based on a measured rod worth in MOATA weighted by a POW flux-adjoint flux correction factor to allow for the difference in rod position in the two reactors.

The value of the prompt neutron decay constant, α, measured in this assembly (see below) was only about half the value measured in MOATA. Detailed measurements of thermal flux distributions in Mockup I were therefore made to investigate the discrepancy. It was found that the vertical buckling component in a Mockup I fuel slab was 12.9×10^{-4} cm^{-2} as apposed to the MOATA value of 18.4×10^{-4} cm^{-2} and that the vertical buckling component in the central graphite was 6.3×10^{-4} cm^{-2}. The original POW calculations had assumed a single value of 18.4×10^{-4} cm^{-2} for the vertical buckling component over the whole reactor. Insertion of the measured buckling values into the POW model gave an α value in agreement with that measured, but at the cost of underestimating the critical mass by some 500 g U5. The earlier

agreement between calculated and observed critical mass noted earlier thus appears to be fortuitous.

A 3-dimensional calculation performed by Theoretical Physics Section indicates that the successful application of the buckling approximation to a 2-dimensional representation of such a reactor as Mockup I will require that space and energy dependent bucklings be used if both α and critical mass are to be correctly computed.

Measurement of the flux distribution in the horizontal direction through the centre of the fuel slab and into the coupling region of Mockup I again revealed a large difference with a similar distribution measured in MOATA and with that predicted by the original POW calculation. Use of a different cell representation, with a discrete region of polythene between fuel and graphite and the use of measured graphite and fuel axial bucklings, improved the calculated flux distribution, but the physical reason for the apparent large difference from MOATA has not yet been ascertained. These flux distributions are shown in Figure 2.6.

Measurements of Prompt Neutron Decay Constant on Mockups I and II

Three methods have been employed to obtain the value of α, the ratio of the effective delayed neutron fraction to the prompt neutron generation time.

(a) The correlation method. The correlation between the fluctuations in the count rates from two neutron detectors is analysed. Data are recorded on magnetic tape and analysed on the Hewlett-Packard correlator of the Noise Analysis Laboratory, Engineering Research Division. The value of α is obtained by least squares fitting of an exponential function to either the cross or autocorrelogram. Corrections are necessary for reactor subcriticality and neutron detector saturation is checked by performing two runs at different power levels. Preliminary results are:

Reactor	α
MOATA	44.4 ± 0.3
Mockup I	25.3 ± 0.4
Mockup II	25.3 ± 0.3

Since β_{eff} is very close to β, α is primarily a measurement of the neutron lifetime. The difference between the values of α for MOATA and Mockup I must therefore be interpreted as showing that the neutron lifetimes in Mockup I is much longer than in MOATA. Possible reasons for this are being investigated.

(b) The variance-to-mean method. The second moment of repeated neutron counts recorded for a given time interval by a high efficiency detector is measured. Counts have been accumulated in multiscaler mode both on a pulse height analyser and a PDP-7 computer. The variance of the number of counts for different accumulation times has been compared with the theoretical realtionship. Preliminary results yield values of α in agreement with those from the correlation experiment, (a).

(c) Interval distribution method. An attempt was made to obtain a value of α by measuring the distribution of the intervals between counts recorded by a high efficiency detector. The low value of α in Mockup I and the source neutron contribution resulting from neutrons leaking from the shielded source flasks, combined to prevent an accurate value of α being obtained by this technique.

The chain reaction in a reactor such as Mockup I is often described in terms of two subcritical slabs with neutron interchange between them, making the system as a whole, critical. In this description the value of the exchanged neutrons is expressed in terms of a 'coupling reactivity'. The cross correlation between two detectors, one in each core slab, can provide data on the coupling processes between the slabs. The coupling between two almost critical cores causes the cross-correlogram to show a negative exponential component at small time lags superimposed on the main prompt neutron exponential distribution. As the coupling becomes weaker, the turn-over at small time lags increases and the effects of the time delays experienced by neutrons in travelling from one slab to the other become important.

A series of cross correlograms has been measured for different detector locations in Mockup I. (The high detection efficiency required for the correlation experiment precluded locating detectors within the core slabs.) These various locations will allow the neutron wave effects from core to detector to be separated from the core coupling phenomena.

A preliminary value for the coupling reactivity for Mockup I is 0.042

which is greater than the coupling reactivity for MOATA. This indicated stronger coupling is supported by the different flux distributions observed in the central graphite region for two reactors.

Different flux levels in each slab can be produced by making the individual reactivity of each slab unequal. As the coupling becomes weaker, this flux tilting becomes more pronounced and in the limit of complete decoupling, the flux levels in the two slabs can be varied independently since each slab is then itself critical.

Flux tilting was produced in Mockup I by scramming a single rod adjacent to one slab. By recording the time behaviour of the flux in each slab before and after the rod scram, it is possible to deduce the reactivity coupling between the slabs. Measurement of the static flux tilt introduced by an asymmetric control rod arrangement has also been used to determine the reactivity coupling.

Measurement of Central Cell Temperature and Void Coefficients of Reactivity

During preparation of a revised MOATA Safety Document, large differences were observed between measured and calculated void and temperature coefficients. Since the magnitude and sign of these coefficients determines the course of a power excursion, it was considered important to discover the basis of the observed discrepancy between measurement and calculation.

A central region of one core slab of Mockup I was so constructed that thin strips of polythene could be withdrawn from the region between a fuel plate and the polythene block containing the fuel plate, thus simulating cell voiding. The volume left was then flooded with water to determine the moderator equivalence of polythene and water. Finally, small nichrome heaters were used to measure reactivity effects following temperature changes, extensive temperature scanning with thermocouples being used to determine region averaged temperatures. Reactivity effects were determined both by change in critical rod settings and change in reactor period.

These measurements supported the calculated values of reactivity changes and indicated the importance of a physically realistic cell model. The underlying reason for the discrepancies between calculation and measurement for MOATA are as follows.

(i) In determining void coefficients, complete voiding of the coolant channel was employed. The effect of neutron streaming in the channel then dominates the reactivity effect and masks the fact that the void coefficient in the absence of complete streaming paths becomes positive in the outer regions of the core slab.

(ii) In measuring the temperature coefficient the reactor coolant was slowly heated over several hours, resulting in both water and graphite reflectors tending to be in temperature equilibrium with the core. Since both these regions have positive temperature coefficients, these experiments led to a much smaller net negative temperature coefficient being determined and incorrectly assigned to the core.

2.4 PULSED NEUTRON AND SPECTRA STUDIES (I. Ritchie)

Pulsed Integral Experiments in Thorium - Experiment (M. Rainbow)

The Elevated Facility (ELF), which allows the thorium assembly to be mounted approximately 5 m above the concrete floor and approximately 3 m from the nearest massive concrete shielding, was commissioned in January 1973. This device provides a greatly reduced probability of backscatter of neutrons into the assembly from the surroundings within the time interval of interest (~500 nsec after the start of the pulse) during pulsed experiments. It has been used for an extensive series of measurements of time and space dependent ^{239}Pu and ^{235}U reaction rates with the following source conditions:

(i) a thick lithium target using the Li(p,n) reaction at 2.3 MeV with a pulse width of ~10 ns;

(ii) a thick lithium target using the Li(p,n) reaction at 2.8 MeV with a pulse width of ~10 ns;

(iii) a thick beryllium target using the Be(d,n) reaction at 2.8 MeV with a pulse width of ~200 ns.

In addition, a series of identical measurements has been performed with the thorium assembly on the ELF and at the old floor level position to assess the improvements afforded by the ELF.

The processing procedures used for the analysis of experimental data obtained from these experiments have been extensively updated and streamlined to facilitate better and more efficient use of the IBM 360 system. This is essentially complete and analysis of the experimental data is proceeding.

Further improvements have been made to the timing resolution with which events in fission detectors can be measured. The most recent results (Figure 2.7(b) and (c) indicate that the detector timing uncertainty distribution has a standard deviation of ~1 ns. These are compared with an earlier result (Figure 2.7(a)) which was obtained with a different electronic configuration. Figure 2.7(b), which presents the result obtained with the basic detector timing system (see inset of Figure 2.7(b)) exhibits a secondary hump which is caused by pulses with long rise times. This hump can be removed by the addition of a simple pulse shape discrimination arrangement to the basic detector timing system (see Figure 2.7(c) and inset).

Pulsed Integral Experiments in Thorium - Theory (S. Moo, I. Ritchie)

Time dependent reaction rates in a pulsed thorium assembly have been

calculated by a one mode, asymptotic diffusion theory code (TENDS). The calculations took into account the experimental pulse shape (~10 ns pulse from a Be(d,n) source), the timing resolution of the detectors and the input neutron spectrom used in the measurements. The code employed a time-dependent, group-independent buckling to validate a direct comparison of the one mode calculation with the lowest Fourier component derived from the experimental time-space distributions. The time dependent reaction rates from the calculations were processed in exactly the same way as the experimental results to provide the 'instantaneous decay constant' of the fundamental mode time distribution.

Figures 2.8(a), (b), (c) show comparisons for the ^{237}Np, ^{235}U and ^{239}Pu reaction rates between the experimental results and theoretical results using 50 group data sets derived from the ENDF/B III and the Winfrith files and also the ABBN 26 group data set. Conclusions to date are as follows:

(i) Discrepancies exist for the ^{237}Np detector data between the ENDF/B II and Winfrith files, but detector data for ^{239}Pu and ^{235}U are in good agreement.

(ii) There is poor agreement between theor and experiment throughout the entire time range of the ^{237}Np reaction rate measurements.

(iii) There is poor agreement at early times (energies $\geq$ 1 MeV for the ^{235}U and ^{239}Pu measurements, but much better agreement at later times (energies $\leq$ 200 keV).

The sensitivity of the experimental parameters $\lambda_{111}(t)$ to changes in the nuclear data for ^{232}Th has been investigated. The results for ^{237}Np and ^{235}U reaction rates using the experimental configuration presently under investigation, are shown in Figure 2.9. The changes to the nuclear data were based on the premise that the absorption, fission, (n,2n), elastic and total cross sections can be measured independently, whereas the inelastic cross section is derived from these independent measurements. It was also assumed that the total cross section is known with high precision so that any change in the partial cross sections must be accompanied by a change in σ_{inel} such that σ_{total} remains constant.

The transport code TDA and the Monte Carlo code MORSE have been applied to the pulsed thorium block problem. The present investigation has been limited to problems of the optimum time step and mesh size to use. The

indications are that the time range used in the experiments can be covered using a reasonable amount of computer time and an adequate number of energy groups and spatial mesh points. These codes will allow an assessment to be made of the adequacy of the TENDS calculations and the importance of thorium assembly geometry, presence of probe holes and the source anisotropy, etc.

Surprisingly little information exists in the literature on the angle-dependent neutron energy spectrum to be expected from the $Li(p,n)^4Be$ reaction using a thick target. As this is one of the neutron sources used in the experiments, an attempt has been made to calculate the spectrum using both published angular distribution measurements and theoretical models for the $Li(p,n)^7Be$ and $Li(p,n)^7Be$ reactions.

Spectrum Measurements by Proton Recoil Proportional Counter (A. Rose)

The energy and angular distribution of neutrons from the (d,n) reaction in beryllium metal have been measured for deuterons with 2.0, 2.4 and 2.8 MeV energies. Problems with the detector gas filling system resulted in rather poor detector resolution (~12 per cent). Nevertheless, neutron energies in the range 50 to 3 MeV were measurable using a combination of gas filling. The analysis program requires details of the neutron energy spectrum above 3 MeV, for which little published data are presently available. Some measurements have been reported by a Japanese group, but there is some doubt as to the effect of target water cooling on their results. Recent time of flight measurements made by Physics Division are still being analysed, and analysis of the Be(d,n) proton recoil data will therefore be deferred until these high energy data become available.

Measurements to determine the energy and angular distribution of neutrons from the (p,n) reaction in thick lithium metal have also been completed for proton energies of 2.4 and 2.8 MeV. As the maximum neutron energy associated with these proton energies is 1.2 MeV, the analysis of the raw proton recoil data is simplified and is well advanced. The problems associated with the gas filling rig were solved prior to these lithium measurements, resulting typically in 7 per cent resolution for the detector system. A comparison of measured spectra and calculated spectra at 0° and 90° is shown in Figure 2.10.

Some further attempts have been made to measure the detector response functions and compare these with the response functions in the SPEC IV code. The major problem in this type of measurement is to obtain a truly mono-energetic source of neutrons. The 3 MeV Van de Graaff accelerator and the

Li(p,n) reaction using a thin target have been used as a primary source of monoenergetic neutrons, and various types of collimators have been used to remove the floor and wall scattered neutrons. The measurements to date show a reasonable agreement with SPEC IV except at the lower end of the pulse height distribution. This could be ascribed either to inadequacies of the theoretical response function, or to a small number of scattered, and hence low energy, neutrons. Measurements on the ELF indicate that in a d.c. mode of operation there is a significant proportion of scattered neutrons. Attempts to discriminate against these scattered neutrons on the ELF by operating in a pulsed mode have been frustrated by the long time scale (~4 to 7 μs) associated with pulse formation in the proportional detectors. A further complication is the correlation between the pulse height and the variation in the time at which the pulse appears (see Figure 2.11). This makes any time discrimination at less than the maximum time variation an effective pulse height discrimination.

Spectrum Measurements by Time of Flight (S. Whittlestone)

Measurements have been completed of the angular distribution of the neutron time of flight spectrum from the $^{9}Be(d,n)^{10}B$ reaction using a thick target at deuteron bombarding energies of 2.0, 2.4 and 2.8 MeV, and the counted down klystrom bunched mode of pulsing on the 3 MeV Van de Graaff. An NE102 scintillator was used as the neutron detector and the system was operated at a sufficiently low discriminator bias to allow detection of neutrons down to 30 keV.

A program has been developed to handle time of flight spectrum analysis. Raw data are read from magnetic tape, corrected for background and the time spectrum unfolded with respect to the 'gamma flash' profile. The resulting neutron time of flight spectrum is stored on disk and can then be used, together with detector efficiency data, to produce energy spectra. Various forms of output (graphs, print, magnetic tape) are available from the second stage of analysis.

As is common elsewhere, a combination of experiment and theory is being used to determine the detector efficiency. Estimates of the efficiency for neutron energies greater than 1 MeV have been made using a Monte Carlo program and the efficiency up to 1 MeV has been measured using neutrons from the Li(p,n) reaction.

A detector system using either of the scintillators NE213 or NE218 has

been built up. A filling system has been set up which allows filling of the detector chambers while preventing contamination of the scintillator with oxygen. To date, problems have been experienced with swelling and peeling of the special liquid scintillator paint used to improve reflection within the chamber.

2.5 SAFETY STUDIES

Over the past three years a considerable effort has been devoted to the improvement of methods for transient two-phase compressible flow calculations, including blowdown calculations. These studies have been continued and their scope extended. The methods developed have potential in application to assessment of power reactor safety under various classes of cooling failure conditions.

Improved methods of transient two-phase compressible flow calculation are incorporated in the code OWEN which treats a single flow path. Brief descriptions of this code and of comparisons with experiments have appeard in earlier progress reports. The transients which can be treated by this code are limited to those in which the flow at the inlet remains inwards. This is because the inlet enthalpy is one of the boundary conditions and this boundary condition only has physical meaning when the flow is inwards. If, for example, rapid heating began within a channel, the resulting expansion could cause fluid to flow out from both ends of the channel; thus the number of boundary conditions can change during the transient. This difficulty also prevents application of the method to multi-flow path problems. A modified finite difference scheme has been developed which removes this restriction.

Because OWEN is in British units it was decided to write a completely new code in SI units incorporating the modified difference scheme. This code NAIAD has been used to repeat the analysis of the CISE inlet blockage experiments. Good agreement with the earlier analysis using OWEN is found.

In loss of coolant calculations, estimation of the coolant flow out of the break is very important. There are two parts to this problem; the first is to calculate the coolant conditions at the break and the second is given these conditions, what is the discharge rate? A number of correlations have been developed for the latter problem; no method is available for the former.

Fauske (1962)[*] carried out experiments in which two-phase water was discharged through a long uniform pipe. He obtained a correlation which gave the critical discharge rate as a function of pressure and quality at the exit. However, he did not find any general method of calculating the conditions at the exit from those at the inlet. This has been attempted here.

---

[*] Fauske, H. K. (1962) - Contribution to the theory of two-phase, one-component critical flow. ANL6633.

Fauske also measured the pressure at 6 points upstream of the break. For each Fauske experiment, the lengths required to produce these five measured pressure drops were calculated. The ratio of these calculated lengths to the actual length in the experiment was plotted. Many different slip and friction models were tested. Considering the scatter of the data, the following model gave reasonable agreement.

(i) Thermodynamic equilibrium.

(ii) Jones slip model.

(iii) Mean square speed of each phase equal to the mean speed squared of that phase.

(iv) Kinetic energy of motion perpendicular to the channel axis negligible.

(v) Annular friction (Beattie 1972)* with zero pipe roughness.

The comparison of the above with Fauske's experiments is shown in Figures 2.12(a) and (b).

The program ASTEM4A for calculation of properties of water has been obtained from the Argonne Code Center and is now operational.

---

*Beattie, D. R. H. (1973) - A note on the calculation of two-phase pressure losses. Nucl. Eng. and Design.

2.6 OTHER TOPICS

SPERT Transient Calculations (J. Connolly)

Reactor physics data for three SPERT cores, B24/32, B16/40 and B12/64, have been calculated with the AUS code. Temperature and void coefficients were calculated with the perturbation theory sub-routine of POW. This work indicates a much larger negative temperature coefficient for the core itself than reported in the literature, due to the larger positive contribution of the water reflector in these cores to the temperature coefficient as usually determined. Use of calculated temperature coefficients for these cores in the reactor transient analysis code ZAP has given good agreement with the power burst observed in non-boiling transients during the SPERT program.

Neutron Streaming (D. J. Wilson, D. B. McCulloch)

Thermal neutron flux distribution measurements were completed in experimental assemblies of Al/water slab lattice arrays with the slabs both parallel and perpendicular to the source plane. Regular arrays with 0.635 cm water gaps between 0.635 cm, 1.27 cm, 2.54 cm and 5.7 cm thick aluminium slabs were studied, plus a further assembly with 1.27 cm water and 0.635 cm aluminium slabs.

Manganese foils were used as neutron detectors and were removed for scintillation counting of their induced activity following irradiation on one thermal column face of the MOATA reactor. Extreme precision of manufacture and assembly of the aluminium plates and attachment of the foils, minimised errors due to the severe fine structure flux gradients in these lattices.

Both 'extrapolated widths' and the 'exponential direction' foil activity distributions were each measured in several lines and planes in each assembly. These have been corrected and reduced to equivalent neutron flux level at each detector location.

Analysis of the distributions in terms of conventional 'cosine' and 'sinh' functions has proved very difficult owing to the pronounced fine structure effects and the small number of lattice cells in some assemblies. Further work is required to improve understanding of the data, but in qualitative terms, the anticipated departures from single exponential behaviour are expected from theory (Clancy et al.)[*] are clearly discernable.

---

[*] Clancy et al. (1968) - J. Nucl. Energy, 22, 445.

Neutron Source Project (G. Hogg, J. Tendys)

The dense plasma focus has been operated at a capacitor bank energy of 13 KJ with 50:50 deuterium-tritium gas fillings. An average neutron yield of 1.1×10^{11} neutrons per pulse was obtained, an increase of ~100 over that obtained with pure deuterium gas fillings. The pulse width was 80 ± 5 ns (FWHM) and the average neutron energy of the pulse, determined by neutron time of flight, was 15.1 MeV in the forward direction with a range 13.5 to 16 MeV. The average energy for D-D and D-T neutrons are respectively 0.4 and 1 MeV greater than those resolved from nuclear reaction data for an assumed ion temperature of ~1 keV. These energy shifts indicate that neutron production is associated with a particle acceleration mechanism rather than being altogether of thermonuclear origin. The closed cycle tritium system has been removed from the gun assembly and dismantled for decontamination.

The electron temperature of the plasma during the compression stages of the dense plasma focus, as a function of time, is being determined by the use of foil absorption techniques. If the electron temperature is assumed to be thermal, the measurement of the ratio of the X-ray transmission through two different absorber foils is sufficient to permit the calculation of the electron temperature. The result obtained from this relatively simple method was found to be too high to be consistent with the operation of the dense plasma focus, indicating that the electron distribution is non thermal. It is therefore necessary to measure the X-ray energy spectrum as a function of time for a single plasma discharge. This can be achieved by the use of band pass filters, whose response is defined by the transmission through thin K-edge filters and absorption in matched thicknesses of scintillator material. The electron temperature is then determined by comparing the measured signals with signal intensities computed for different electron temperatures.

A four channel devise using photomultipliers as signal detectors has been constructed and tested. This unit will cover the X-ray energy region of 1 to 10 keV. A four channel device using filters followed by surface barrier detectors has been constructed and this will permit measurements in the 50 to 200 keV energy range. However, the lack of recording equipment will not permit simultaneous usage of these two spectrometers.

Several modifications to the vacuum system, including a new stainless steel vacuum chamber, have been made to improve the repeatability of the focus. The new chamber can be maintained at a high state of cleanliness, thus reducing the contamination of the filling gas.

3.1 NEUTRON DATA MEASUREMENTS

Nubar Absolute for ^{252}Cf (J. W. Boldeman)

A number of additional sources of error in liquid scintillation $\bar{\nu}$ measurements have been investigated. These included:

(i) Representation of the fission neutron spectrum in a Watt form instead of a Maxwellian.

(ii) Variation in the scintillation detector efficiency for neutron capture gamma rays as a function of position within the scintillator including effects caused by the axial hole through the scintillator.

(iii) Possible dead time errors caused by the triple coincidence on the liquid scintillator photomultiplier lines.

None of the effects listed above had a significant influence on the absolute value of $\bar{\nu}_p$ for ^{252}Cf. However a number of slight corrections were found necessary. The experiment has now been completed and the final value is 3.738 ± 0.015.

Energy dependence of $\bar{\nu}$ for ^{235}U and ^{233}U (J. W. Boldeman, J. Caruana, R. L. Walsh)

Some measurements of the variation of $\bar{\nu}$ with neutron energy in the fission of ^{235}U have been repeated with improved accuracy to confirm earlier findings of no fine structure. Two measurements have been made at 375 ± 70 keV and 550 ± 70 keV. Both measurements confirm the previous data. In addition, some measurements are in progress to confirm a suspected minimum in the $\bar{\nu}_p(E_n)$ dependence for ^{233}U at 150 keV.

Neutron Capture Cross Sections (B. J. Allen, J. W. Boldeman, D. M. H. Chan, M. J. Kenny, A. R. Musgrove, Hla Pe)

Analysis has continued of the high resolution neutron capture cross section data measured previously at the Oak Ridge Electron Linear Accelerator by B. J. Allen (on attachment from AAEC) and R. L. Macklin (ORNL, research sponsored by the USAEC under contract with Union Carbide Corporation. A number of improvements have been implemented in the FORTRAN analysis library, particularly in the resonance parameter analysis program (RESPR2). Exchanges of analysis programs and results have continued during the year between ORNL and Lucas Heights. Work at Lucas Heights has involved contributions to the

following items.

Silicon: Cross section results for silicon have been published. An additional high bias measurement in natural silicon was made during the year at ORELA in an effort to investigate the reported asymmetry of the 760 keV resonance in the inverse photonuclear reaction $^{29}Si(\gamma,n)$. Adjacent narrow resonances were observed in the high bias data which leaves the (γ,n) result open to some doubt.

Calcium: The neutron capture cross section of ^{40}Ca, ^{42}Ca, ^{43}Ca and ^{44}Ca have been measured with separated isotopes at ORELA. Results were obtained from 2.5 keV up to 350 keV, with an energy resolution of 0.2 per cent. Total energy detectors were used to observe the capture yield and a thin ^{6}Li glass scintillator monitored the neutron beam. Resonance parameters, average cross sections and strength functions have been deduced. The radiative widths of the s-wave resonances are found to be four to seven times that for the $\ell > 0$ resonances for the even isotopes and a factor of two greater for ^{43}C. Capture yields (including background) are shown for $^{40,42,43,44}Ca$ in the neutron energy range 12 to 50 keV in Figure 3.1. These data extend from 2.5 to over 300 keV. Average resonance parameters for these iotopes are given in Table 3.1 and average capture cross sections are listed in Table 3.2.

Chromium: Data for a separated isotope sample of ^{52}Cr has been analysed for neutron energies between 5 and 210 keV. The capture cross section is dominated by two strong s-wave resonances at 50.3 and 97.2 keV. There are also a number of small p-wave resonances. Table 3.3 shows the preliminary resonance parameters with probable ℓ value assignments. Good agreement is obtained with previous RPI data for the two large s-wave resonances.

Barium: Analysis of the capture γ-ray yields in $^{134,135,136,137,138}Ba$ is well advanced and preliminary average resonance parameters for these isotopes are given in Table 3.4. High level densities limit the analysis of resolved resonances to energies below 10 to 15 keV, except for ^{138}Ba where resonances are well resolved to 80 keV.

TABLE 3.1

AVERAGE RESONANCE PARAMETERS IN CALCIUM ISOTOPES

Target isotope	E keV	N	N_0	D_0 keV	S_0 x 10^{-4}	S_1 x 10^{-4}	$\Gamma_\gamma(s)$ eV	$\Gamma_\gamma(p)$ eV
^{40}Ca	2.5-355	59	14	26 ± 6	2.0 ± 1.0	0.03 ± 0.02	2.4 ± 1.3	0.37 ± 0.27
^{42}Ca	1.5-364	92	22	17 ± 3	1.3 ± 0.7	0.1	1.5 ± 0.6	0.4 ± 0.3
^{43}Ca	2.5-101	135	44	2.3 ± 0.4	2.5 ± 0.7	0.46 ± 0.10	0.77 ± 0.31	0.4 ± 0.3
^{44}Ca	2.5-187	35	11	19 ± 5	3.0 ± 1.5	0.1	1.2 ± 0.7	0.2 ± 0.2

TABLE 3.2

AVERAGE CAPTURE CROSS SECTIONS (mb) IN CALCIUM ISOTOPES

Target isotope	σ_{MB}	RI	Neutron Energy (keV)										
	KT=30	E_n 2.5	10-20	20-30	30-40	40-50	50-60	60-70	70-80	80-90	90-100	100-200	200-300
^{40}Ca	6.1	220	11.3	11.6	3.0	9.7	3.4	1.0	0.0	4.6	0.0	3.3	5.0
SD	0.4	20	0.6	1.7	0.2	0.9	0.3	0.1		0.3		0.3	0.4
^{42}Ca	14.2	372	2.5	13.5	26.3	10.1	4.2	6.5	7.8	9.3	8.7	6.4	3.5
SD	0.7	70	0.1	1.2	2.0	0.6	0.4	0.5	0.5	0.6	0.5	0.5	0.4
^{43}Ca	46.5	3132	70.5	64.9	33.6	29.7	20.2	23.4	14.6	22.0	15.6		
SD	4.9	480	8.5	7.8	4.1	3.6	2.5	2.9	1.8	2.7	2.0		
^{44}Ca	7.3	339	13.4	11.8	0.0	6.8	10.8	1.2	4.4	4.4	0.0	4.6	
SD	0.9	44	2.4	1.8		1.1	3.4	0.3	0.7	0.7		0.8	

σ_{MB} is the Maxwellian averaged capture cross section at 30 keV

RI is the resonance integral above 2.5 keV

SD = standard deviation

TABLE 3.3

RESONANCE PARAMETERS IN $^{52}Cr(n,\gamma)$

Energy keV	$g\Gamma_\gamma\Gamma_n/\Gamma$ eV	Area beV	Error %	ℓ	Γ_n eV	$g\Gamma_\gamma$ MeV	Γ_n^o eV
5.272	0.000	0.4	74	1	0.000	(599)	
19.425	0.009	2.0	35	1	0.005	(599)	
23.001	0.241	44.5	7	1		241	
27.655	0.268	41.2	7	1		267	
31.711	0.118	15.8	12	1		118	
33.993	0.139	17.4	13	1		139	
34.388	0.093	11.5	17	1	0.062	(599)	
48.030	0.384	34.0	17	1		399	
48.359	0.280	24.6	15	1		287	
50.180	0.167	14.1	20	1		169	
50.261	1.128	95.3	8	0	1140.000	1128	5.085
57.809	0.432	31.8	16	0	179.269	433	0.746
68.300	0.056	3.5	42	1	0.036	(599)	
79.250	0.024	1.3	115	1	0.015	(599)	
95.157	0.466	20.8	25	0	359.600	466	1.166
97.211	6.633	289.8	5	0	6120.398	6640	19.630
106.660	0.810	32.3	20	0		881	
109.990	0.582	22.5	24	1		617	
111.929	0.813	30.8	19	0		812	
113.167	0.425	15.9	25	1		424	
115.256	0.160	5.9	49	1		160	
123.100	1.143	39.5	20	0		1142	
130.800	0.897	29.2	21	0		897	
139.650	0.949	28.9	24	0		949	
153.250	0.635	17.6	28	1		635	
165.098	0.745	19.2	32	1		744	
185.140	0.535	12.3	40	1		534	
190.389	1.303	29.1	24	0		1302	
198.684	0.609	13.0	42	1		609	
201.263	0.821	17.3	38	0		821	
204.847	0.391	8.1	56	1		391	
207.023	0.560	11.5	42	1		559	

TABLE 3.4

AVERAGE RESONANCE PARAMETERS IN BARIUM ISOTOPES

Target isotope	E keV	MB (30)	N_0	N_1	D eV	S_0 x 10^{-4}	S_1 x 10^{-4}	Υ eV
^{134}Ba	3-10.6		24	31	300	0.5	0.1	0.12
^{135}Ba	3-10.5		143	28	48	1.5	0.16	0.13
^{136}Ba	3-11	47	10	21	950	1.2	0.3	0.18
^{137}Ba	3-11		9	46	450	0.5	0.2	0.14
^{138}Ba	3-80	3	8	14	10000	0.5	0.01	0.19

$\sigma_{MB}(30)$ is the Maxwellian averaged capture cross section at 30 keV

Compilation of 30 keV Maxwellian Averaged Capture Cross Sections

(B. J. Allen)

A significant amount of new capture data has been published in recent years. With the increased astrophysical interest in neutron capture cross section data for the lighter nuclei, it is appropriate to compile a computer file of 30 keV average capture cross sections. When resolved resonance data are available, these are weighted by the Maxwellian thermal distribution for kT = 30 keV to obtain $\langle\sigma(kT)\rangle = \langle\sigma \cdot v\rangle / vT$.

The compilation will be updated periodically and will be available on request.

Neutron Strength Function Card Library (A. R. Musgrove)

A computer card library of neutron strength function data was earlier compiled and published as AAEC/E277. This has been now updated to January 1974 and is available on application.

Similar files of average radiative width information and evaluated average level spacing (see e.g. ^{135}Ba writeup) are in preparation.

3.2 NEUTRON REACTIONS

Neutron Emission from Individual Fission Fragments of ^{252}Cf

(R. L. Walsh)

The $\nu(Z)$ and $\nu(A)$ analyses are now complete and some of the main results are as follows.

The relative neutron emission $\nu(Z)$ is shown in Figure 3.2. The small variation of $\nu(Z)$ for the heavy fragment disagrees with earlier lower X-ray resolution data*. However, it results in a substantial slope for the $\nu_{total}(Z)$ curve (shown in Figure 3.2) which is in good agreement with recent data on total neutron emission**. The measured average excess of even-Z total neutron emission over odd-Z emission was 0.15 ± 0.25 neutrons.

The $\nu(A)$ data are shown in Figure 3.3(a) and are compared with the double-velocity data of Bowman et al.† and the double energy data of Signarbieux et al.†† in Figure 3.3(b). The present data have been corrected for neutron backscatter and detection geometry, but not for mass resolution. The present data agree with the high neutron emission near mass 120 reported by Bowman et al.† ν_L/ν_H was found to be 1.19. Figures 3.4(a) and 3.4(b) show the total neutron emission $\nu_T(A)$. The peaks at masses 90, 96 and 156 in the present $\nu(A)$ data and at masses 134, 140, 152, 156 and 162 in the $\nu_T(A)$ data correspond exactly to the locations of the peaks seen in the ^{252}Cf and ^{235}U mass yield curves†.

The $\nu_T(Z)$ data of Nifenecker et al.** definitively found no odd-even Z effect in the fragment neutron emission. Because of low count rates, the statistical accuracy of the present $\nu(Z)$ work is rather too poor to permit a conclusion one way or the other. However, the negative result found in ** is somewhat at variance with the observation of fine structure in the present $\nu_T(A)$ work.

---

*Nifenecker et al. (1969) - Nucl. Phys. A131, 261.

**Nifenecker et al. (1973) - LBL-1950.

†Bowman et al. (1963) - Phys. Rev. 129, 2133.

††Signarbieux et al. (1972) - Phys. Lett. 39B, 503

Neutron Capture Mechanisms (B. J. Allen, R. Barrett, K. Bray, L. C. Carlson, M. J. Kenny)

In an endeavour to obtain more information on the mass dependence of anomalous gamma ray spectra observed after neutron capture, measurements have been made with a NaI detector at neutron energies between 30 keV and 1 MeV. A survey of capture spectra has been made across the periodic table at a neutron energy of 460 keV. Background subtracted results at 460 keV are shown in Figure 3.5. It is seen that in some mass regions, e.g. A $\sim$ 50, the 'anomalous bump' is quite strong, while in other regions, e.g. A $\sim$ 90, there is virtually no bump. The neutron capture mechanisms responsible for the non-statistical behaviour are under investigation.

In the case of iron, high resolution measurements have been made using a Ge(Li) detector for neutron energies up to 460 keV. The results showed that the anomalous gamma ray strength, while having a stationary centroid as seen in the NaI data, is composed of increasing transition strengths to higher energy excited states as the neutron energy increases. Figure 3.6 shows the high energy portion of the spectra for neutron energies of 50, 150, 250 and 450 keV.

Interference Effects in ^{48}Ti and ^{58}Ni (J. B. Garg, B. J. Allen, M. J. Kenny)

Partial capture gamma ray yields in ^{48}Ti and ^{58}Ni in the 10 to 100 keV range were obtained with a Ge(Li) detector. The yields were normalised relative to the total capture yields.

The aim of the experiment was to observe interference between s-wave resonances and perhaps the non-resonant cross section in the partial capture channels. Monte Carlo calculations for ^{48}Ti, however, showed that multiple scattering would mask this effect, if present, and that thinner targets would be required.

p-wave Neutron Strength Functions (Hla Pe, B. J. Allen, M. J. Kenny, J. R. Bird)

An attempt has been made to measure directly the energy dependence of the p-wave capture cross section in the mass region of the p-wave maximum (A $\sim$ 100) by detecting specific gamma rays which are probable only after p-wave capture. A natural cadmium target was used and transitions to four low-lying positive-parity states in ^{112}Cd and ^{114}Cd have been studied. Such transitions are either weak or not observed in thermal capture and are presumed

to be E1 following p-wave capture. The intensities of these transitions as a function of neutron energy do not follow the calculated p-wave capture cross section and further measurements are being made to confirm this result.

3.3 FACILITIES AND TECHNIQUES

3 MeV Accelerator (H. Broe, A. Van Heugten, J.Copland, P. Lloyd, S. Kanard, M. J. Kenny)

The accelerator was used in experiments for 4840 hours distributed as shown in Table 3.5. Maintenance accounted for 1190 hours and involved routine service only.

Major technical developments during the year were improvements to the experimental areas with particular reference to the low scattering facility and the proton channelling rig. Beams of up to 15 μA of singly charged helium ions were run for periods of up to 15 hours without deterioration of the ion source.

The experimental area was increased in size by shifting the east wall by 3 m. The effectiveness of the wall was improved by using paraffin filled boxes 34 m high on top of the concrete. A central magnet selection system for quadrupoles, switch magnets and analyser magnets was installed. New monitoring systems were installed for target and aperture current measurements and slit controls. The load on the cell air conditioning was decreased by removing the motor generator sets to the plant room. The chiller in the accelerator cell was rewired and a new motor was installed.

A turbo pump was installed in the alcove to give improved vacuum to the long beam lines used for proton channelling and (p,γ) spectroscopy. The changeover to metric units involved conversion of approximately 40 vacuum gauges.

The 'count down' mode of beam pulsing has been improved to allow the usual 1 μs interval between the 'nanosecond' pulses to be increased by multiples of 1 μs.

(a) 'Nanosecond' system

This formerly operated with its own internal 1 MHz oscillator. 'Count down' requires that the pulsing be synchronous with an oscillator outside the tank. An existing system to provide the external 1 MHz involved a pulsed light source driving a photomultiplier. After considerable modification of the circuitry in 1972 this system has been made quite reliable, though it is still affected by the poor regulation of H.T. for the photomultiplier. This is essentially the same problem as that of the 'microsecond' mode, discussed later.

In the course of these developments a study was made of the long standing problem of the interaction between the two 1 MHz driver stages, one for each pair of deflection plates. On the bench the anode current in the main oscillator is 19 mA to produce 3.8 kV output. Both auxiliary and main amplifiers can be tuned without interaction. In the confined space of the top terminal, field lines are severely distorted so that the two amplifiers interact. If the main amplifier is tuned with the auxiliary off, the anode current ia approximately 25 mA. When the auxiliary is switched on the current in the main amplifier may exceed 40 mA. To bring this down to a reasonable value (approximately 35 mA) the auxiliary must be de-tuned. Simple shielding of the auxiliary had no effect, indicating that a major re-design is needed to eliminate the interaction.

(b) 'Microsecond' system

This unit provides a gating pulse to let through the desired 'nanosecond' pulse. The major difficulty with this system is in obtaining reliable operation of the 'on' and 'off' pulse systems, in which a light emitting diode at the tank base sends a signal up a light pipe to a photomultiplier. A thorough examination of this system has been made to improve its sensitivity and reliability. New higher output light emitting diodes have been purchased and attempts are being made to obtain more output from the pulsing system. It is hoped that it will be possible to reduce the duration of the light pulse and so reduce the rise time of the photomultiplier output. This would reduce timing jitter.

Data Acquisition Facilities (M. D. Scott, R. J. Cawley)

The PDP-15 has been connected to the site Dataway - a bus system allowing several small computers to communicate with each other and indirectly with the IBM 360 facility. The PDP-15 software has been rewritten around Dataway operations. Routine program loading is now done from the IBM 360 disk system and jobs can be submitted to the IBM 360 job stream from the PDP-15 console. Dumping data from the PDP-15 to IBM 360 is possible, but is a little cumbersome at present.

The IBM 360 analysis program PTANAL has been improved in performance and the plotting features made more flexible. New features include energy calibration, peak searching and identification, spectrum differentiation and energy conversion for time of flight spectra.

Two new programs have been written for the PDP-7. The two parameter data acquisition program AUTDIG provides automatic 'command string' execution on cue and program controlled target positioning. A slow multiscaling program KNOTTY uses one of the PDP-7's 5 MHz scalers, with program controlled channel stepping on receipt of external timing signals.

A 13 bit ADC (Canberra Industries 8060), purchased by AINSE, was provided with connectors for the existing ND2200 interfaces. Signal mismatches and a fault in the ADC, however, have delayed utilisation until 1974.

A Hewlett Packard 7004B XY plotter was interfaced to the PDP-15, but was found to suffer approximately 1 cm overshoot when drawing lines. An overshoot compensation circuit was developed, which successfully removed Y axis overshoot, but led to instability when applied to the X axis.

A large screen (Hewlett Packard 13004) display monitor was connected to the PDP-7, allowing its use with the existing light pen.

Interface modifications were carried out to allow the use of longer cables linking the PDP-7 to the PDP-15. Subsequently, the computers were repositioned in a new laboratory layout.

No mainframe faults occurred in the PDP-15, but the ADC interface gave intermittent trouble which was finally traced to dirty card contacts.

Approximately 15 man days were spent on PDP-7 maintenance, of which 5 were on mainframe faults, including dirty memory contacts and inhibit driver failures. Peripheral troubles accounted for 3 man days, with faults in the paper tape reader, interference from the BRPE paper tape punch and failures in the ND160 ADC. The remaining 6½ man days were devoted to interface faults, of which approximately half required design modifications.

An 8K PDP-11 was purchased for fission studies and interfaced by Instrumentation and Control Division to the existing data collection hardware. A program has been written to calculate mean and variance parameters for the frequency distribution of ν. An intermittently recurrent fault in the PDP-11 has severely disrupted development work and has not yet been identified.

Neutron Capture Analysis (J. R. Bird, L. H. Russell, I. F. Bubb)

An improved Ge(Li) detector shield has been constructed for use in analytical measurements employing prompt gamma rays from thermal neutron capture. A neutron beam from the MOATA reactor operated at 100 kW was used in determining the chlorine content of 20 g samples of wheat. Automatic

peak search and attributor routines have been used in studying the gamma ray spectra from various rock samples.

Prompt Nuclear Analysis (J. R. Bird, B. L. Campbell, P. B. Price)

The bibliography of papers on analysis by measurements of the prompt radiation from nuclear analysis has been updated to the middle of 1973.

Nuclear Reaction Analysis (J. R. Bird, L. H. Russell, G. E. Murch)

Scattering, channelling and reaction measurements have been applied in the analysis of the surface of various samples. On-line differentiation of thick target backscattering spectra produces peaks for each mass number present in the sample. These results are complemented by measurement of gamma ray and charged particle spectra to obtain concentrations and diffusion profiles for isotopes of C, N, O and F.

TABLE 3.5

ACCELERATOR TIME ALLOCATION 1973

Topic	Expt. No.	Title	Personnel	Origin	Running Time (hours)
Fission	11	$\bar{\nu}$ vs E_n	Boldeman, Walsh	Physics	34
	12	Nubar absolute	Boldeman	Physics	572
	13	Kinetic Energy Studies	Walsh	Physics	12
	15	Fragment Angular Distribution	Caruana	Wollongong	683
Capture Cross Sections	18	^{238}U Capture Cross Section	Kenny, Allen	Physics	46
Neutron Capture	21	Ge(Li) Capture Spectra	Kenny, Allen, Pe, Garg	Physics	496
	23	Capture Mechanisms	Allen, Kenny, Barrett, Bray, Carlson	Physics/Melb/ ANU	367
Neutron Transport	31	Pulsed Integral - Th	Rainbow	Physics	594
	32	Pulsed Spectra - Th	Whittlestone	Physics	71
	33	Spectra - fast assemblies	Rose	Physics	542
Nuclear Analysis	41	Oxygen Analysis	Russell, Murch	Physics/Flinders	102
	42	Applications	Bird, Russell	Physics	163
	43	Dosimetry	Cripps	Health Physics	261

TABLE 3.5 (cont'd)

Topic	Expt. No.	Title	Personnel	Origin	Running Time (hours)
Atomic Physics	51	Channelling	Kelly, Price	UNSW	76
Radiation Damage	55	Crystal Damage	Pollard, Anderson	UNSW	183
Analysis	57	Light Element Analysis	Atkinson	Melbourne	59
Charged Particle Reactions	59	(p,γ) Spectroscopy	Lasich	Queensland	63
	60	(p,γ) Spectroscopy	Boydell, Read, Solomon	Melbourne	392
	61	(d,nγ) Spectroscopy	McKenzie, Noonan	Melbourne	38
	62	(d,n) Reactions	McKenzie, Armitage	Melbourne	34

Tests: 56 hours

Total operating time : 4840 hours

Maintenance : 1190

4. THEORETICAL PHYSICS

4.1 AUS Modular Scheme (J. Pollard, G. Robinson, B. Clancy)

The AUS modular scheme consists of a suite of 'modules' (computer codes) communicating with each other via disk 'data pools' (cross section, geometry, flux libraries, etc.) and provides a general purpose neutronics calculational tool on the IBM 360. A design philosophy of the scheme has been to provide essential multiscope basic modules required as part of neutronic studies on various reactors. No effort has been directed to providing modules to study fine detail of particular reactors, but rather the scheme is written in a way which permits later addition of these modules as the need arises. Even so, the present suite of modules enables physics analysis to be undertaken on a wide range of possible reactor experiments, particularly those undertaken on site with the Critical Facility.

Because of the general purpose nature of AUS little or no provision exists for the introduction of correction ('fiddle') factors in either theory or data. Rather the principle adopted has been to develop modules that rely heavily on physics, mathematics and numerical analysis in-depth studies undertaken on site over the past decade. Essentially these studies have concentrated on understanding 'clean' reactor experiments. The cross section data is to be progressively updated from the ENDF/B file, although for many nuclides the present AEE Winfrith based data may suffice.

Both fast and thermal reactor studies have been undertaken with the scheme since the initial release some two years ago. The scheme is continually being developed and should serve as a valuable check on special purpose overseas programs used for specific reactor studies.

A schematic representation of AUS follows and recently available modules are discussed in an expanded presentation.

A SKETCH OF THE COUPLING OF SOME AUS MODULES AND DATA POOLS

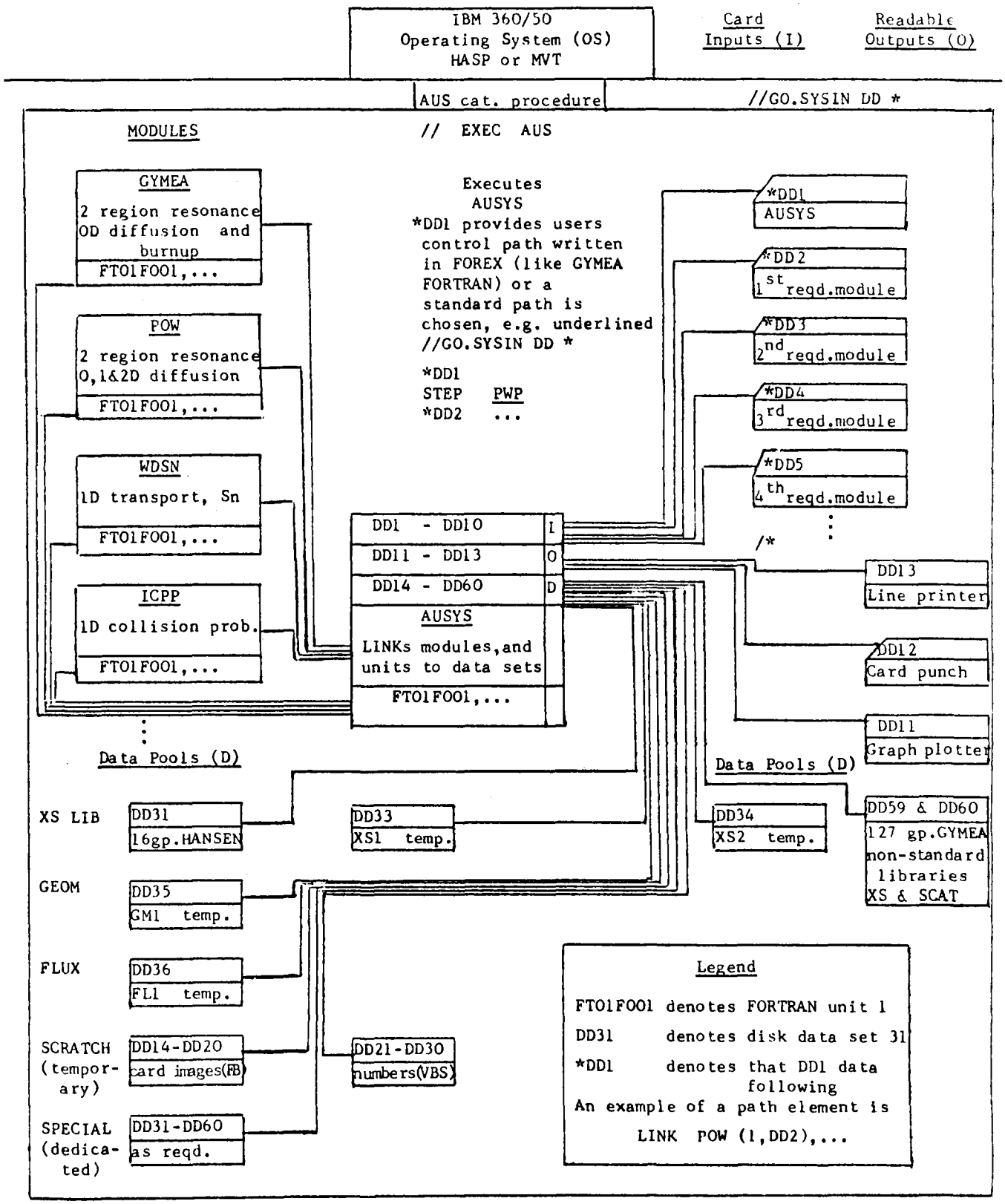

The modules and data pools are connected together at run time in a programmable fashion with usually simple FOREX (FORTRAN like) statements in an AUSYS control program which runs under the IBM 360 HASP/OS system. The inclusion of new modules and data pools is trivial - a highly desirable feature of a developing system.

Modules available are:

0D data preparation modules

MIRANDA — multiregion resonance theory, B_N
- usually used as the first step of a calculation and replaces

GYMEA — 2-region resonance theory, P_o.

1D transport theory modules

ICPP — collision probability theory, P_o (particularly for slabs)
- usually used as a second step for few regions and many groups.

ANAUSN — transport theory S_n, P_N (particularly for cylinders)
- flexible module with search and fixed source options.

WDSN — transport theory S_n, P_o
- used as an alternative to ANAUSN although largely replaced.

1D editing module

EDIT1D — general purpose editing
- used to collapse groups and smear materials from 1D calculations.

0, 1 and 2D diffusion theory module

POW — diffusion theory, P_o, steady state and kinetics
- flexible module with search options, etc., editing capabilities including perturbation theory (as well as 2 region resonance theory data preparation - largely replaced by MIRANDA).

0, 1 and 2D burnup module

CHAR — analytic solution of general chain burnup
- uses cross section anf flux data pools from earlier modules.

3D diffusion theory modules

ZHEX — diffusion theory, P_0, hexagonal cylinders.

DXYZ — diffusion theory, P_0, rectangular cylinders

- both the above are not highly integrated into the scheme as their usually long running nature (10 hours) discourages general use!

Special purpose modules

AUSED — cross section library maintenance module.

MERGEL — cross section library merge utility.

POW (KINDATA) — delayed neutron data preparation.

FIVE — flux spectra CALCOMP plotting

Data Pools

Library cross section data pools

GYMEA — 127 group data, resonance information in Russian subgroup form

- largely obtained from AEE Winfrith with some data from ENDF/B (and derived from the GYMEA libraries).

HANSEN — 16 group Hansen and Roach data, resonance tabulation (300K only).

ABBN — 26 group Russian data, resonance tabulation

Temporary cross section data pools

XS1 — temporary data pool which may be saved.

XS2 — as above.

Other data pools

Other data pools exist for geometry, flux, status (mixing rules, etc., for CHAR burnup) etc.

AUS Module MIRANDA (G. Robinson)

The MIRANDA module, which is currently under development, is a cross section data preparation code suitable for both fast and thermal reactor calculations. The present data library for the code is basically a reformatting of the 127 group GYMEA library to an AUS cross section library in which resonance information is given by the Russian subgroup method.

The MIRANDA resonance calculation involves a multi-region collision probability calculation for the subgroups with the source obtained from the Hill-Schaeffer $\wedge$ method. Corrections for non-isolated resonances, resonance overlap and group flux depression are included. Calculations for ^{238}U metal and oxide rods for a range of rod size, pitch and moderators, have given excellent agreement with the numerical slowing down solution of the PEARLS code (to within 1 per cent in resonance captures).

The resonance calculation is followed by a homogeneous B_n flux solution, group condensation and extensive output where required. The code is at present limited to cylindrical and slab lattices though the extension to more complex geometries is easy in principle. The various options have been thoroughly tested and the initial release of the code and 127 group library will be available shortly.

AUS Module CHAR (G. Robinson)

The CHAR module solves the isotope depletion equations for any number of spatial divisions of a system with any number of isotopes represented. Input from the various AUS data pools enables reaction rates to be calculated in each discrete material which is to be burned up. The module can be used in conjunction with any code which solves the neutron transport equation to undertake either lattice or whole reactor burnup. The specification of isotopic compositions and spatial smearing rules in the STATUS data pool is the basis of this approach to burnup calculations. Besides being essential for burnup, the incorporation of the STATUS data pool in the AUS system has improved the integration of the modules of the system. All editing facilities can now be much improved.

AUS Module ANAUSN (B. Clancy)

The original one dimensional discrete ordinates transport module available to the AUS system was a refined version of the UK program WDSN-ST. While extremely efficient for cell calculations, this module was unable to handle multigroup P_N anisotropic scattering data, to perform criticality searches or to deal efficiently with fixed source problems. Because these capabilities were deemed necessary, an appropriate module had to be provided and the possibility of using the US code ANISN for this task was studied. This was rejected because the code's internal structure made it unsuitable for the AUS scheme and because of dissatisfaction with ANISN's convergence strategy for certain problems. A new module ANAUSN was therefore coded and is available

for general use both within AUS and as a stand alone program.

Three Dimensional Diffusion Codes (G. Doherty)

Two multigroup, finite difference diffusion codes ZHEX and DXYZ were written for hexagonal-z and x-y-z geometries, respectively. Both use a plane by plane over-relaxation solution procedure and are structured to accommodate very large problems. The codes were written for an IBM 360/50 run in MVT mode using HASP and employ dynamic storage allocation, direct access data sets and some double precision arithmetic.

ZHEX was written to assess the feasibility of performing multigroup fast reactor calculations in three dimensions. Each channel is assigned seven mesh points (centre and corners) which is barely adequate for typical fast reactor dimensions, but allows a considerable economy of mesh points over alternative internal mesh point schemes. The code is restricted to down-scattering problems and uses coarse mesh rebalancing and Chebyshev source extrapolation. The inner routine which solves for the fluxes in a plane is written in ASSEMBLER. The routine solves from the centre outwards using a further over-relaxation. Channel centre points are treated as discrete while all the corner points on the periphery of each ring of channels are solved simultaneously using an elimination technique which takes advantage of the almost tridiagonal form of the matrix equation. A typical 6 group, 18 axial mesh calculation of a 250 MW fast reactor converges from a flat flux guess to 10^{-4} in source in 300 minutes on the IBM 360/50.

DXYZ allows upscattering problems and incorporates a group rebalance procedure to accelerate convergence on this type of problem. Coarse mesh rebalancing and Chebyshev source extrapolation are again employed. The inner routine (again in ASSEMBLER) uses standard successive line over-relaxation to solve for the fluxes in a plane. The edge mesh representation is used for all directions. A four group calculation of an Argonaut reactor, starting from a cosine shape in each direction and converging to 10^{-4} in source takes about 150 minutes.

The codes are available as AUS modules or as stand-alone codes.

4.2 MULTIGROUP DATA PREPARATION (H. Ferguson)

Overall Summary of Data Processing

Currently multigroup cross section and scattering matrix data are produced from evaluated microscopic point data that come essentially from two

sources, namely, the UK Nuclear Data Library (UKNDL) and the Evaluated Nuclear Data File (ENDF). The UKNDL provides tabular neutron cross sections and secondary-neutron energy-angular distributions, while the more comprehensive ENDF gives in addition fission product yield and decay data, resolved and unresolved resonance parameters and thermal neutron scattering law data, amongst other information. ENDF also contains cross sections and energy-angular distributions for photon reactions.

The major programs for processing the UKNDL data into multigroup form are BOMB which averages group cross sections and a series of programs collectively known as BOMBO which produces elastic and inelastic epi-thermal scattering matrices. ENDF data is processed into multigroup form primarily by the Oak Ridge program SUPERTOG which produces cross sections and epi-thermal elastic, inelastic and (n,2n) scattering matrices. Thermal scattering matrices are prepared from ENDF thermal law scattering data (in $S(\alpha,\beta)$ form) by the UKAEA program PIXSE. These thermal and epi-thermal matrices are then judiciously combined using the local program MERGER. Multigroup pseudo resonance parameters for GYMEA may be emulated using the program AVRAGE4G (see below). Multigroup cross sections can also be prepared from miscellaneous microscopic point cross section data and/or resolved resonance parameters using the program GUNYA.

The bulk of the multigroup neutron cross section and scattering data produced are ultimately loaded onto the GYMEA libraries using the locally written loading and editing programs XSEDIT (for cross section libraries) and SCATLD (for scattering matrix libraries). However, a significant effort has gone into the production of thorium data for the pulsed neutron experiments. While the GYMEA libraries are primarily oriented to reactor calculations spanning neutron energies between 10 MeV and 10^{-3} eV, a special purpose library of moderator cross sections and matrices has been prepared in GYMEA format. This spans the range 10 MeV to 10^{-6} eV. This library represents, in final form, cross section data for analysis of the now completed pulsed neutron and neutron wave studies of polycrystalline moderators.

Unresolved Multiresonances for GYMEA

For certain nuclides it is desirable to have resonance parameters for self-shielding calculations that extend well beyond the range of measured resonances. The partial widths of the actual resonances are not all the same, but are distributed randomly about their means with distributions that can be readily parameterised. One way to overcome this lack of experimentally

measured resolved resonances is to generate a large number of single pseudo resolved resonances by taking random samples from the assumed statistical distribution for the various partial widths. The result of this is on average, a set of pseudo resonances with more or less the same general properties as the true resonances (the method of the program GENEX). However to be adequate, this method requires so many individual samples that the processing becomes prohibitive for our purposes.

The approach that is adopted here is to lump together large numbers of similar resonances. Thus many resonances are replaced by a single set of parameters and associated with this single 'multiresonance' is an additional parameter, the 'multiplicity factor', equal to the number of resonances it represents. The parameters are not strongly energy dependent, but are strongly dependent on the particular compound nucleus state to which they correspond. It was initially assumed that for each state all the resonances in a single multigroup could be replaced by a single multiresonance, however this had two main disadvantages. Firstly, the parameters chosen for each multiresonance could not fully reflect the distributions of the individual partial widths and consequently each of the multiresonances had to be a compromise value that could never be fully consistent with the corresponding group averaged partial cross sections. Secondly, the resonances with the smallest fission widths give rise to the strongest temperature dependent effects. However, these resonances cannot be represented at all by a single multiresonance whose partial fission width must lie near the mean.

To overcome these two objections, the single multiresonance for each group and spin state has been replaced by a number of multiresonances whose partial widths are taken from successive subdivided portions of the assumed partial width distributions. Each of these subdivided multiresonances represents equal numbers of actual resonances. This method, while largely preserving the overall characteristics of the actual statistical distributions, greatly reduces the necessary number of resonances. The program AVRAGE4G uses the parametrised ENDF cross sections in the unresolved region to produce parameters in form suitable for loading onto the GYMEA libraries. To date, only ^{235}U multigroup data has been produced in this way, but the method is general and may be applied to any ENDF material that has suitable unresolved parameters.

^{232}Th Multigroup Data for the Pulsed Neutron Experiments

The space-time behaviour of fast neutron fluxes in pulsed heavy metal assemblies is under study. Multigroup cross sections and scattering matrix data ranging from 10 MeV to 1 keV is required for use in the 0-dimensional time dependent diffusion program TENDS, the 1-dimensional time dependent transport program TDA and the Monte Carlo program MORSE. The UKNDL and ENDF were used to produce two separate data sets from essentially independent sources using the local BOMB-BOMBO programes for the UKNDL set and SUPERTOG for the ENDF set as outlined above.

Initially a 37 group structure was used taking the standard GYMEA group boundaries at the high energy end, but it soon became apparent that these group boundaries were not specifically suited to the ^{232}Th data and so a special 50 group structure and lastly, a special 100 group structure, was used. The ENDF ^{232}Th data gave the elastic scattering angular distributions (quite in accordance with the ENDF specifications). However, the specifically ENDF oriented program SUPERTOG can only process angular distributions that are given in Legendre coefficient form (although this restriction is undocumented). Consequently it was necessary to first write a program to convert the tabular distributions to Legendre coefficients to produce a reformatted ENDF material. Apart from this setback, the data preparation was relatively straightforward.

4.3 FISSION PRODUCT STUDIES (J. L. Cook, H. D. Ferguson, A. R. deL Musgrove, G. Trimble)

Fission Product Yield Data

In any reactor, the yields from fission of the various fission products are important since it is the building up of such fission products which eventually terminates the operating lifetime of the reactor with a given charge of fuel. In the fission event, most secondary neutrons are emitted from the highly excited fission fragments, so one has to consider two types of yields, the 'prompt' yields, or yields before neutron emission, and the 'delayed' yields or yields after neutron emission. Comprehensive measurements of yields are available for thermal fission of ^{233}U, ^{235}U, ^{239}Pu and ^{241}Pu, while yields from fission neutrons are available for ^{232}Th, ^{233}U, ^{235}U, ^{238}U and ^{239}Pu. No fast yield measurements are available for ^{240}Pu or ^{241}Pu which are nuclides of significance in any ^{239}Pu fuelled reactor.

We have investigated the delayed yields for the above fissile materials

by firstly conjecturing a 'two mode' hypothesis of the fission process whereby the curve of yields versus fission product masses is assumed to consist of a Gaussian for a symmetric mode and an independent Gaussian for an asymmetric mode. The fits of measured yields to this functional form was very poor, deviations averaging around 100 per cent in some cases, with the single exception of ^{235}U yields from 14 MeV neutrons, for which an excellent fit was obtained. From the shapes of the yield curves, we conjectured that the fission process might take place through three modes, two asymmetric and one symmetric. The fits obtained by assuming independent Gaussians for each mode was excellent in all cases with a mean deviation averaging around 10 per cent.

With the eight parameters obtained by fitting each fissile nuclide, we are investigating the possibility of extrapolating to yield values that have not been measured for other incident neutron energies and parent mass numbers, particularly for ^{239}Pu, ^{240}Pu and ^{241}Pu. To date it appears that linear interpolation is not possible, but quadratic interpolation holds some promise.

With the fitted parameters we have carried out a survey of the yield requirements for thermal and fast reactors. It was found that one considers all yields greater than 10^{-6} per cent then some 750 fission products must be taken into account. Taking this requirement down to 10^{-12} per cent enlarges the number of nuclides to 1,100. At the present time 758 fission products have measured half-lives ranging down to 0.2 s. If we neglect half-lives shorter than this, then from the point of view of fuel management, 758 appears to be around the number one should consider in thermal or fast reactors, for a complete survey.

Cross Sections and Decay Data

We propose to prepare a fission product data library suitable for fuel management studies. It will contain information on yields, decays and activation cross sections. Much of this information, particularly the decay data, will be obtained from other libraries, but the section on activation cross sections will be evaluated by us. To this end, a survey of neutron strength functions has been carried out while compilations of radiation widths and level spacings are in progress.

Much overseas interest has been shown in our previous fission product library and a number of shortcomings have been discovered. Information about comparisons with experiment has been conveyed to us. Using visual display facilities these deficiencies are being overcome in the light of the new measurements.

Fuel Management

Towards the end of the life of a fuel element in a thermal or fast reactor, there is more material present in the form of fission products than there is fuel. Detailed studies have shown that for an adequate description of nuclide burnup in such a system, one may need to know cross sections for nuclides with yields down to about 0.003 per cent. A number of low cross section nuclides can be neglected, but it appears that some 80 nuclides must be included to obtain satisfactory results.

It is proposed that theoretical studies of thermal and fast systems be carried out using burnup programs to assess the concentrations of the various nuclide species at the end of life of the fuel element. Experimental measurements of fission product worths have been made which indicate large discrepancies for some nuclides, particularly ^{153}Eu and by such comparisons we hope to be able to amend our data to obtain better agreement.

Waste Management

When fission products are removed from exhausted fuel elements and concentrated in liquid form, the beta and gamma activity of the unstable products generates considerable heat, which poses a storage problem. Just how this heat generated varies with time is not known precisely, but preliminary studies show that some 800 nuclides contribute significantly. To calculate the heat as a function of time, one would require a massive library of beta and gamma decay schemes for such nuclides, a project which is beyond the capacity of the data group. However, an ENDF/B library containing this material will shortly become available and we propose to use this in studies of decay heating. As part of this project, we will be investigating ways of removing the biologically hazardous long-lived isotopes such as ^{90}Sr from the wastes, either by burnup in a reactor, or a proton accelerator. For this purpose the library has decay data for 823 nuclides and yield data for 1016 isotopes. The 823 set consists of 701 isotopes in their ground state, 116 isotopes in their first isomeric excited states and 6 isotopes in second excited isomeric states.

4.4 SHIELDING

Monte Carlo Codes (B. McGregor)

Several major calculational tools obtained from ORNL have been made operational. These include KENO, a Monte Carlo code developed from the 05R system to allow the calculation of criticality in array systems. Useful

features include reflective and albedo boundary conditions with precomputed albedos, modified Hansen and Roach 16 group cross section set, ability to include the user's own cross sections or to calculate them using XSDRN, statistical analysis of results, various source routines. KENO has been used for several years at ORNL and is regarded as a reliable calculational method.

A combination version of the ORNL general purpose Monte Carlo code, MORSE, has also been made operational. The combinational geometry is easy to use and gives the power of the original 05R general geometry description without the difficult data preparation problems. MORSE uses the same cross sections as the ORNL S-N transport codes ANISN and DOT which allows ready comparison of alternative methods.

Eigenvalues of the Discrete Ordinates Equations in Slab Geometry

(I. Donnelly)

The discrete ordinates form of the one group, time independent, source free neutron transport equation has been solved analytically for slab geometry in order to obtain the dependence of the solution on the angular quadrature and spatial mesh used in deep penetration problems. Expressions for the neutron flux have been obtained in terms of the resulting eigenvalues, but the most interesting results are found for large homogeneous systems in which the flux is determined by a dominant eigenvalue K. The dependence of K on the angular quadrature and spatial mesh size used in the discrete ordinates approximation has been evaluated.

The one group, time independent, source free neutron transport equation in slab geometry can be written as

$$\mu \frac{\partial \psi(x,\mu)}{\partial x} + \psi(x,\mu) = \frac{c}{2} \int_{-1}^{1} \psi(x,\mu')\, d\mu' \qquad \ldots(1)$$

In the discrete ordinates approximation the angular flux is only evaluated at N discrete directions $\{\mu_m\}$ with associated weights $\{\omega_m\}$. This leads to a set of N coupled equations

$$\mu_m \frac{\partial \psi(x,\mu_m)}{\partial x} + \psi(x,\mu_m) = \frac{c}{2} \sum_{n=1}^{N} \omega_n \psi(x,\mu_m) \quad , \quad m = 1,2,\ldots,N \qquad \ldots(2)$$

The dominant eigenfunction solution of these equations has the form

$$\psi(x,\mu_m) = \psi(\mu_m)\, e^{Kx} \quad . \qquad \ldots(3)$$

Assuming a symmetric quadrature, the substitution of equation (3) in equation (2) results in the equation

$$\sum_{m=1}^{N/2} \frac{\omega_m}{1 - \mu_m^2 K^2} = \frac{1}{C} \qquad \ldots(4)$$

for the eigenvalue K. In the limit $N \rightarrow \infty$, equation (4) becomes

$$\frac{\tanh^{-1} K_e}{K_e} = \frac{1}{C} \qquad \ldots(5)$$

where K_e is the exact value of the dominant eigenvalue. In general a closed equation cannot be obtained for K unless $N \leq 8$; however it can be shown that for $|1 - C| < 1$,

$$K^2 = K_e^2 + 0\left((1 - C)^{J+1}\right) \qquad \ldots(6)$$

as long as the angular quadrature correctly evaluates the moments $\sum_{m=1}^{N/2} \omega_m \mu_m^{2n} = 1/(2n+1)$ for $0 \leq n \leq J$.

Spatial discretisation results in equation (2) being replaced by the set of coupled difference equations

$$\mu_m \left[\psi(x + \Delta, \mu_m) - \psi(x, \mu_m)\right] + \Delta\psi(\bar{x}, \mu_m) = \frac{C}{2} \sum_{n=1}^{N} \omega_n \psi(\bar{x}, \mu_m)$$

$$m = 1, 2, \ldots, N \qquad \ldots(7)$$

where Δ is the mesh size, x has discrete values only and $\bar{x}$ lies in the interval x to $x + \Delta$. Two alternative methods are commonly used to express $\psi(\bar{x}, \mu_m)$ in terms of $\psi(x, \mu_m)$ and $\psi(x + \Delta, \mu_m)$, and thus allow the solution of equation (7). One is the diamond difference approximation which is highly accurate for small Δ, but which can give negative flux values for larger Δ. The other is the step function approximation which is not as accurate for small Δ but always gives positive fluxes.

In the diamond difference approximation the relationship

$$\psi(\bar{x}, \mu_m) = \tfrac{1}{2}\left[\psi(x, \mu_m) + \psi(x + \Delta, \mu_m)\right] \qquad \ldots(8)$$

is used to eliminate $\psi(\bar{x}, \mu_m)$ from equation (7). For small Δ, solutions of

equation (7) are of the form

$$\psi(x, \mu_m) = \psi(\mu_m)\, e^{K^d x} \quad . \qquad \ldots(9)$$

The dominant eigenvalue K^d is related to the eigenvalue K by the relationship

$$K^d = \tanh^{-1} (K\Delta/2)/(\Delta/2) \quad , \quad \left|\frac{K\Delta}{2}\right| < 1 \qquad \ldots(10)$$

$$= K\left[1 + \frac{(K\Delta)^2}{12} + \frac{(K\Delta)^4}{80} + \ldots\right]$$

and hence the diamond difference approximation overestimates the size of the eigenvalue for $C < 1$. For $C > 1$, $K \longrightarrow iB$ and $K^d \longrightarrow iB^d$, so the eigenvalue B^d is smaller than B. The error in K^d is seen to be second order in Δ and is small for $|K\Delta| < 0.5$.

In the step function approximation the relationship

$$\psi(\bar{x}, \mu_m) = \psi(x + \Delta, \mu_m) \quad , \quad \mu_m > 0$$

$$= \psi(x, \mu_m) \quad , \quad \mu_m < 0 \qquad \ldots(11)$$

is used. Solutions of equation (7) are of the form

$$\psi(x, \mu_m) = \psi(\mu_m)\, e^{K^s x} \quad . \qquad \ldots(12)$$

No closed relationship holds between the dominant eigenvalue K^s and K; however for small Δ the following expression has been obtained

$$K^s = K\left[1 - d\Delta + O(\Delta^2)\right] \quad , \quad \Delta << 1 \qquad \ldots(13)$$

where d is a function of C and the angular quadrature used. The error in K^s is first order in Δ. A typical value of d is 0.4 and even a mesh size as small as 0.1 mean free paths will give a 4 per cent error in K^s relative to K.

Site Service Work

Advice has been given on problems concerning shielding ^{252}Cf sources and the MOATA dump tank area.

Other Calculations

The Monte Carlo method often provides an alternative means of calculating at least part of a problem. A study of the pulsed thorium assembly is now

underway using MORSE and two finite difference codes TDA and POW. KENO is being used to calculate a MOATA mockup in the Critical Facility.

Comparisons with the diffusion code calculations of this problem have shown unexpected differences which are not presently understood.

4.5 NEUTRON SPECTRA STUDIES

Unfolding of Resolution Functions for Experimental Data (D. W. Lang)

The computer techniques used to study a gedanken problem* have now been applied to the analysis of experimental data.

(a) Time of Flight Data

The raw data are in the form of apparent time of flight spectra of neutrons and gammas emitted from a target bombarded by a pulse of charged particles. The time spread of the gamma distribution reflects the time spread of the original beam pulse. It is the effect of this which must be unfolded from the apparent neutron spectrum to give a better approximation to the actual time of flight spectrum of neutrons from which the energy spectrum follows.

The unfolding program developed for a gedanken problem to obtain a spectrum from data uses an iteration process in which the residual errors after each step are used to determine the next step. First a test is made to see if the residuals can reasonably be ascribed to random errors of measurement of the data. If not, a further vector to be added to the spectrum is generated. Two of the criteria to be satisfied by the vectors are:

(i) The new vector must not interfere with the fit that has already been achieved. Two vectors are required to be conjugate, i.e. an interference term in the expression for chi-square is required to be zero.

(ii) The amplitude of the added vector is constructed to minimise the new value of chi-square.

It is necessary to have a third criterion to give mathematical effect to the intuitive idea that the calculated spectrum should be as simple as possible. The form of the criterion is crucial since it involves a choice between the

---

*AAEC/PR37, section 4.4.1)

many spectrum vectors that are compatible with the data on statistical grounds. The form used was re-written for the time of flight spectrum problem and has been found to have considerable general application.

For each spectrum point a measure of acceptable error is defined. This is taken to be the change required in the spectrum value at that point, keeping all other values constant, in order to change the value of the chi-square from zero to unity, using the given data points and the variances of the associated data values. For any vector to be added to the spectrum an associated vector can be defined in which each element is the ratio of the change of spectrum value at a given spectrum point to the associated error measure at that spectrum point. A third criterion is then set up to be satisfied by the vector to be added to the spectrum.

The associated vector of the type just described is selected to be proportional to the gradient of the chi-square in the space of such associated vectors. The program is required to make the largest variation of spectrum values in regions of the spectrum that make least contribution to chi-square for the fit to the data set. The effect is that as far as possible the errors at the individual spectrum points all contribute equally to the residual value of the chi-square.

The program strategy is similar to the conjugate gradient method to obtain the most important portion of an inverse to a matrix. The program produces an estimate for the spectrum values which would be observed with a zero time spread for the original beam pulse. There is no intrinsic requirement that the data should be unfolded to this number of spectrum points. The measure of error for the spectrum points produced does, however, depend on the number of points in the spectrum and neglects covariances. It is biassed to produce a smooth form of the spectrum, even if the spectrum could be fitted by a few sharp lines and hence should be interpreted with commonsense.

(b) Proton Recoil Data

Neutron spectra are often obtained from an examination of the spectra of protons produced by collisions of the neutrons in hydrogenous material. A program (SPEC-IV) developed at Aldermaston to unfold the neutron spectrum from the measured recoil spectrum has been modified to local conditions and preferences and is in use on the IBM 360. To satisfy some doubts about the validity of various steps in the procedures of SPEC-IV a program has been written using the unfolding techniques described above and is now available on

the IBM 360. Results for the two programs are in agreement where they have been compared. The iterative procedure combined with plotting of results allows flexibility in deciding what errors are acceptable in the fit to the data, but is more demanding on computer time.

(c) One of the most longstanding problems in nuclear physics has been the measurement of photonuclear spectra. These are often produced by gamma rays originating in bremsstrahlung and the final yield data is therefore a folding of the photonuclear cross section with the bremsstrahlung spectrum. A program has been written and shown to be effective on data supplied by Dr. H. H. Theis of the University of Western Australia.

Detector Efficiency Studies (E. Clayton)

The percentage of neutron flux incident on a detector that gives rise to recorded events is called the detector efficiency for neutrons of that energy. The interpretation of time of flight experiments require the variation of detector efficiency with energy. It is surprising that efficiency measurements are still bedevilled by difference between experiment and theory (see Plasek et al. 1973)* and also between experiment and experiment (see Thornton et al. 1971).**

The AAEC effort is directed toward the use of organic detectors at low neutron energies. The consequent need for low threshold detectors means that processes normally neglected become important. Carbon recoils, which yield a much smaller pulse than proton recoils of the same energy, may give a pulse large enough to exceed the threshold. Hence the presence of resonances is the carbon cross section gives rise to a rapid variation in the detector efficiency over a small energy range. The statistical nature of signal formation in the detector and photomultiplier also becomes more important at low energies.

A study is in progress with the aim of calculating efficiencies for the detectors NE102 and NE213. The project may reasonably be split into two parts. Firstly, a calculation of energy deposited in the detector and secondly, conversion of deposited energy into an output pulse from the photomultiplier.

---

* Plasek, R., Miljanik, D., Valkovic, V., Liebert, R. B. and Phillips, G. C. (1973) - NIM, 111, 251.

** Thornton, S. T. and Smith, J. R. (1971) - NIM, 96, 551.

A Monte Carlo program has been written to simulate the manner in which neutrons deposit energy when incident on a cylindrical detector normal to one of the two parallel flat faces. Neutrons are followed as they undergo collisions with carbon or hydrogen and consequently change direction and kinetic energy. The kinetic energy lost in each collision is assumed to be deposited in the detector.

The major work of the project is now directed to the study of the conversion of energy deposited into output signal. The problems here are the variation of light output from different detectors for a given deposited energy and the statistical nature of the process at all stages. A literature search for this part is still in progress. One difficulty is the accurate calculation of the output pulse height for low energy protons. Data for proton energies above 200 keV has been given by Smith et al. (1968)[*]. This data as parameterised by Lindstrom and Anderson (1972)[**] is used in our calculations. This parameterisation is being investigated to determine whether it is sufficiently accurate below 200 keV or whether it will be necessary to measure the proton response.

---

[*] Smith, P. L., Polk, R. G. and Miller, T. G. (1968) - NIM, 64, 157.

[**] Lindstrom, W. W. and Anderson, B. D. (1972) - NIM, 98, 413.

5.0 PUBLICATIONS

5.1 Papers

Allen, B. J., Macklin, R. L., Winters, R. R., Fu, C. Y. (1973) - Comments on the doorway state in ^{206}Pb. Phys. Rev. C, 7, 6, 2589.

Allen, B. J. and Macklin, A. L. (1973) - ORELA neutron capture and stellar nucleosynthesis. Atomic Energy in Aust. 16, 2, 14.

Allen, B. J., Macklin, R. L., Winters, R. R., Fu, C. Y. (1973) - Neutron capture cross sections of the stable lead isotopes. Phys. Rev. C, 8, 4, 1504.

Bird, J. R. Allen, B. J., Bergqvist, I., Biggerstaff, J. (1973) - Compilation of keV neutron capture gamma ray spectra. Neutron Data 11, 6, 433.

Cook, J. L. (1973) - The international compilation, evaluation and exchange of nuclear data for reactors and AAEC participation. Atomic Energy in Aust. 16, 20.

Cook, J. L. (1973) - A note on inverse scattering calculations of energy-independent potentials. Aust. J. Phys. 26, 561.

Hogg, G. R. (1973) - Some problems of fusion reactors. Atomic Energy in Australia, July 1973, pp.7-12.

Rose, E. K., Cook, J. L. and Bertram, W. K. (1973) - Statistics of Adler-Adler resonance parameters. Aust. J. Phys. 26, 725.

Wasson, O. A., Allen, B. J., Winters, R. R., Macklin, R. L., Harvey, J. A. (1973) - Neutron resonance parameters of ^{92}Mo. Phys. Rev. C, 7, 4, 1532.

Wasson, O. A. and Allen, B. J. (1973) - p-wave resonances in ^{111}Cd(n,γ)^{112}Cd. Phys. Rev. C, 7, 2, 780.

5.2 Reports

Broomhall, G. J., Kenny, M. J., Martin, P. W., Bird, J. R. (1973) - Measurement of partial capture cross sections for neutron energies above 10 keV. AAEC/E302.

Culley, D. and Donnelly, I. J. (1973) - Neutron and gamma ray flux levels in PWR pressure vessels. AAEC RP/TN152.

Reports (cont'd)

Clifford, C. E., McGregor, B. J., Muckenthaler, F. J. and Mysatt, F. R. (1973) - ORNL TSF pipe chase neutron streaming experiment - Phase One. ORNL-TM-4176.

Donnelly, I. J. (1973) - Evaluation of boundary conditions for the heterogeneous reactor code SOS-1. AAEC/E288.

Hogg, G. R. (1973) - The dense plasma focus as a pulsed D-T neutron source. AAEC/E279.

Hogg, G. R. and Tendys, J. (1973) - Some X-ray and neutron measurements on the dense plasma focus. AAEC/E280.

McGregor, B. J. and Myatt, F. R. (1973) - Effects of air density perturbations on the transport of gamma rays produced by point gamma ray sources. ORNL-TM-4266.

Pollard, J. P. (1973) - Numerical methods used in neutronics calculations. Ph.D. Thesis, UNSW (Wollongong).

Walsh, R. L. (1973) - Neutron emission from fission fragments. M.Sc. Thesis, UNSW (Wollongong).

5.3 Conference Papers

Allen, B. J. and Macklin, R. L. (1973) - Fast neutron capture cross sections in Si. Int. Conf. on Photonuclear reactions and applications, California. CONF 730301.

Allen, B. J., Kenny, M. J., Bray, K. H., Barrett, R., Carlson, L. E. (1973) - Neutron capture by ^{56}Fe for neutron energies to 460 keV. Nat. Sov. Conf. on Neutron Physics, Kiev.

Allen, B. J., Musgrove, A. R. deL., Chan, D. M. A., Macklin, R. L. (1973) - Neutron capture cross sections of the Ca and Ba isotopes. Nat. Sov. Conf. on Neutron Physics, Kiev.

Boldeman, J. W. (1972) - Prompt neutron yield from the spontaneous fission of ^{252}Cf. 2nd IAEA Panel on Neutron Standard Reference Data, Vienna.

Boldeman, J. W. (1972) - Revised values of nubar for the thermal neutron fission of ^{233}U, ^{235}U, ^{239}Pu and ^{241}Pu. 2nd IAEA Panel on Neutron Standard Reference Data, Vienna, Nov. 1972.

Boldeman, J. W. (1973) - Prompt neutron yield from the spontaneous fission of ^{252}Cf. Nat. Sov. Conf. on Neutron Physics, Kiev.

Conference Papers (cont'd)

Boldeman, J. W. (1973) - Recent relative $\bar{\nu}_p$ measurements. Nat. Sov. Conf. on Neutron Physics, Kiev.

Boldeman, J. W. and Walsh, R. L. (1973) - Energy dependence of the average total fission fragment kinetic energy in the neutron fission of ^{233}U. Nat. Sov. Conf. on Neutron Physics, Kiev.

Hogg, G. R. Tendys, J. and Daniel, J. A. - The dense plasma focus X-ray and neutron emission. 9th AINSE Plasma Physics Conf., Sydney, Feb. 1973.

Musgrove, A. R., Cook, J. L. and Trimble, G. T. (1973) - Prediction of unmeasured fission product fields. IAEA Panel Meeting on Fission Product Nuclear Data, Bologna.

Pollard, J. P. (1973) - Solution of neutron diffusion equations. Seminar on 'Computational Methods in Mathematical Physics', ANU, Canberra, Dec. 1973 (to be p8blished).

6.0 RESEARCH CONTRACT

Title: Neutron Strength Function Calculations
Reference No: 72/E/2
Period: 31/10/72-30/4/73
Supervisor: Professor I. E. McCarthy
University: School of Physical Sciences, Flinders University
Liaison Officer: D. W. Lang

Objective: (a) To predict the single particle eigenvalues for single neutron states labelled $2d\frac{5}{2}$, $2d\frac{3}{2}$ and $3S\frac{1}{2}$ in the nuclear mass region 60 to 100. (b) To investigate the effect of deforming a nucleus with special reference to any isotopic effects. (c) To use the calculated wave functions to investigate strength functions for low orbital angular momentum (s, p and d waves) and nuclei of mass less than 120.

Status: The early part of the year was devoted to writing and checking a computer program for neutron strength functions. The program admits a considerable number of alternative types of nuclear potential as well as the numerical values that can be ascribed to them. First calculations were done with the simplest potentials to determine our ability to duplicate the work already reported in the field.

During the year it became more difficult to obtain computer time in Adelaide and Mr. Peter Cooke, the student associated with the project, came to Lucas Heights for two months. Programs written for the CDC 6400 in Adelaide were swiftly translated for the IBM 360. Some extra checking proved necessary and strength functions were then obtained in reasonable agreement with experiment and previous calculations.

A second program is still in the process of checking. The object is to extend calculations with imaginary and non local components of a potential into the negative energy region. Strength function calculations are to follow.

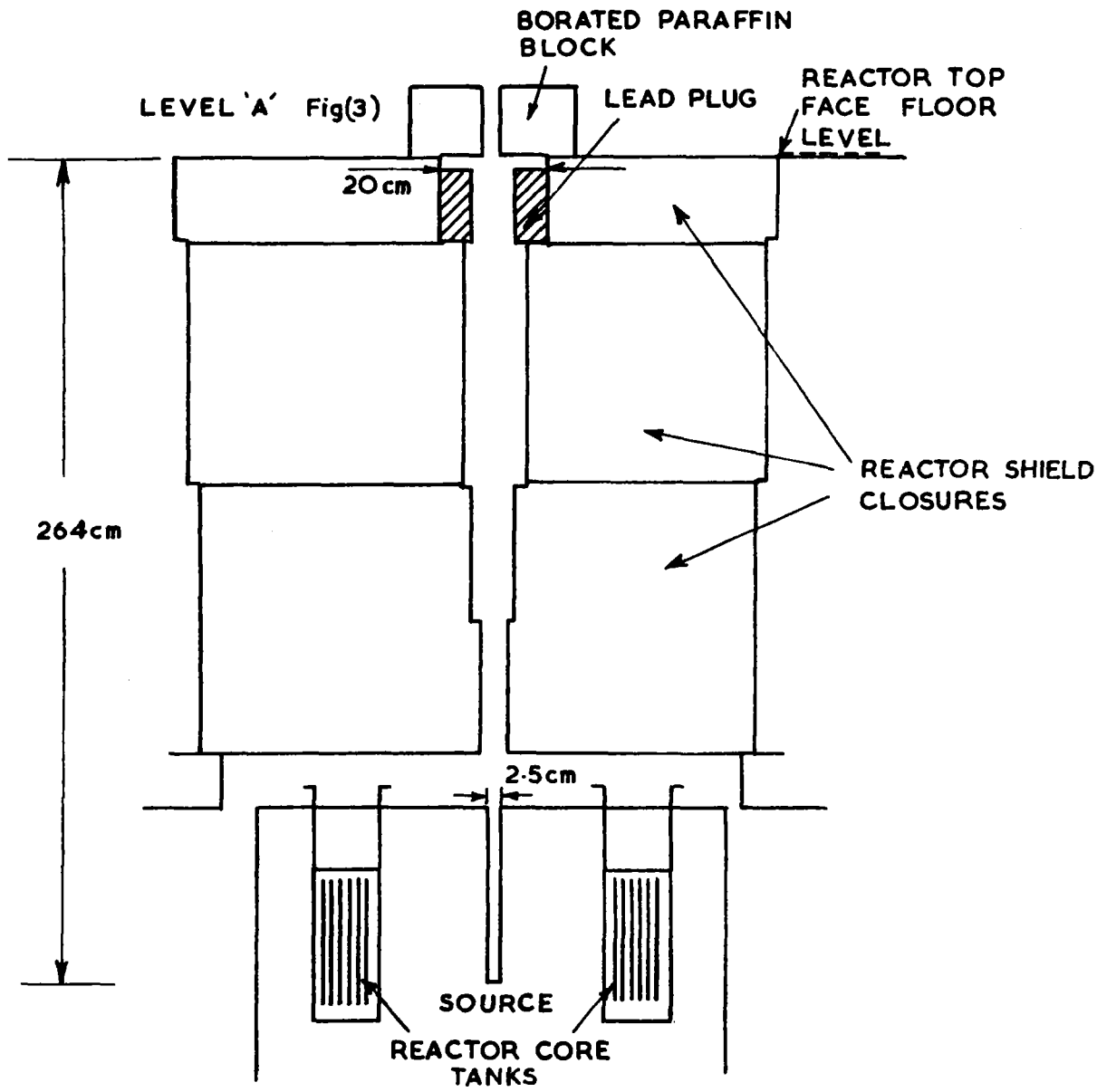

FIGURE 2.1 GENERAL ARRANGEMENT OF THE MOATA IRI BEAM HOLE FOR NEUTRON RADIOGRAPHY

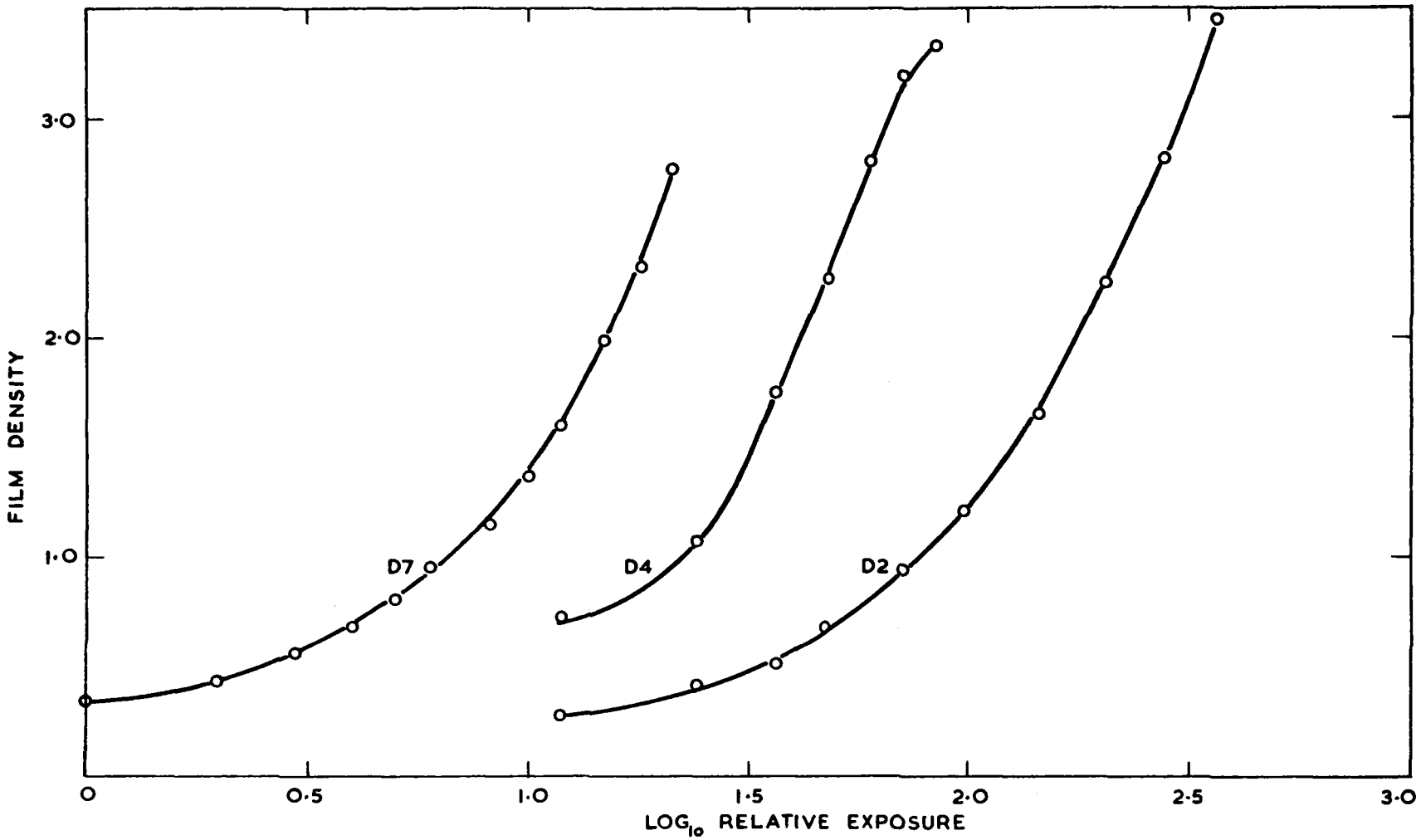

FIGURE 2.2(a) SENSITOMETRIC CURVES FOR 0.004 cm THICK GOLD FOIL

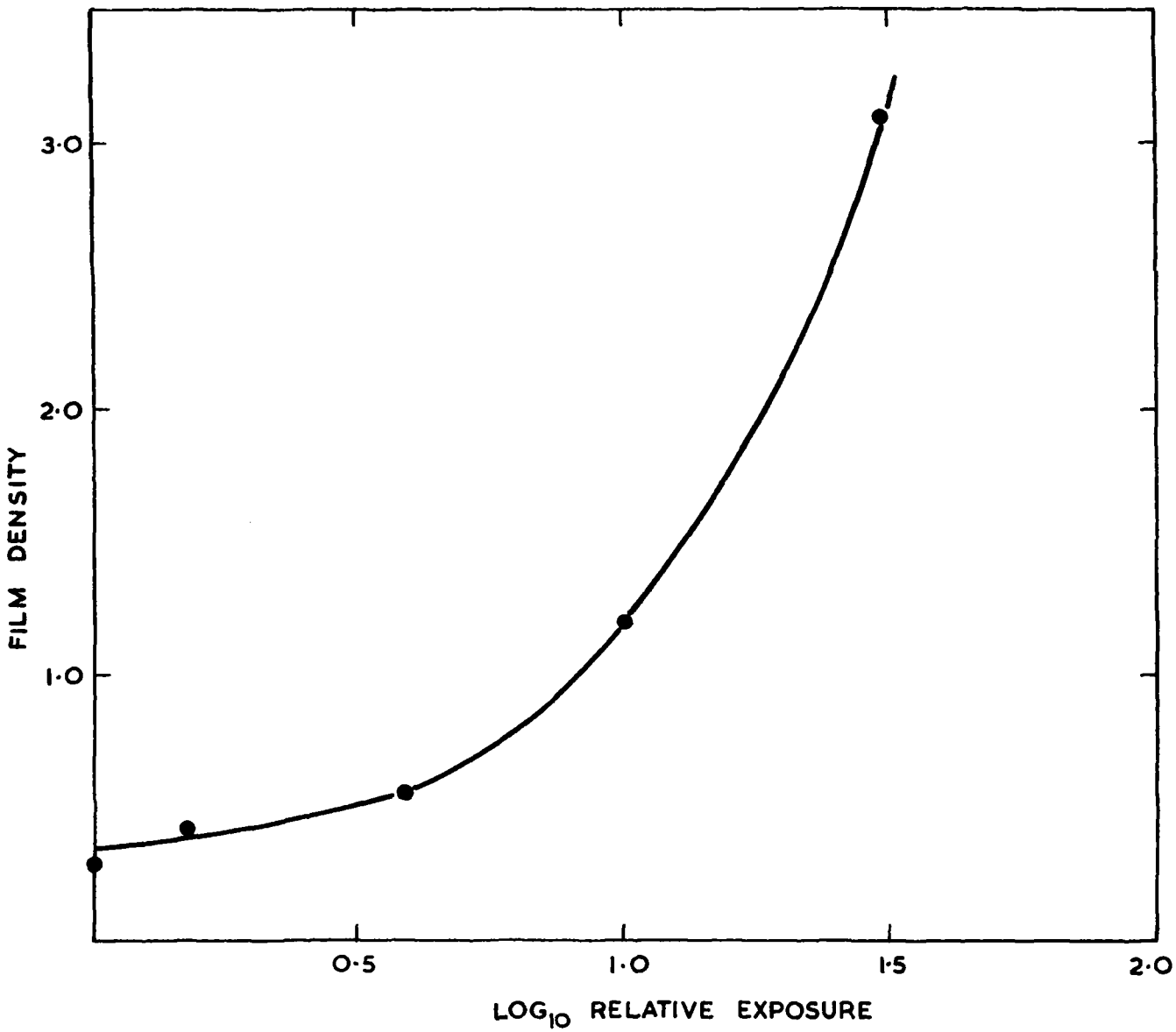

FIGURE 2.2(b) SENSITOMETRIC CURVES FOR 0.0127 cm THICK INDIUM FOIL

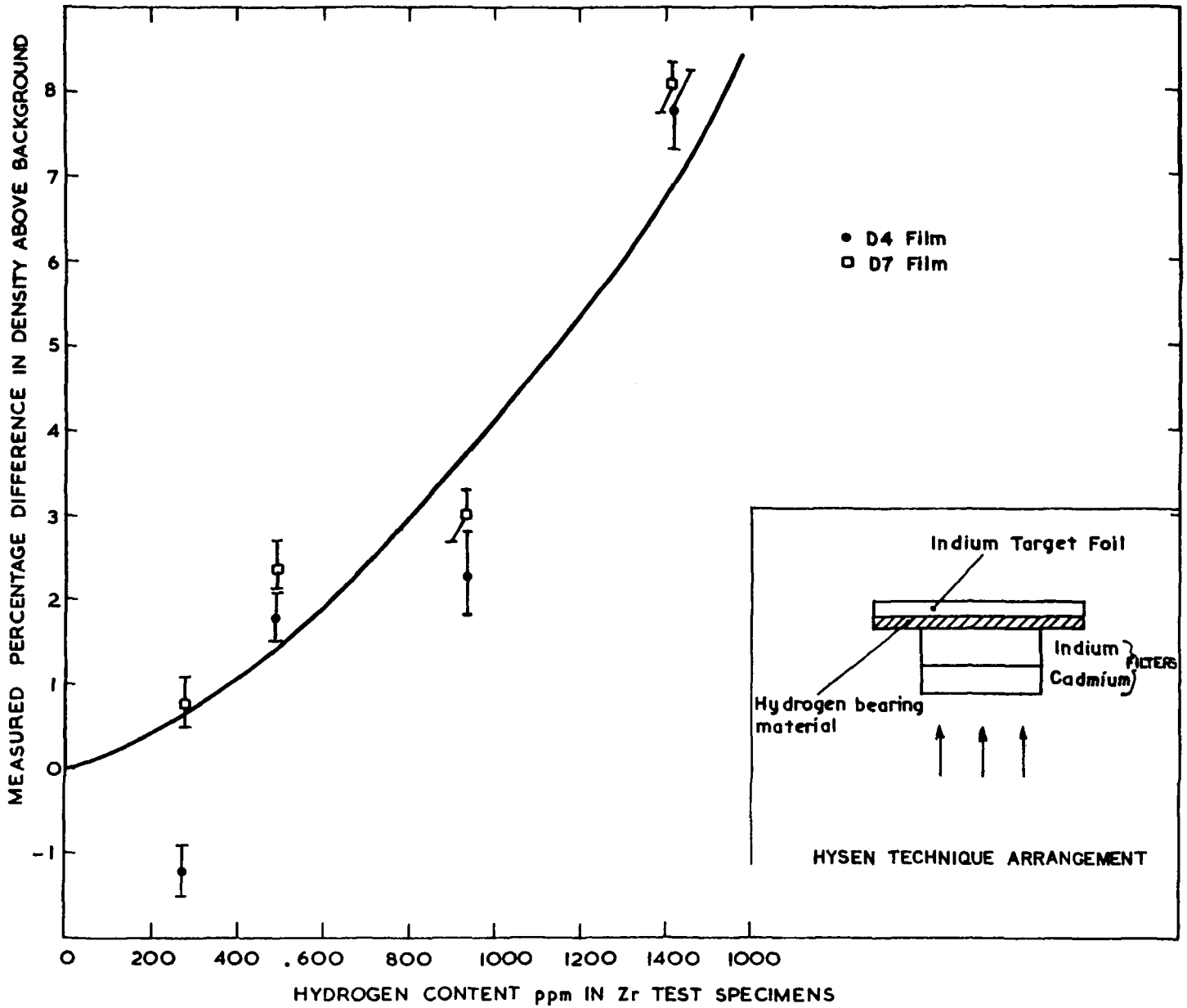

FIGURE 2.3 THE ASSAY OF HYDROGEN IN ZIRCONIUM

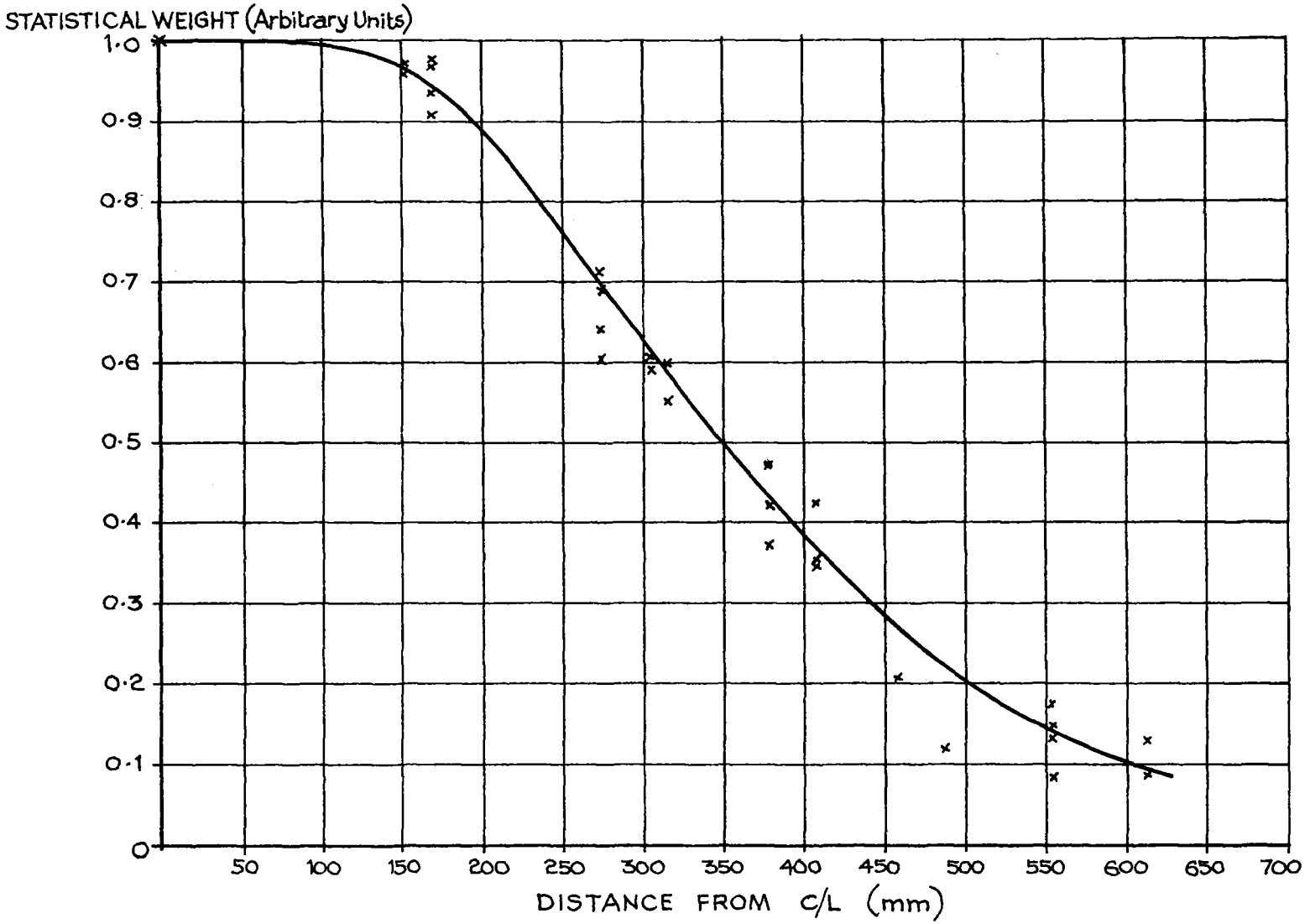

FIGURE 2.4 HIFAR STATISTICAL WEIGHTS FOR A FUEL ELEMENT AND 2V POSITIONS

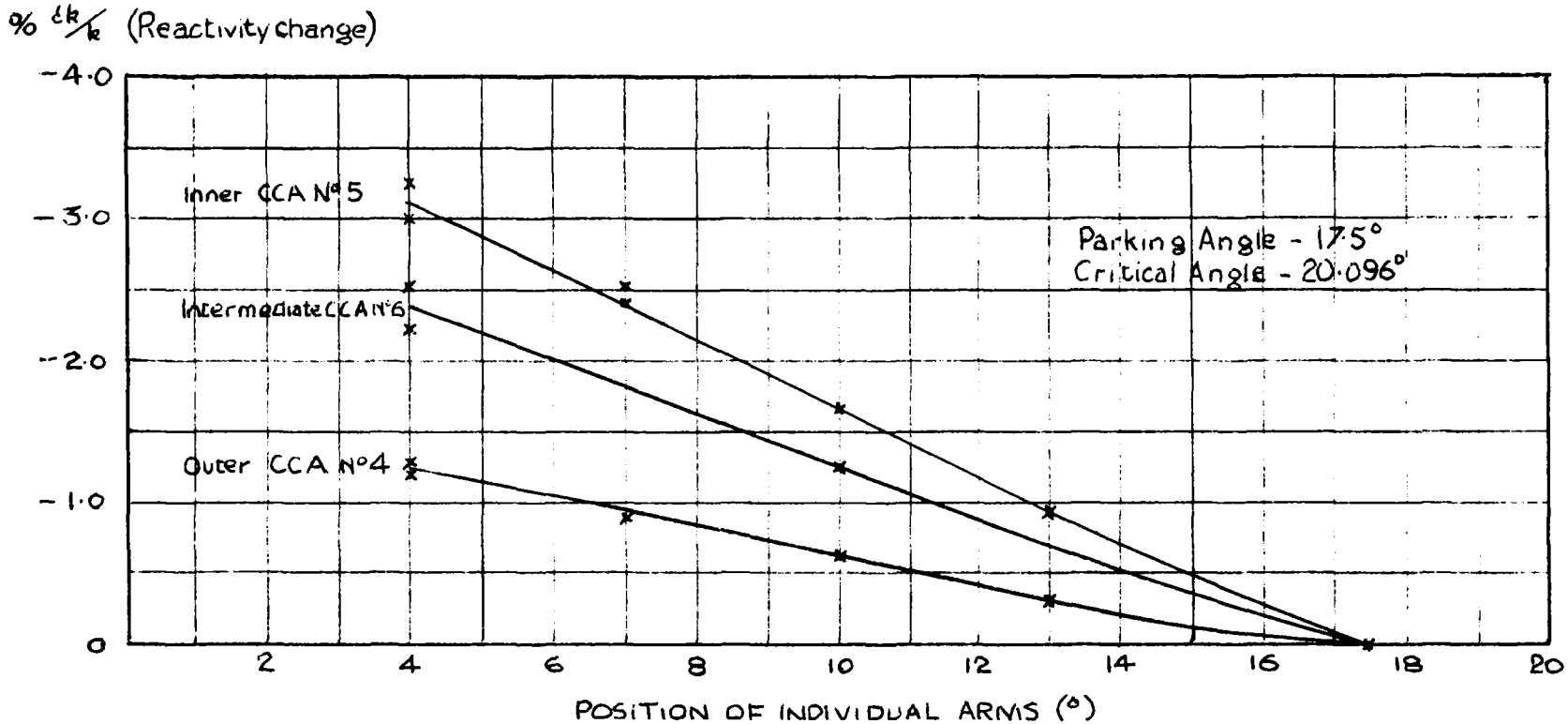

FIGURE 2.5 HIFAR REACTIVITY CHANGES PRODUCED BY INDIVIDUAL CCA MOVEMENT

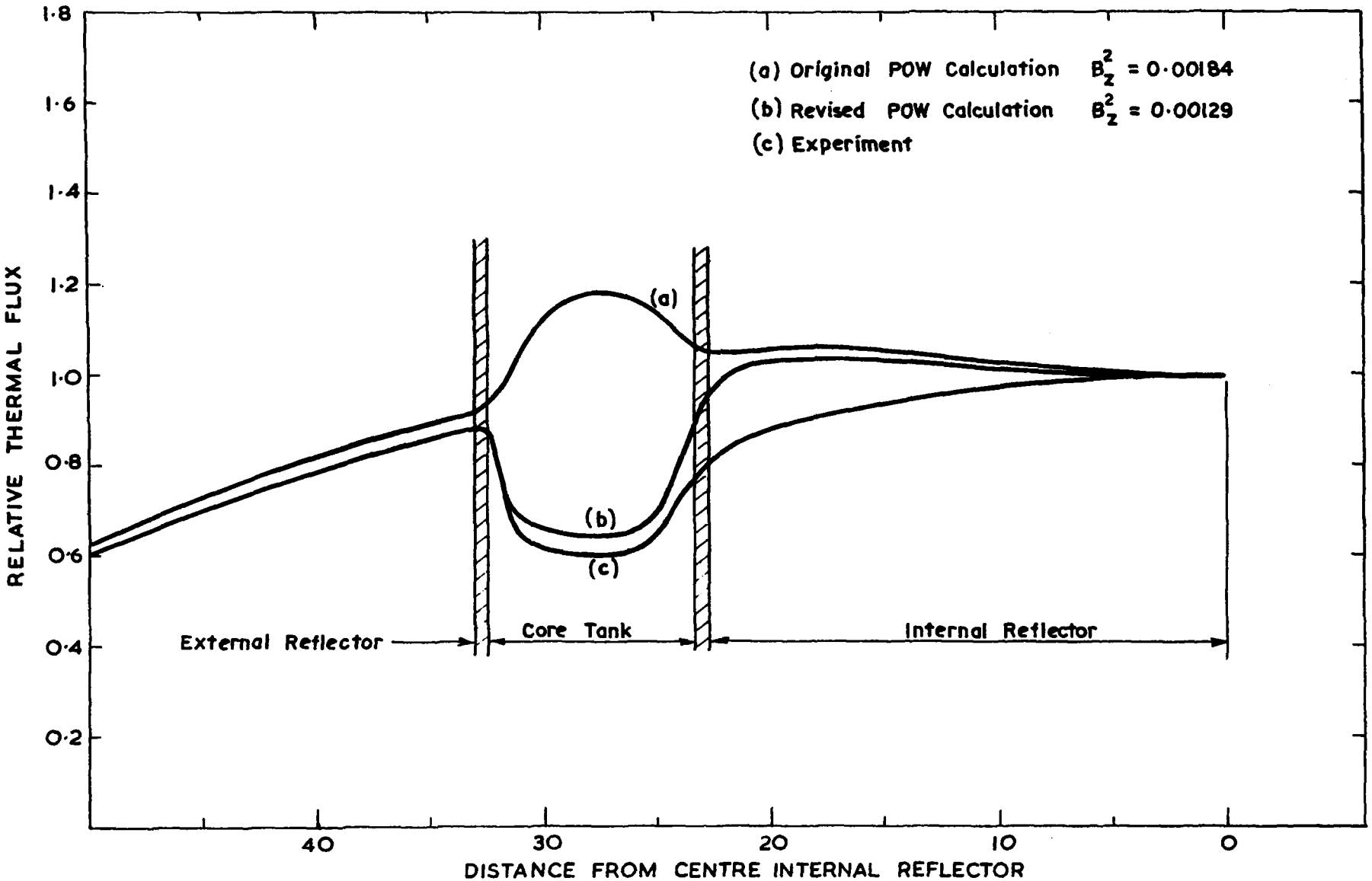

FIGURE 2.6 EXPERIMENTAL AND CALCULATED FLUX DISTRIBUTIONS FOR MOATA MOCKUP I

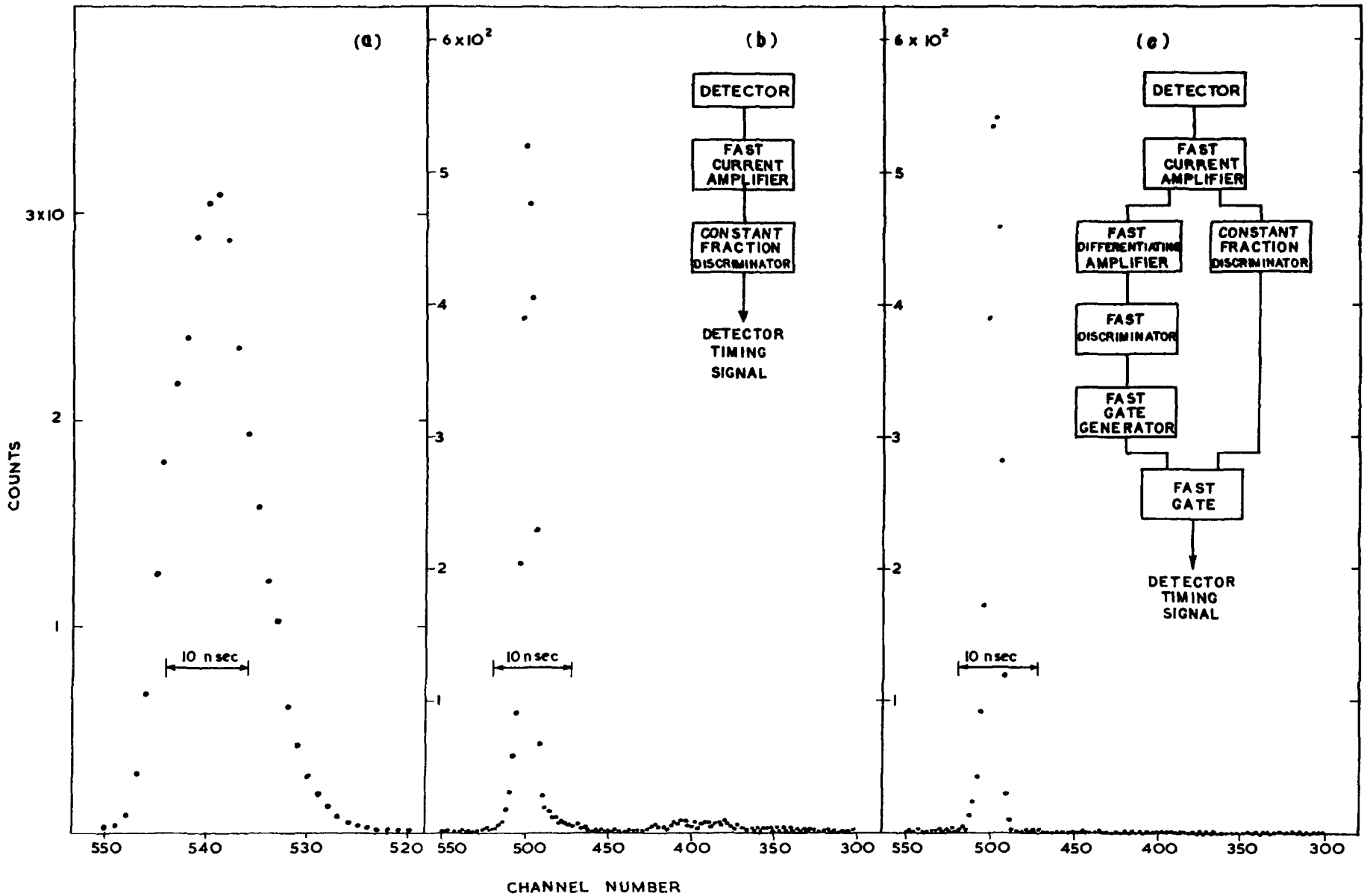

FIGURE 2.7 PULSE FISSION CHAMBER TIMING RESOLUTION: IMPROVEMENTS FROM VARIOUS ELECTRONIC ARRANGEMENTS

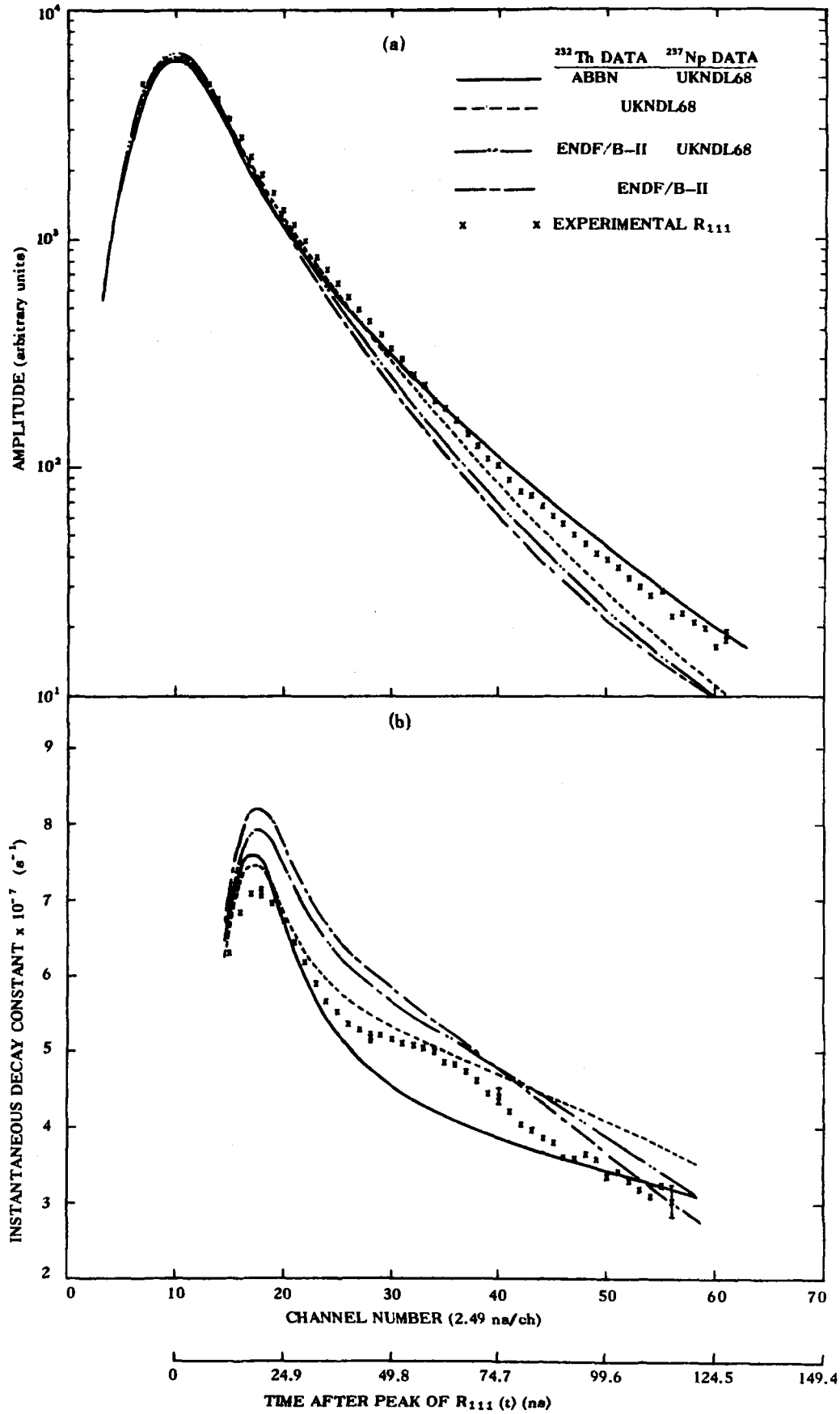

FIGURE 2.8(i) CALCULATED AND EXPERIMENTAL VALUES OF FUNDAMENTAL MODE FISSION RATES FOR ^{237}Np AS A FUNCTION OF TIME. (a) FUNDAMENTAL MODE TIME DISTRIBUTION (b) $\lambda(t)$ THE INSTANTANEOUS DECAY CONSTANT

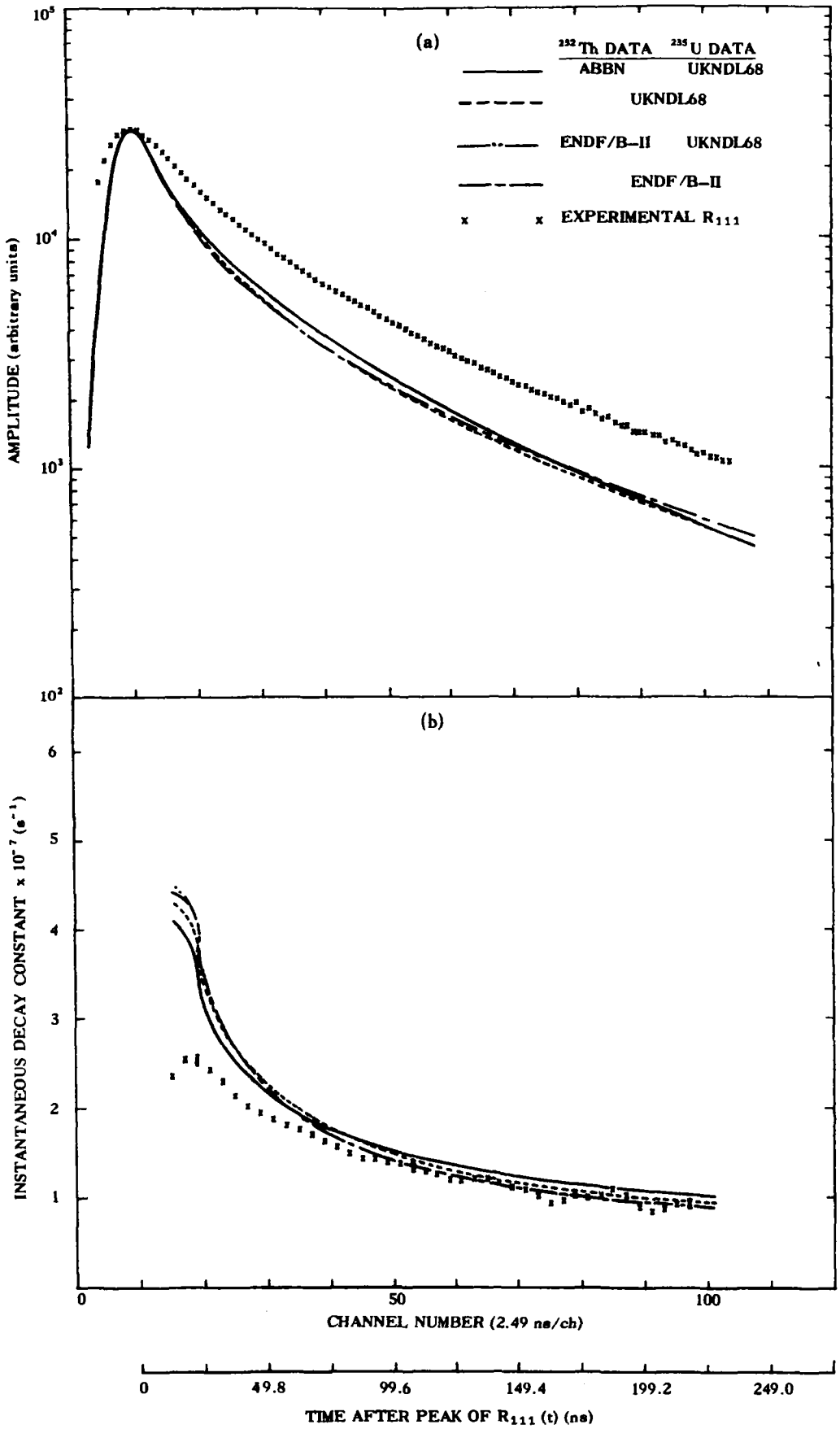

FIGURE 2.8(ii) CALCULATED AND EXPERIMENTAL VALUES OF FUNDAMENTAL MODE FISSION RATES FOR ^{235}U AS A FUNCTION OF TIME. (a) FUNDAMENTAL MODE TIME DISTRIBUTION (b) $\lambda(t)$ THE INSTANTANEOUS DECAY CONSTANT

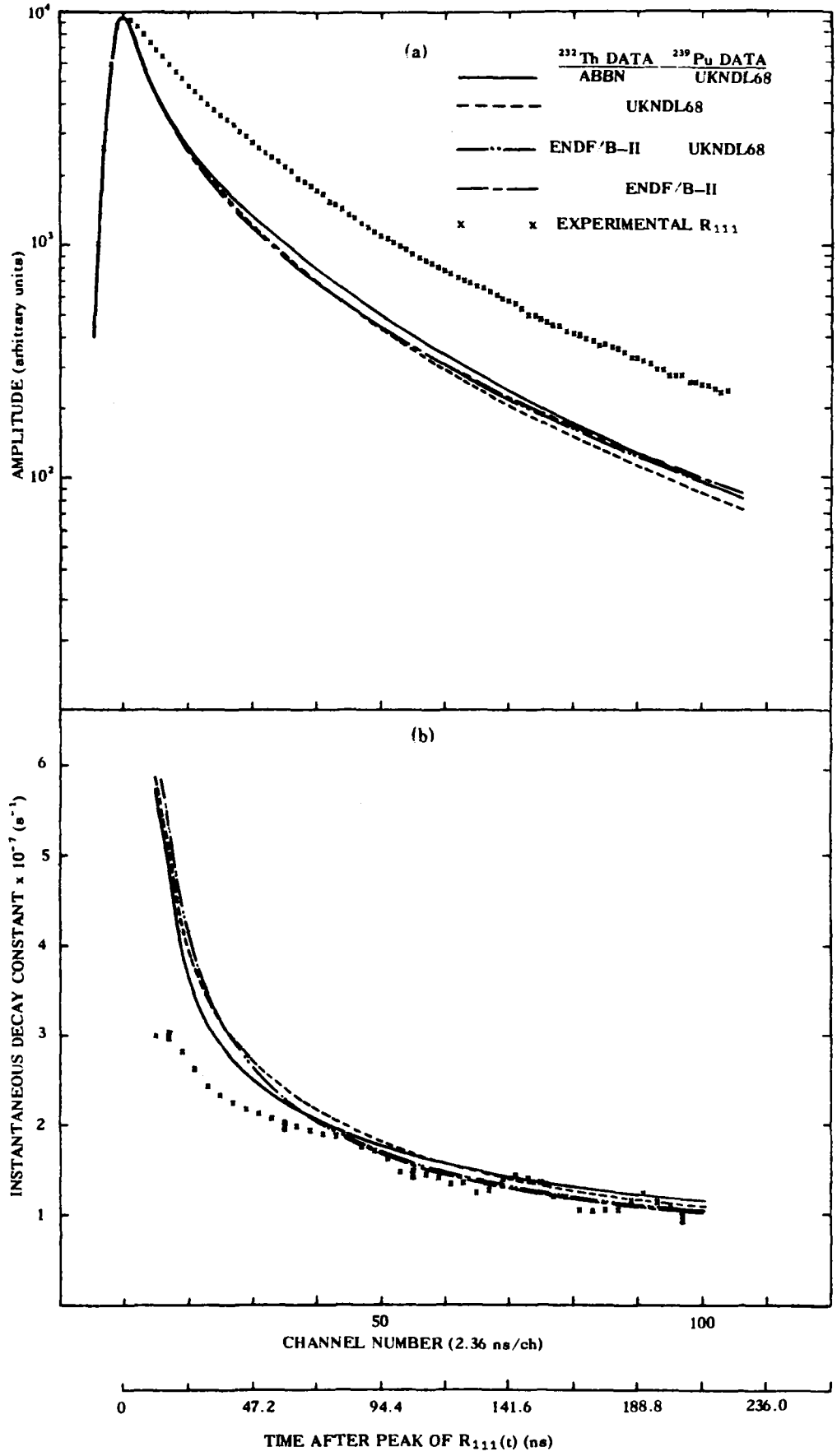

FIGURE 2.8(iii) CALCULATED AND EXPERIMENTAL VALUES OF FUNDAMENTAL MODE FISSION RATES FOR ^{239}Pu AS A FUNCTION OF TIME. (a) FUNDAMENTAL MODE TIME DISTRIBUTION (b) $\lambda(t)$ THE INSTANTANEOUS DECAY CONSTANT

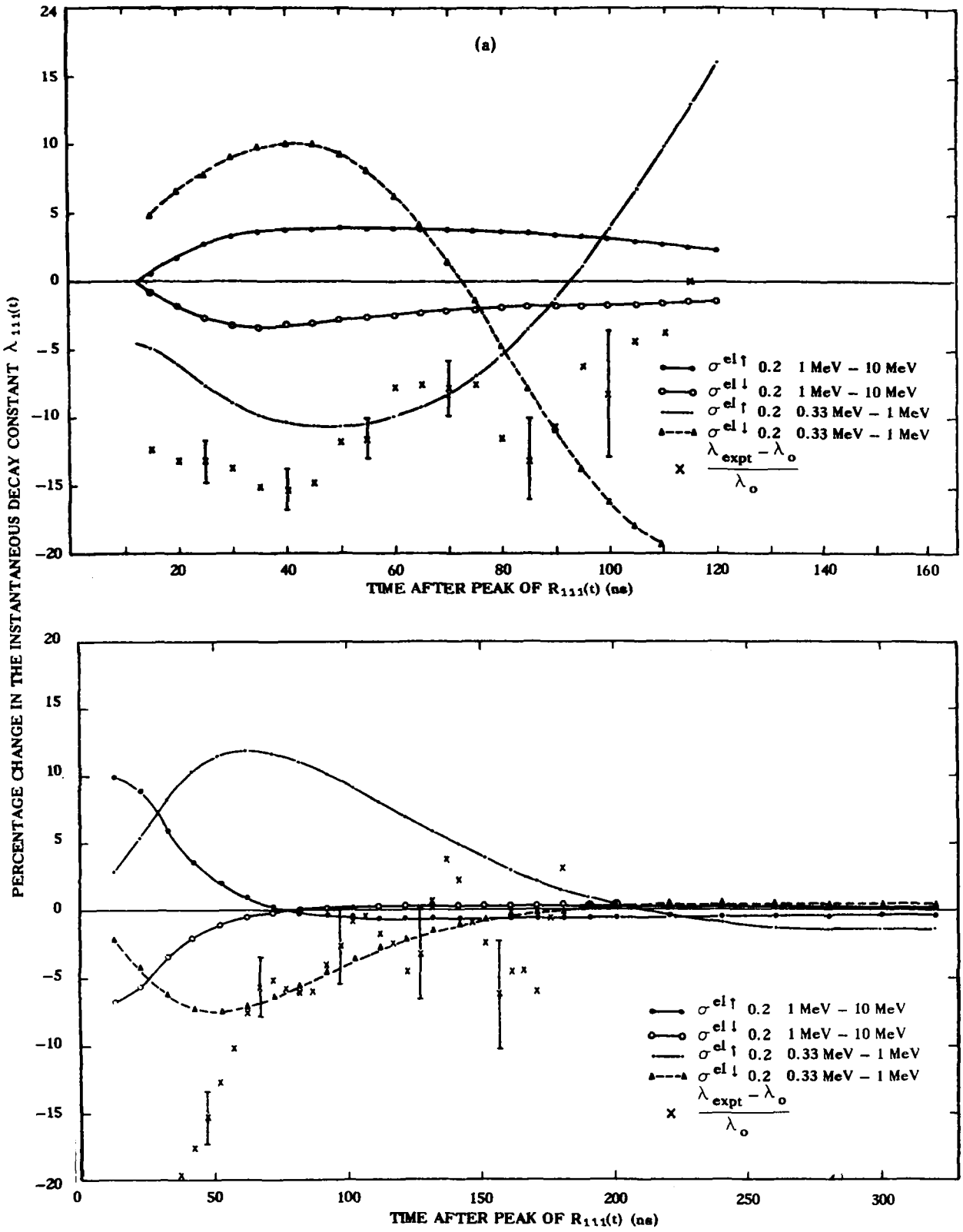

FIGURE 2.9 CHANGES IN λ(t) OF (a) ^{237}Np AND (b) ^{235}U FISSION RATES FOR GIVEN CHANGE IN ^{232}Th ELASTIC CROSS SECTION

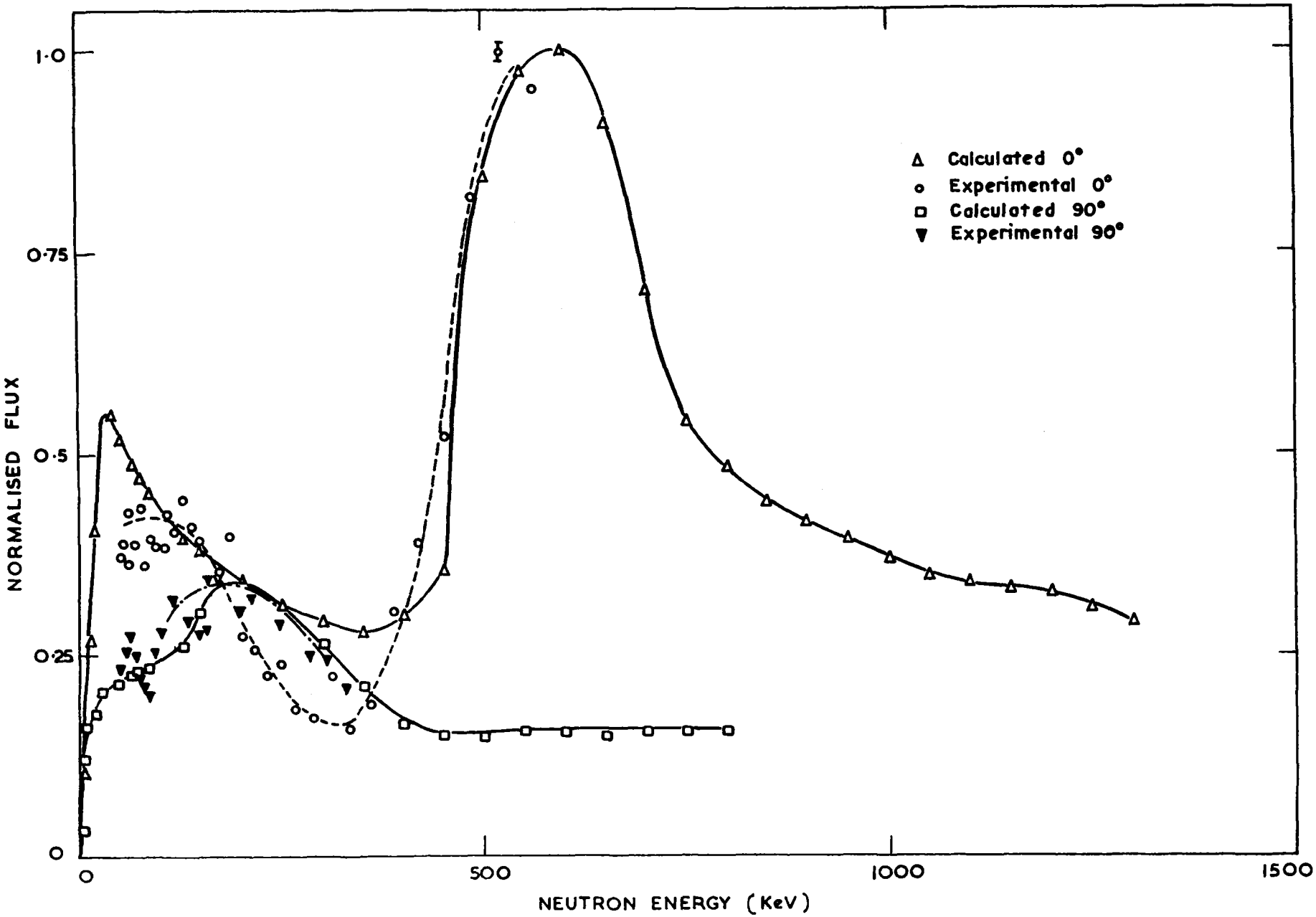

FIGURE 2.10 CALCULATED AND EXPERIMENTAL NEUTRON SPECTRA FROM Li(p,n) REACTION AT 0° AND 90°

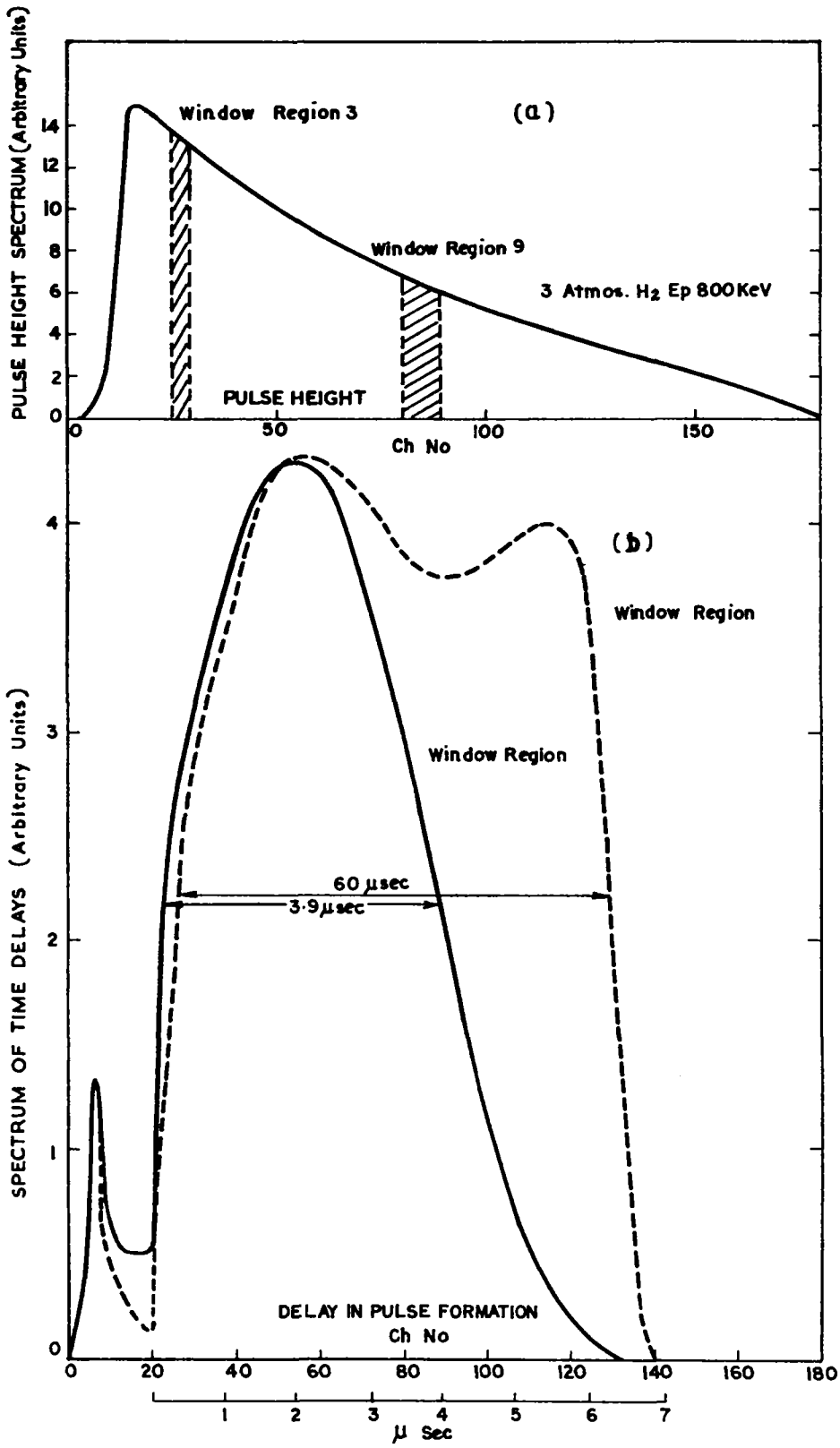

FIGURE 2.11(a) THE TIME DELAY SPECTRUM OF PULSES INITIATED BY PROTON EVENTS IN A GAS FILLED PROPORTIONAL COUNTER AS A FUNCTION OF PULSE HEIGHT
(b) PULSE HEIGHT SPECTRUM SHOWING PULSE HEIGHT WINDOWS FOR WHICH DELAY SPECTRA IN (a) WERE MEASURED

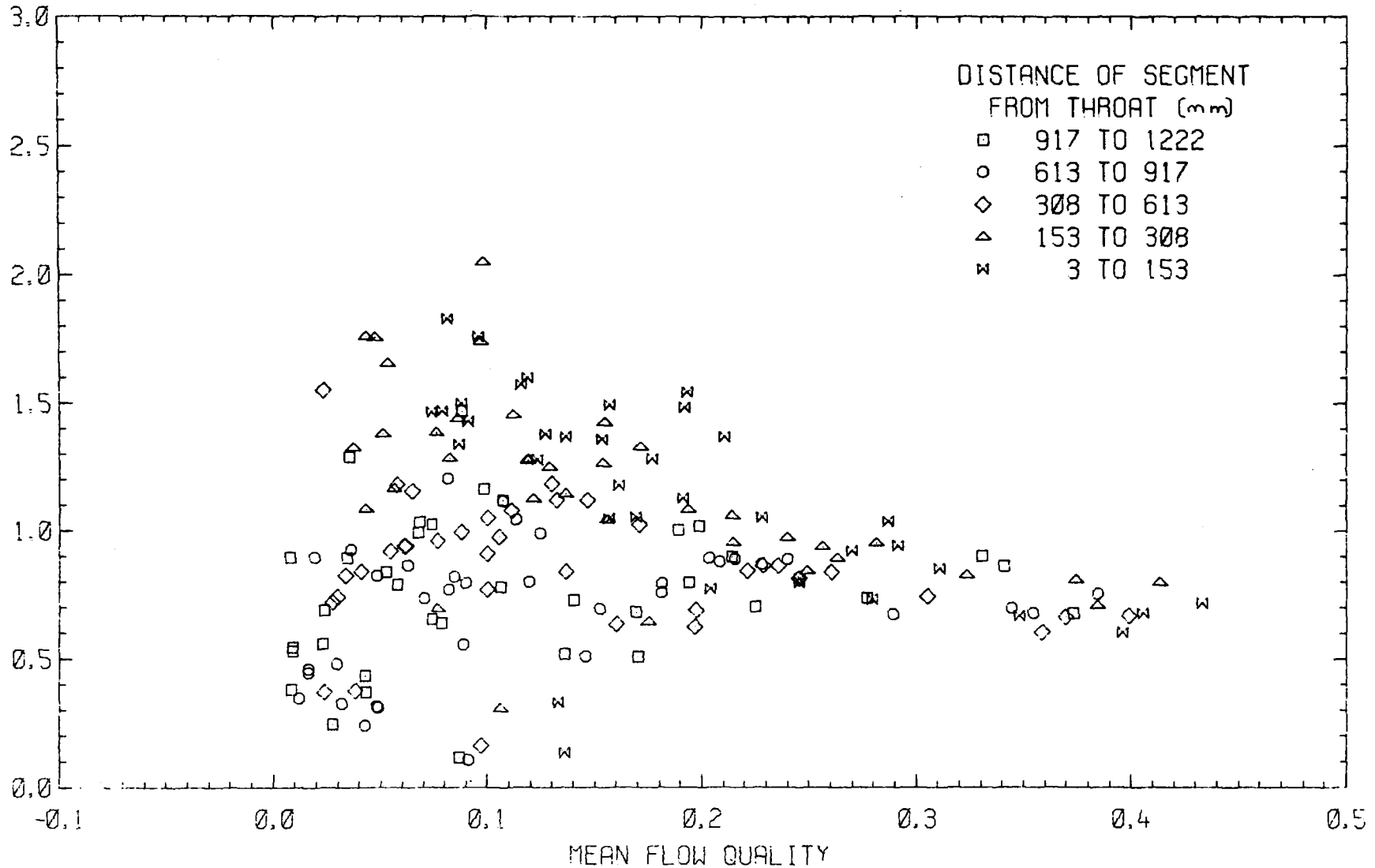

FIGURE 2.12(a) CALCULATED AND MEASURED PRESSURE PROFILES AT NEAR CRITICAL FLOW RATES, 3.175 mm DIAMETER

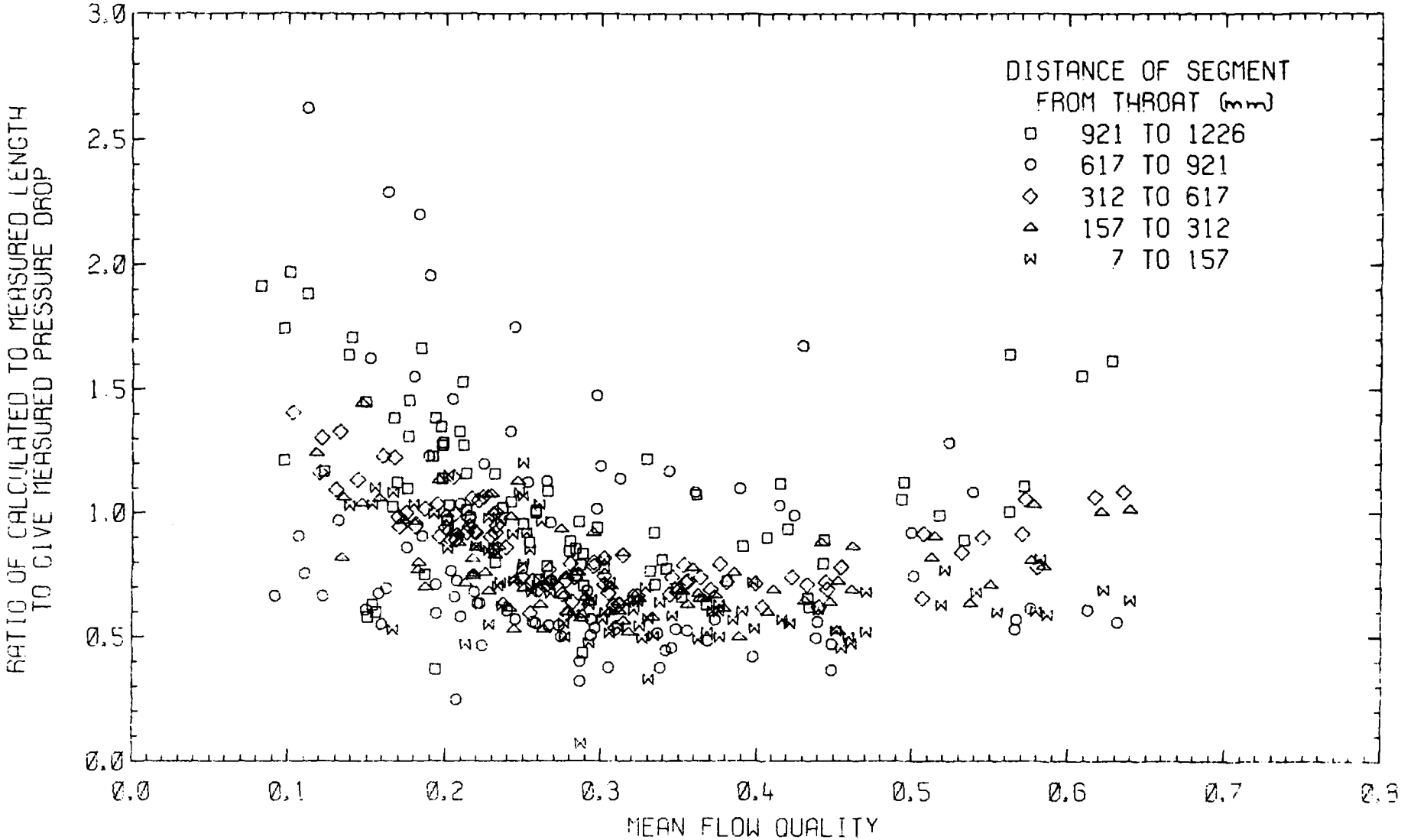

FIGURE 2.12(b) CALCULATED AND MEASURED PRESSURE PROFILES AT NEAR CRITICAL FLOW RATES, 6.833 mm DIAMETER

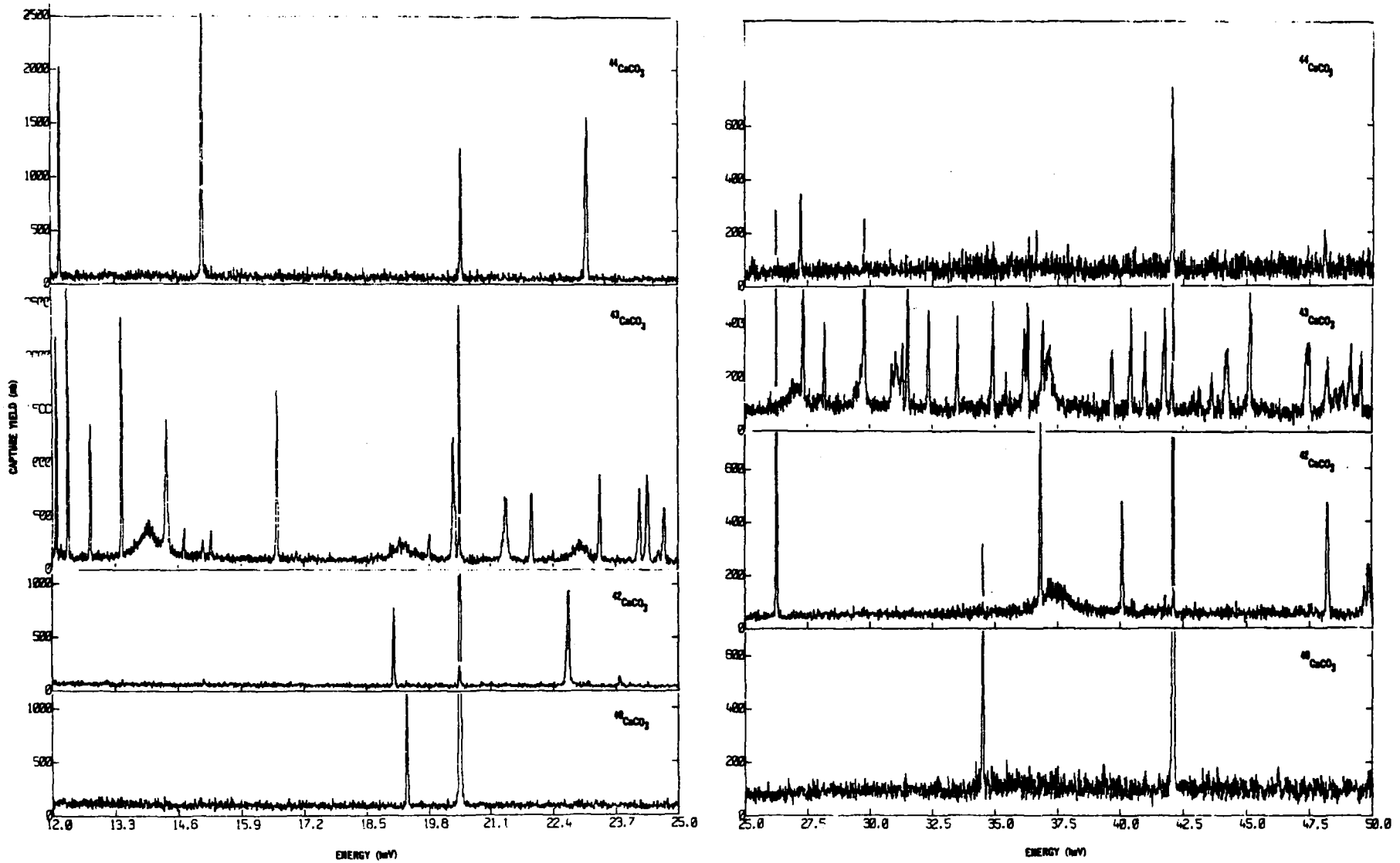

FIGURE 3.1 AVERAGE CAPTURE γ RAY YIELDS IN CALCIUM ISOTOPES

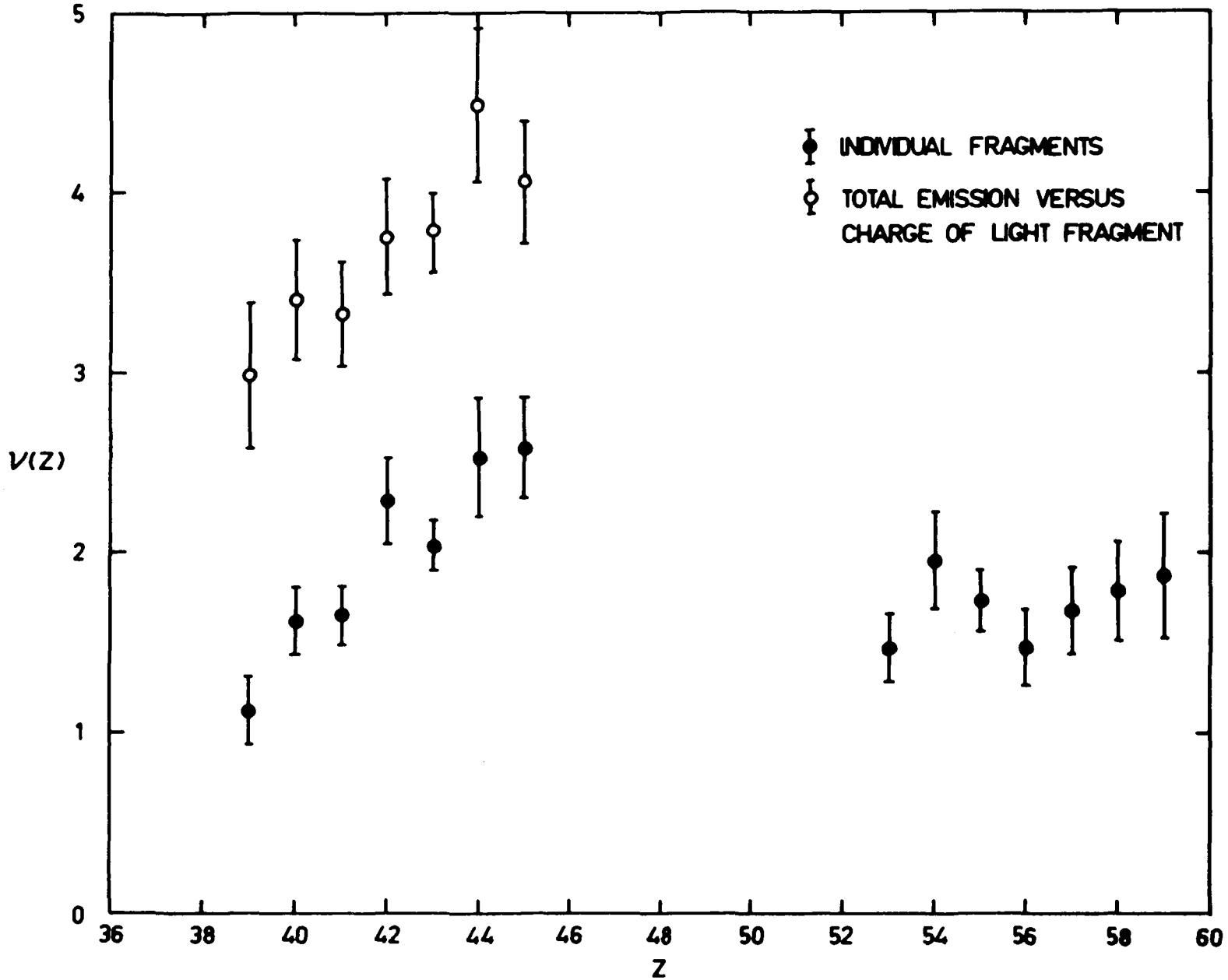

FIGURE 3.2 NEUTRON EMISSION AS FUNCTION OF ^{252}Cf FRAGMENT CHARGE ν(Z)

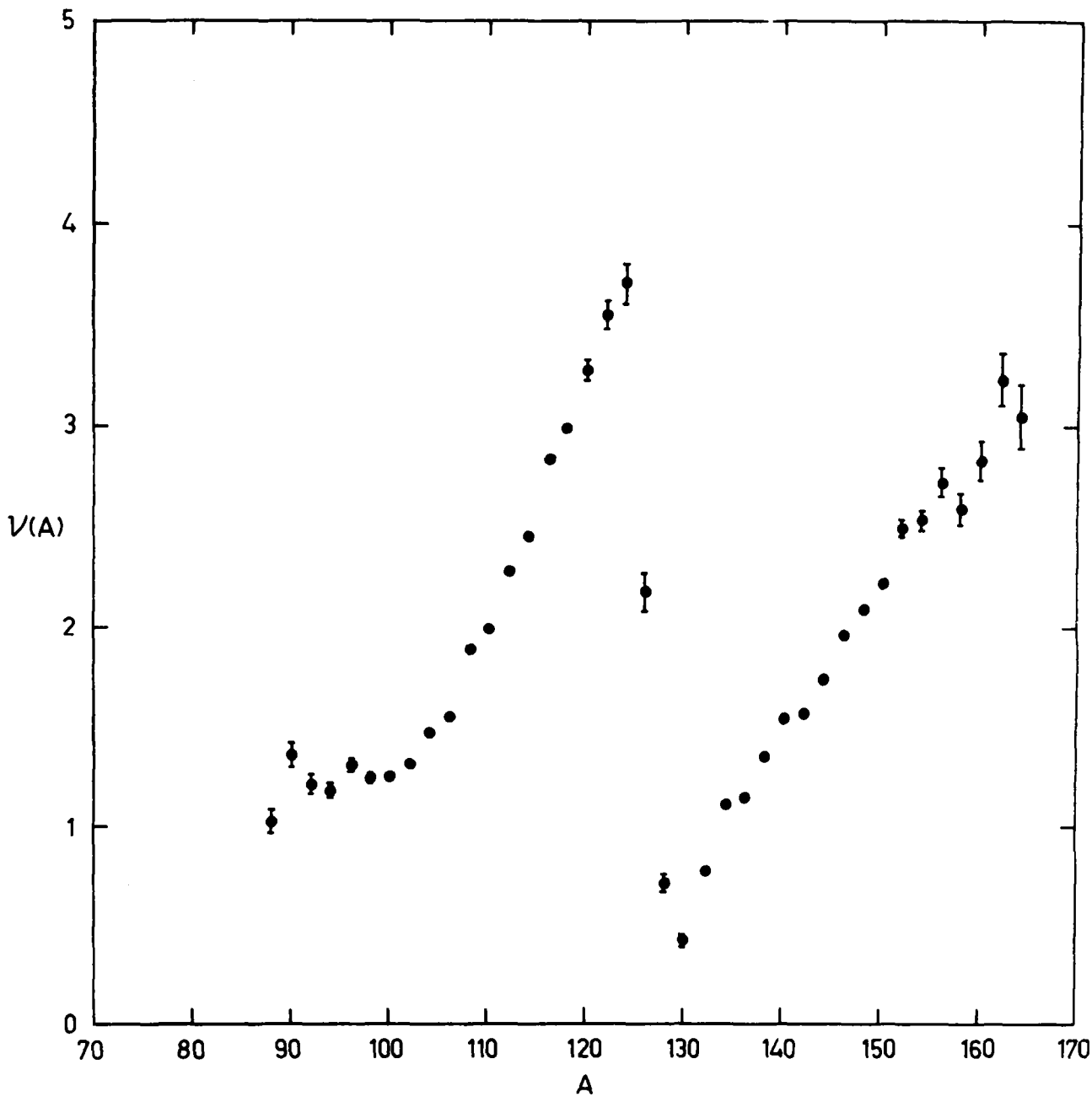

FIGURE 3.3(a) NEUTRON EMISSION AS FUNCTION OF ^{252}Cf FRAGMENT MASS $\nu(A)$

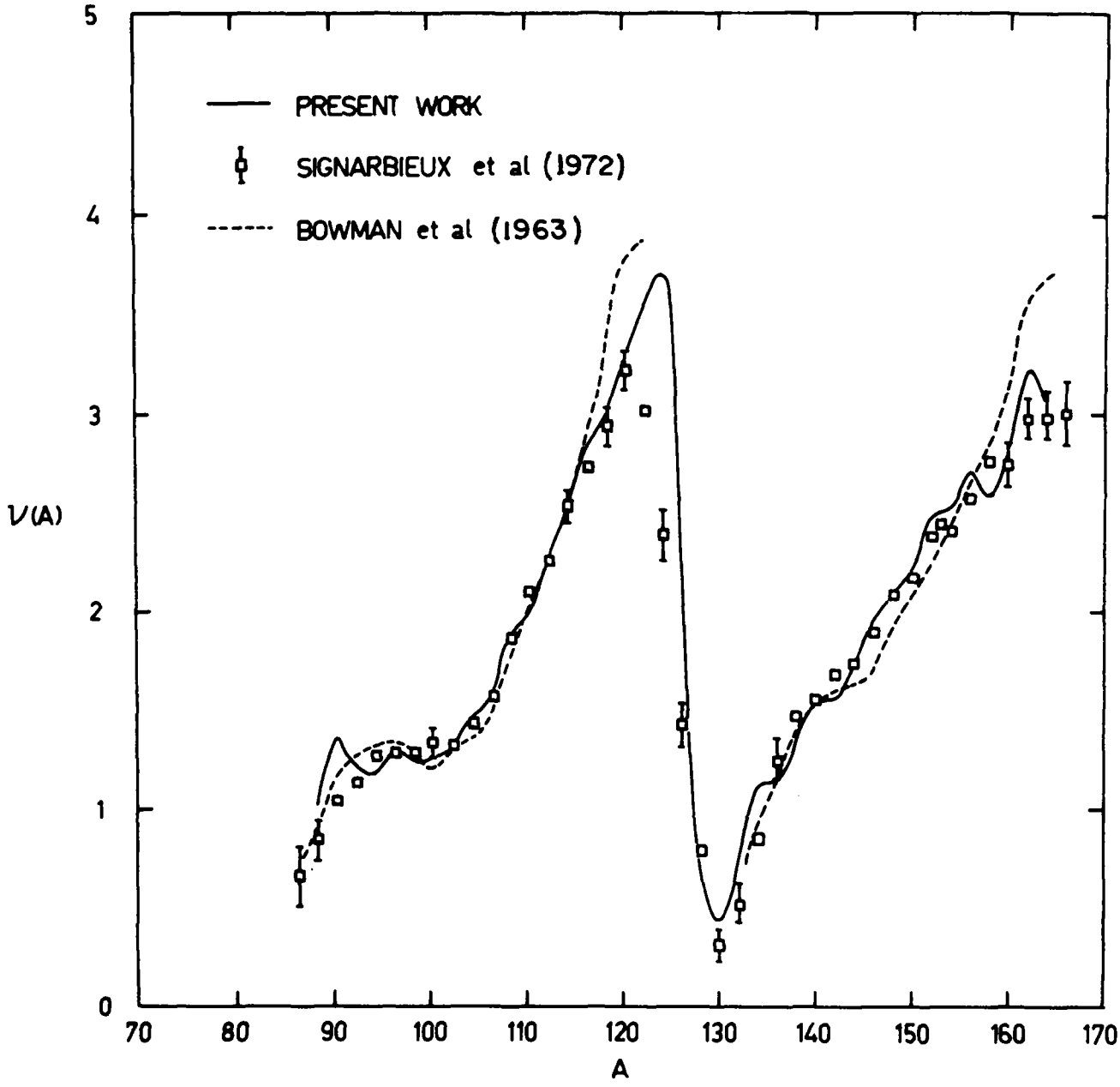

FIGURE 3.3(b) COMPARISON OF ν(A) FROM VARIOUS EXPERIMENTS

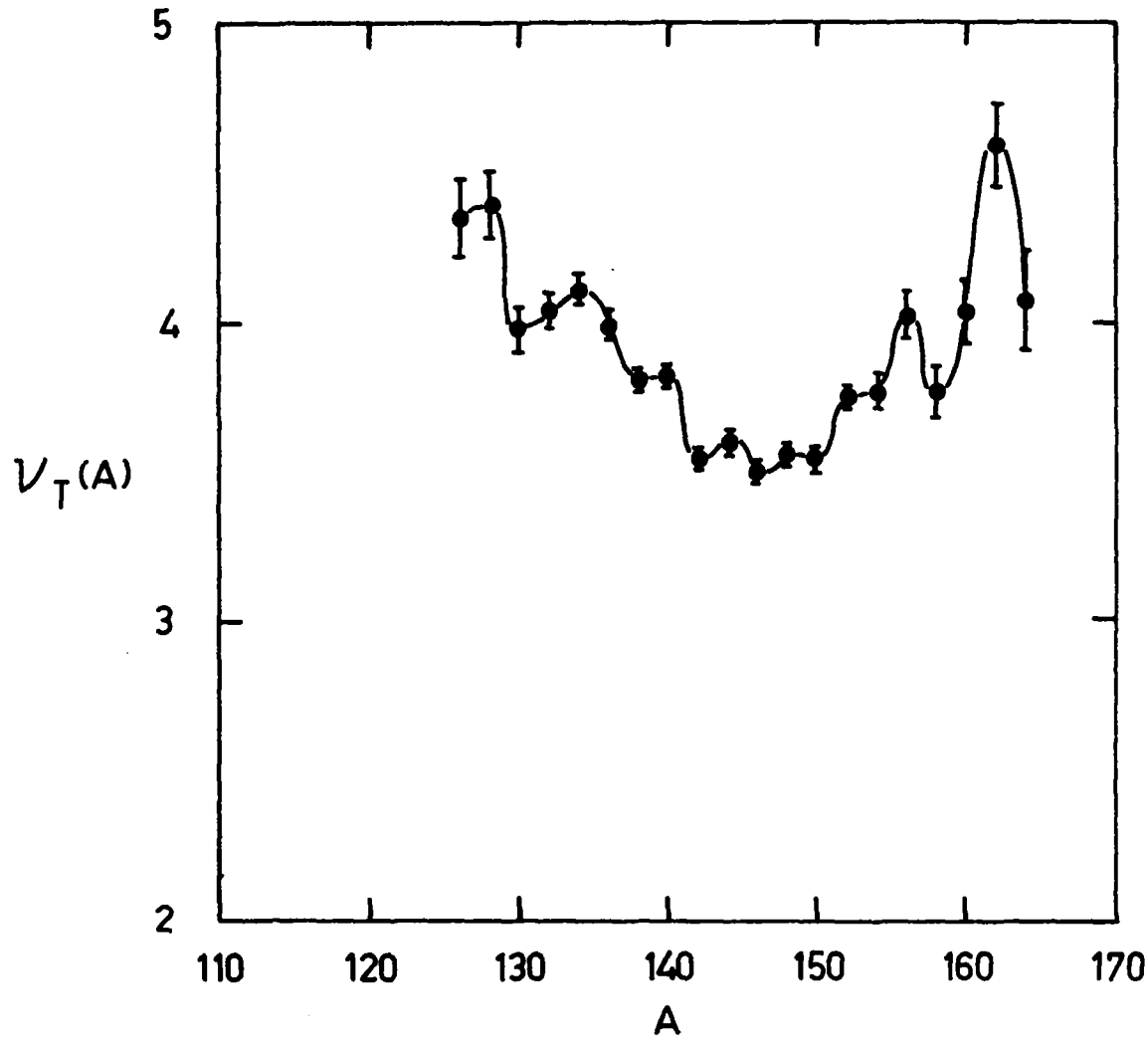

FIGURE 3.4(a) TOTAL NEUTRON EMISSION AS FUNCTION OF HEAVY FRAGMENT MASS

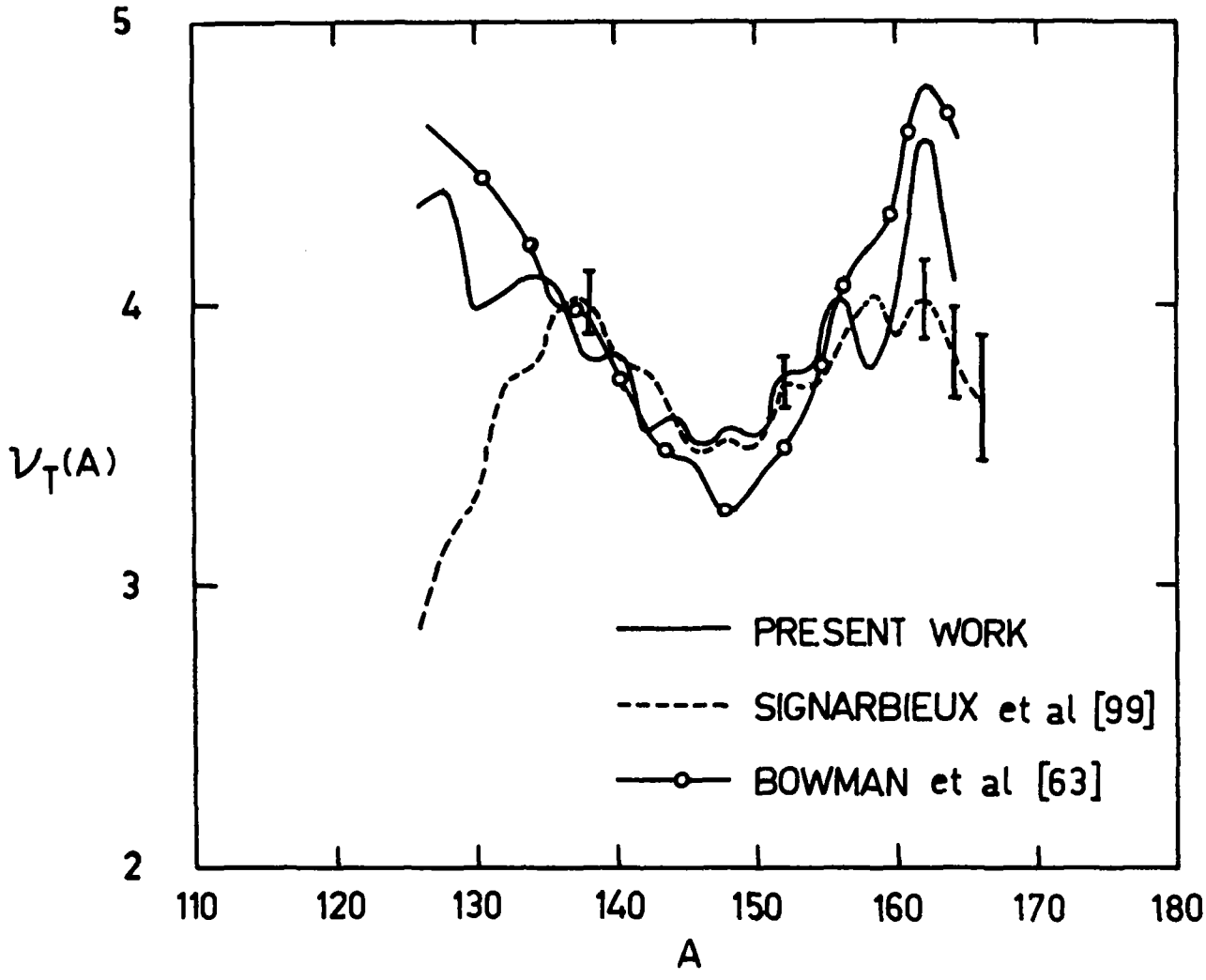

FIGURE 3.4(b) COMPARISON WITH OTHER EXPERIMENTAL MEASUREMENTS

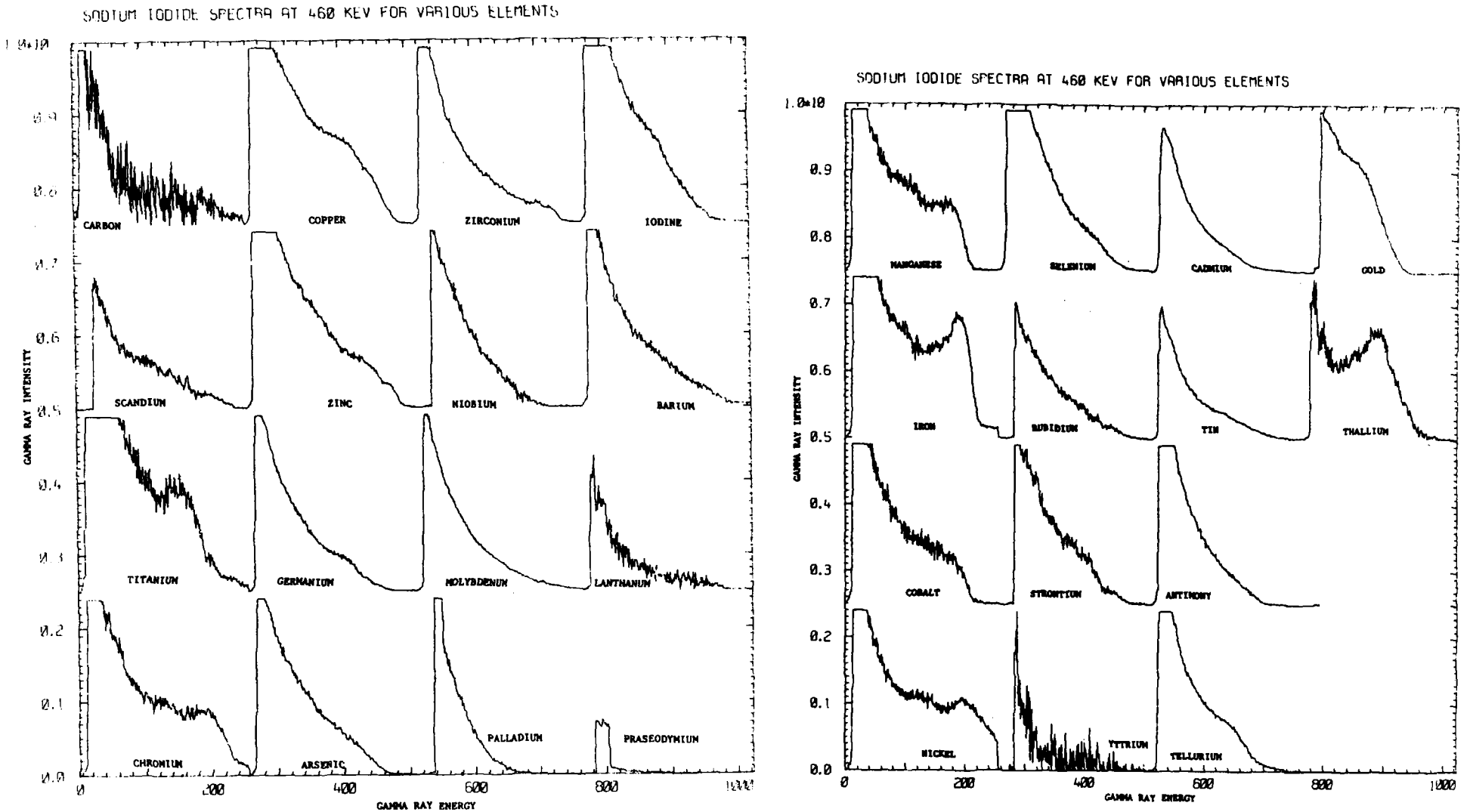

FIGURE 3.5 BACKGROUND SUBTRACTED CAPTURE SPECTRA FOLLOWING CAPTURE OF 460 keV NEUTRONS IN WIDE RANGE OF NUCLEI

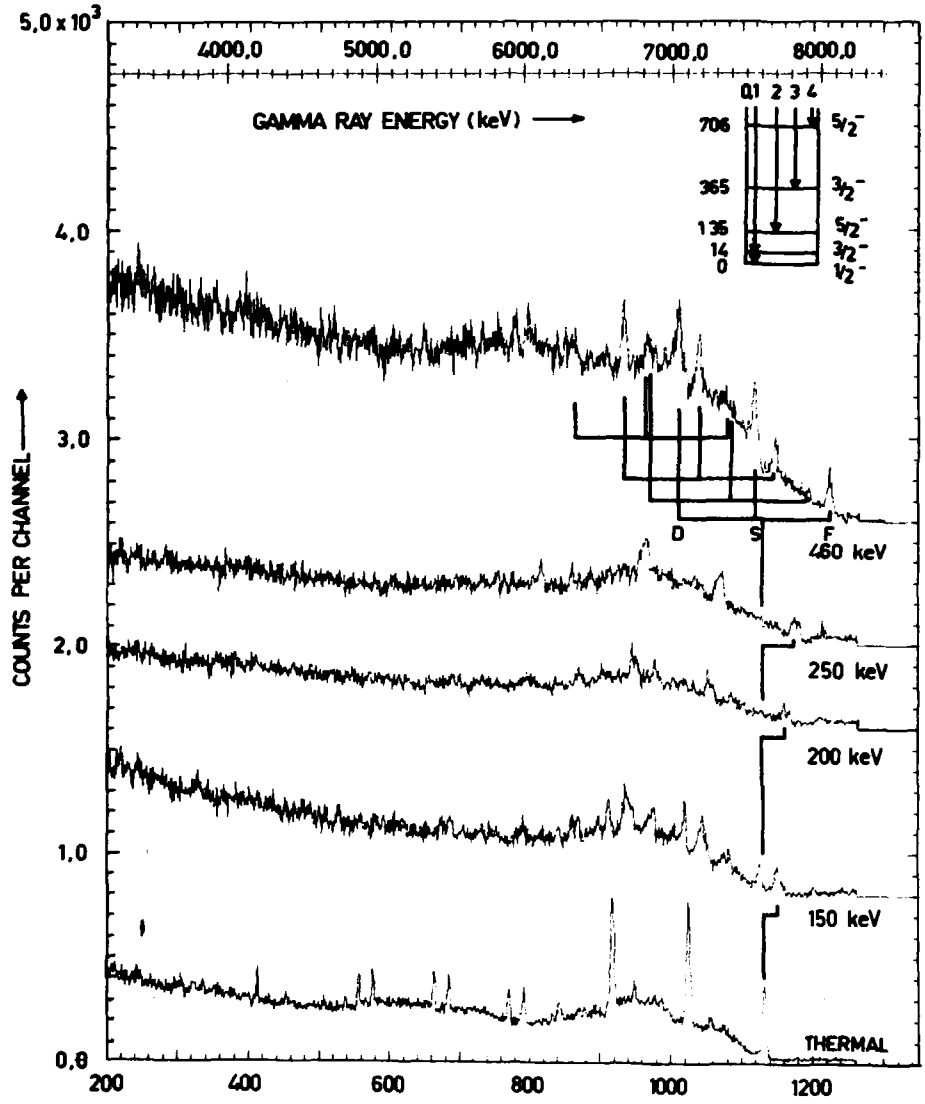

FIGURE 3.6 IRON BACKGROUND SUBTRACTED SPECTRA FOR NEUTRON ENERGIES UP TO 460 keV

APPENDIX (PHYSICS)

STAFF

ACTING DIVISION CHIEF: MR. W. GEMMELL

EXPERIMENTAL REACTOR PHYSICS SECTION (A/Head: Mr. D. B. McCulloch)

Pulsed Neutron and Spectrum Group

RS: A. I. M. Ritchie
M. Rainbow

EO: A. Rose
S. Whittlestone

Technical Staff

TO: K. McMaster

Reactor Experiments Group

RS: J. Connolly
A. Dalton
J. Harries

EO: D. J. Wilson
G. Durance
R. Knott

TO: J. P. Sawyer
D. Stevenson
I. F. Senior

Special Duties

RS: W. J. Turner
P. Duerden

EO: T. Wall
D. Culley

TO: G. K. Brown

OA: W. Leebold (C)

NEUTRON PHYSICS SECTION (Head: Dr. J. R. Bird)

Neutron Data Group

RS: J. Boldeman
M. Kenny
B. J. Allen

EO: R. Walsh
R. J. Cawley

TO: J. Copland
H. Broe

Nuclear Techniques Group

EO: M. Scott

TO: A. van Heugten
L. Russell

OA: J. Carroll (C)

ATTACHED STAFF

R. Barrett (AINSE Fellow, Melbourne University)
K. H. Bray (AINSE Fellow, Australian National University)
I. F. Bubb (Caulfield Institute of Technology)
L. Carlson (AINSE Fellow, Australian National University)
J. Caruana (AINSE Student, Wollongong University College)
D. M. H. Chan (Melbourne University)
J. B. Garg (SUNY, New York, USA)
F. Hille (Wollongong University College)
S. Kannard (AINSE)
P. Lloyd (AINSE)
J. B. Mathur (Wollongong University College)
G. E. Murch (Flinders University)
Hla Pe (Colombo Plan, University of New South Wales)
P. B. Price (University of New South Wales)

THEORETICAL PHYSICS SECTION (Head: Dr. B. Clancy)

Nuclear Physics Group

RS: D. Lang
A. Musgrove
EO: E. Clayton

Nuclear Data Group

RS: J. Cook
W. Bertram
EO: H. Ferguson
E. Rose

Reactor Physics Group

RS: G. Doherty (R)
I. Donnelly
EO: K. Maher

APPENDIX (cont'd)

Reactor Codes Group

RS: J. Pollard

EO: B. McGregor
G. Robinson
B. Harrington
G. Trimble

Technical Staff

TA: M. Inkster (R)
L. Sullivan
J. Miles (C)

Neutron Source Group

RS: G. Hogg
J. Tendys

EO: J. Daniel

Technical Staff

TO: J. Fredericks

(C) Commenced

(R) Resigned

DISTRIBUTION LIST

AAEC/PR 39-P

1.	Chairman	
2.	Deputy Chairman	
3.	Commissioner (Sir Lenox Hewitt)	
4.	Commissioner (K. F. Alder)	
5.	Programme Manager, Nuclear Science and Applications	
6.	Programme Manager, Power and Energy	
7.	Programme Manager, Uranium Fuel Cycle	
8.	Site Manager	
9.	Chief, Materials Division	
10.	Chief, Physics Division	
11.	Chief, Engineering Research Division	
12.	Chief, Chemical Technology Division	
13.	Chief, Instrumentation and Control Division	
14.	Chief, Environmental and Public Health Division	
15.	Chief, Isotope Division	
16.	Head, Applied Mathematics and Computing Section	
17.	Head, Mechanical Development Section	
18.	Head, Regulatory and External Relations Branch	Head Office
19.	Secretary	
20.	Assistant Secretary	
21.	Director, Information Services	
22.	Library	
23.	Director, Nuclear Plant Safety Unit, Mascot	
24.	Head Nuclear Studies Group	
25.	Mascot Library	
26.	Professor Sir Sidney Sunderland, Dean, Faculty of Medicine, University of Melbourne	Safety Review Committee
27.	Dr. C. J. Cummins, Director, NSW Department of Health	
28.	Mr. D. J. Stevens, Director, ARL	
29.	Controller, Site Information Services	
30.	Controller, Site Administration	
31.	Controller, Site Operations	
32.	Controller, Engineering Services	
33.	Controller, Site Planning	
34.	Manager, Commercial Applications	
35.	Nuclear Materials Officer	
36.	ASNT	
37.	Executive Officer, AINSE	
38.	RE Library	
39.		
40.		
41.	Washington Office	
42.	London Office	
43.		
44.	Vienna Office	
45.	Tokyo Office	
46.	Head, Experimental Reactor Physics Section	
47.	Head, Neutron Physics Section	
48.	Head, Theoretical Physics Section	

DISTRIBUTION LIST (cont'd)

49. Head, Reactor Performance Section
50. Head, Engineering Physics Section
51. Head, Chemical Physics Section
52. Head, Applied Physics Section
53. Head, Health Physics Research Section
54. Head, Radioisotope Services Branch
55. Head, Pharmaceutical & Chemical Products Section
56. Head, Irradiation Research Section
57. Head, Reactor Operations Section
58-98. W. Gemmell for INDC and Bilateral Agreement correspondents
99. B. Allen
100. J. Boldeman
101. J. Connolly
102. J. Cook
103. G. Doherty
104. P. Duerden
105. G. Durance
106. J. Harries
107. G. Hogg
108. M. Kenny
109. D. Lang
110. B. McGregor
111. A. Musgrove
112. J. Pollard
113. M. Rainbow
114. I. Ritchie
115. J. Tendys
116. W. Turner
117-147. J. R. Bird (for special distribution)
148. D. Byers (University of Canterbury, N.Z.)
149. V. Deniz (BARC, India)
150. S. Kapoor (BARC, India)
151-171. Bilateral Agreements (UKAEA 5, USAEC 11, AECL 5) via H.O.
172-180. Spares